TU/e EINDHOVEN UNIVERSITY OF TECHNOLOGY

Eindhoven University of Technology

MASTER

Wet selective oxidation of AlAs layers and its application to DBR mirrors

Volpe, D.

Award date:
1997

Link to publication

Disclaimer
This document contains a student thesis (bachelor's or master's), as authored by a student at Eindhoven University of Technology. Student theses are made available in the TU/e repository upon obtaining the required degree. The grade received is not published on the document as presented in the repository. The required complexity or quality of research of student theses may vary by program, and the required minimum study period may vary in duration.

General rights
Copyright and moral rights for the publications made accessible in the public portal are retained by the authors and/or other copyright owners and it is a condition of accessing publications that users recognise and abide by the legal requirements associated with these rights.

- Users may download and print one copy of any publication from the public portal for the purpose of private study or research.
- You may not further distribute the material or use it for any profit-making activity or commercial gain

Faculty of Electrical Engineering

EEA 537

Wet selective oxidation of AlAs layers and its application to DBR mirrors

Davide Volpe

537

September 1996 - February 1997

This master's thesis is written in the framework of the final graduation project for the study of Material Engineering at Politecnico di Torino.

This work was performed as a graduate project under the Erasmus programme at the Eindhoven University of Technology.

Supervisors: Dr.ir. T.G. van de Roer
Ir. M. P. Creusen

Place: Electronic Devices Group
Faculty of Electrical Engineering
Eindhoven University of Technology

The Faculty of Electrical Engineering of the
Eindhoven University of Technology is not
responsible for the content of this report

Abstract

The vertical cavity surface emitting laser (VCSEL) is a new type of opto-electronic device with several important advantages compared to conventional edge-emitting semiconductor lasers. Comparison between VCSELs and conventional lasers along with a brief description of the VCSEL developed at the Electronic Device Group of the T.U.E. are presented in the Introduction section.
Among the several options for current confinement we will concentrate on a relatively recent one which uses wet selective oxidation of AlAs-layers. A complete overview of what can be found in literature about this relatively new oxidation process is presented in chapter 2 and will act as an introduction to two main aspects of intra-cavity contacted VCSELs treated in this master's thesis:

- a general insight into the wet selective oxidation of $Al_xGa_{1-x}As$-layers in order to obtain a reliable and uniform process which transforms epitaxially grown and high Al-content compounds into stable dielectric material. This process is exploited for the current confining in the intra-cavity contacted VCSEL of the T.U.E.

- development of the technological steps required for the realization of a oxide-based Distributed Bragg Reflector (DBR) mirror for visible light applications (λ=650nm).

Concerning the first task of this project, several MBE-grown samples containing multilayers GaAs/AlAs were prepared by using wet or dry process techniques. Oxidation of AlAs-layers was carried out in a quartz furnace at 400-450°C in a saturated environment; since the oxidation rate of $Al_xGa_{1-x}As$ strongly increases with Al-content this process is very selective and only the AlAs-layers are transformed into a mechanically and thermally stable oxide (polycrystalline γ-Al_2O_3).
While the vertical oxidation of $Al_xGa_{1-x}As$ shows a diffusive character and saturation for long oxidation times, the lateral oxidation remains reaction-limited for all of the times inspected. This behavior is probably due to the formation of "canals" along the oxide/semiconductor interface as a result of the contraction of the oxide: the canals are responsible for the fast transport of the oxidizing gasses to and from the oxidation front.
Although the oxidation process is still not fully controlled due to the large number of parameters which affect the mechanism and the kinetics, the experimental observations carried out during this project will allow a better awareness of the whole process when new material will be available.

Table of Contents

1 Introduction 1

2 Wet selective oxidation (literature) 5

2.1 Historical review 5
2.2 Vertical and lateral oxidation 7
2.3 Structure of oxide 8
2.4 Mechanism of wet oxidation 10
2.5 Reaction or diffusion mlimited-process 11
2.6 Parameters which influence the oxidation rate 13
2.6.1 Temperature dependance 13
2.6.2 Al-content 14
2.6.3 Crystallografic preference 15
2.6.4 Doping type and level 15
2.6.5 Heterointerface structure 15

3 Manufacturing process 17

3.1 Introduction 17
3.2 Wet chemical process 17
3.3 Dey process 19
3.4 Plasma etching theory 21

4 Wet selective oxidation (experimental overview) 23

4.1 Experimental set-up for wet oxidation 24

4.2 Uniformity of wet oxidation 26
4.2.1 oxidation of wet-etched mesas 31
4.2.2 oxidation of dry-etched mesas 32
4.3 Thermal stability of AlGaAs/AlO multilayers 37
4.3.1 Introduction 37
4.3.2 First results 37
4.3.3 Improvements in thermal stability 39
4.3.3.1 RTA of graded linear DBRs 39
4.3.3.2 Over-oxidation of AlAs-layers 40
4.3.4 Conclusion 42

4.4 Vertical contraction of wet oxidized AlAs **43**
4.4.1 Introduction 43
4.4.2 Shrinkage valuation 45
4.4.2.1 SEM inspection *45*
4.4.2.2 alpha-step inspection *46*
4.4.3 Conclusion 48
4.5 Atomic Force Microscope measurements **49**
4.5.1 Introduction 49
4.5.2 Preparation of the samples 49
4.5.3 Measures 50
4.5.4 Conclusions 55
4.6 Weight loss during wet oxidation **57**
4.7 Distributed Bragg Reflector for visible light **61**
4.7.1 Introduction 61
4.7.2 Oval defects 63
4.7.3 Realization of a semiconductor/oxide DBR 65
4.7.4 Conclusion 68

5 Conclusions and acknowledgements 69

Appendix 73

A Overview of processed samples **73**

B MBE-growth menu **79**

C Recipes **85**
C.1 process overview 85
C.2 recipe for the new TUE-VCSEL 89
C.3 recipe for wet etched mesas 96

D Aluminum oxides and hydroxides **97**

Reference 101

CHAPTER 1

Introduction

Vertical cavity surface emitting lasers (VCSELs) have several important advantages compared to conventional edge-emitting semiconductor lasers. Emission of coherent light perpendicular to the substrate offers the possibility of fabricating large two-dimensional arrays for optical computing and the new generation of displays; the low divergence of the circular output beam with symmetric profile is more efficiently coupled into a single mode fiber and makes the VCSEL an ideal light source in applications like short-haul optical fiber communication systems, data storage and read-on systems. Relatively simple integration with other devices (Opto Electronic Integrated Circuits), on-wafer testing and wafer-scale fabrication without cleaving the substrate are also interesting characteristics of VCSELs for low cost and mass production.

The structure and the operation of these two types of laser are depicted and compared in fig.1.1 and fig.1.2.

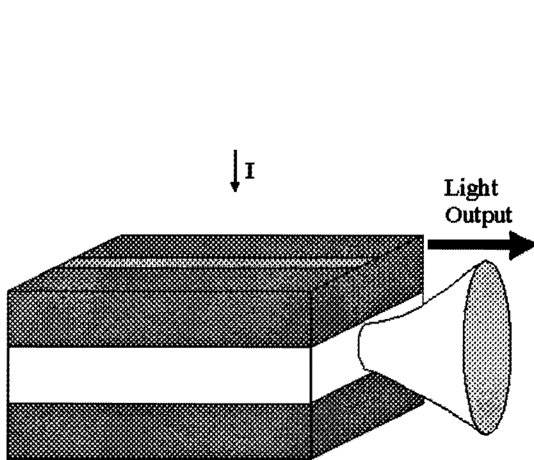

Fig.1.1: conventional semiconductor laser

- large size (about 300μm)
- cleaved mirror facet
- in-plane output (parallel to the substrate)
- high divergence
- elliptical beam

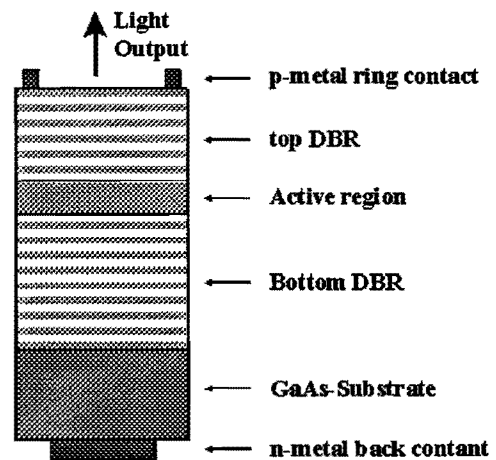

Fig.1.2:Vertical Cavity Surface Emitting Laser (VCSEL)

- lateral dimension in the order of 2-20μm
- built-in DBRs grown by MBE or MOVPE
- vertical emission (perpendicular to the substrate)
- low divergence
- circular beam

The major disadvantages of the VCSEL compared to the conventional edge-emitting laser are the increased difficulty of processing and the lack of polarization selectivity.

The VCSEL designed and fabricated at the T.U.E. by the Electronic Device Group is an intra-cavity contacted VCSEL operating in the 980 nm wavelength regime. InGaAs quantum wells and AlGaAs-based Distributed Bragg Reflector (DBR) mirrors have been used for generating the coherent light in the active region. A detailed description of the technological steps for the realization of the TUE-VCSEL is depicted in appendix C.1.

In the intra-cavity design the charge carriers are not injected into the active region through the DBR mirrors as in the early VCSEL designs, but through two doped contact layers on either sides of the active region. Hence the substrate and both DBRs can remain undoped and the free carrier optical losses will be greatly reduced.

Although the electrical and optical VCSEL design can now be optimized separately, an extra current constriction mechanism is needed to force the charge carriers into the lasing region; this will also minimize the non-radiative surface recombination and therefore external quantum efficiency will be considerably enhanced. The current constriction is achieved in the TUE-VCSEL by lateral selective oxidation of two AlAs-layers placed close to the active region. A cross section of the device is shown in fig.1.3

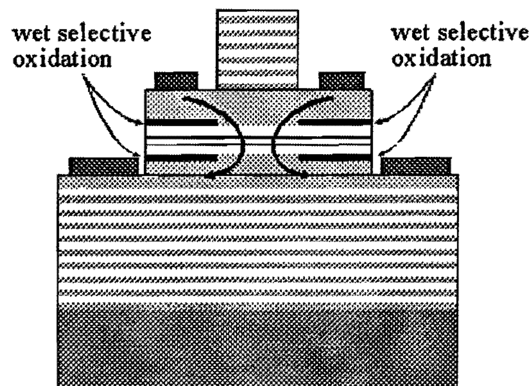

Figure 1.3: schematic cross section of an intra-cavity contacted VCSEL.
Al_2O_3 current constrictions are used to align the electrical and optical density profiles.

Wet oxidation is a relatively new technique for the formation of high-quality oxides and has already been proven to be an extremely useful fabrication technology for the realization of opto-electronic devices. Due to the high selective character of the oxidation (oxidation rate of $Al_xGa_{1-x}As$ with x=1 is about two order of magnitude greater than with x = 0.8) dielectric structures can easily be defined inside a fully epitaxial grown device.

Fabrication of current constriction layers during the VCSEL process is only one of the several applications. Other uses include: diffusion masking, crystal stabilization from

atmospheric degradation, formation of planar waveguides and index-guided lasers and realization of semiconductor/oxide DBR mirrors with high reflectivity.

Although wet oxidation has already been extensively used, the exact properties of the oxide and the mechanism of oxidation are still not fully understood. In this report it is intended to give a collection of experimental observations about this process, a characterization of the formed oxide and practical suggestions for the realization of visible light DBR-mirrors.

CHAPTER 2

Wet Selective Oxidation (literature)

Wet selective oxidation is a relatively new process and it was accidentally discovered by Dallesasse et al. [1] in 1990 during his studies on room-ambient hydrolization of AlGaAs quantum well heterostructures (QWHs). Since then wet oxidation of AlGaAs has been successfully employed in the fabrication of edge emitting lasers and it has recently been applied to several vertical-cavity surface emitting lasers. Nevertheless many aspects of this process are still not well understood: not much is known about the real mechanism behind it and the real properties of the oxides formed by this technique.

This chapter gives a complete review about all the developments made in the last seven years and a good overview of actual research activities concerning the oxide properties. After a brief description about several oxidation techniques for the oxidation of ternary compound semiconductor, the attention will be focused on wet selective oxidation.

2.1 Historical review

Three methods have been established until now for oxidation of $Al_xGa_{1-x}As$:

Anodic oxidation.

Anodic oxidation of $Al_xGa_{1-x}As$ is accomplished by applying a DC voltage between the sample to be oxidized (anode) and a platinum electrode (cathode) in an electrolyte solution. The final thickness of the oxide depends on the applied voltage and the time of the process (the growth rate decrease with time because of the insulating character of the oxide layer). The selectivity of this technique is poor.

Plasma oxidation

Plasma oxidation is carried out in a radio-frequency excited plasma, and as oxidizing agent is used ionized O_2. The DC voltage applied to the substrate controls the deposition rate and the oxide thickness. However this method is not selective for certain Al-compositions. These oxides, very similar to anodic oxidation products, find applications in planar device fabrication as surface passivation layers.

Thermal oxidation

For thermal oxidation the samples are exposed to several types of oxidizing gases (O_2, CO_2, N_2O) at temperatures ranging from 350 to 500°C. Native oxide films of $Al_xGa_{1-x}As$ produced by this method are not uniform and not stable to mechanical and thermal stresses and their electrical and optical properties are poor. The oxidation growth rate depends on the Al-content in the compound and therefore selective oxidation of AlAs-layers is theoretically feasible.

Wet selective oxidation.

Wet selective oxidation is a special case of thermal oxidation; it consists in the exposure of $Al_xGa_{1-x}As$ at elevated temperature ranging from 400 to 450°C to a water vapor flow with N_2 as carrier gas. The oxide formed is a stable phase of Al_2O_3 with high quality and insulating properties and differs significantly from the oxides formed by conventional thermal oxidation.

This process is a powerful tool in the processing of new opto-electronic devices due to the ease of processing and the possibility to selectively and laterally oxidize $Al_xGa_{1-x}As$-layers at a speed of about 2 μm/min.

As already mentioned, this process was first discovered by Dallesasse and coworkers in 1990 during their studies on long-term stability of AlGaAs/GaAs quantum well heterostructure (QWH) devices. After exposure to normal conditions of temperature (25°C) and humidity for 2-10 years, $Al_xGa_{1-x}As$ layers with composition $x > 0.7$ and thickness > 0.1 μm were found instable and transformed into compressively strained oxide layers [2]. The compressive stress caused the formation of microcracks and peeling when the layers were on the top surface, and complete delamination when the layers were buried into the structure and surrounded by unaffected GaAs.

The mechanism of this degradation and selectivity to high composition $Al_xGa_{1-x}As$ was ascribed to hydrolysis and to the extreme reactivity of Aluminum to form several oxygen-rich compounds. A detailed description of the Al-hydroxides and products of thermal decomposition is presented in appendix D.

With help of electron dispersion x-ray spectroscopy (EDS) Dallesasse also found a reduction of As in the hydrolyzed region, probably lost in form of AsH_3 when the water vapor in the air reacted with AlGaAs; the remaining As was ascribed to formation of As_2O_3 still present in the structure. Nevertheless the exact reaction causing the degradation and the chemical composition of the new product were unclear; Dallesasse suggested the following reactions:

$$AlAs_{(s)} + 3\ H_2O_{(v)} \rightarrow Al_2O_{3(s)} + 2\ AsH_{3(v)} \quad (1)$$

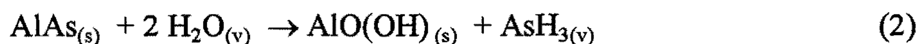

$$AlAs_{(s)} + 2\ H_2O_{(v)} \rightarrow AlO(OH)_{(s)} + AsH_{3(v)} \quad (2)$$

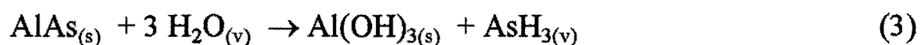

$$AlAs_{(s)} + 3\ H_2O_{(v)} \rightarrow Al(OH)_{3(s)} + AsH_{3(v)} \quad (3)$$

Afterwards, by considerations about the standard heat of formation and on phase diagram (see appendix D) Sugg and coworkers [4] proposed reaction (3) to be responsible for the atmospheric hydrolysis.

In order to obtain new samples for their studies on degradation of $Al_xGa_{1-x}As$, Dallesasse [1] tried to accelerate this process following the classic method (Frosch, 1955) established for wet oxidation of silicon; therefore N_2-flow saturated with water vapor was passed over samples at 400°C; in this way he discovered the so-called "wet oxidation" process for III-V compounds; instead of the low quality product of atmospheric hydrolization, this procedure resulted in the formation of smooth, dense and transparent native oxides with good properties of adhesion.

2.2 Vertical and lateral oxidation

Before dealing with the general aspects of wet oxidation, an explanation of the two main methods for wet oxidizing Al-rich compounds is necessary. The outlines of those two different schemes are drafted in fig. 2.1 .

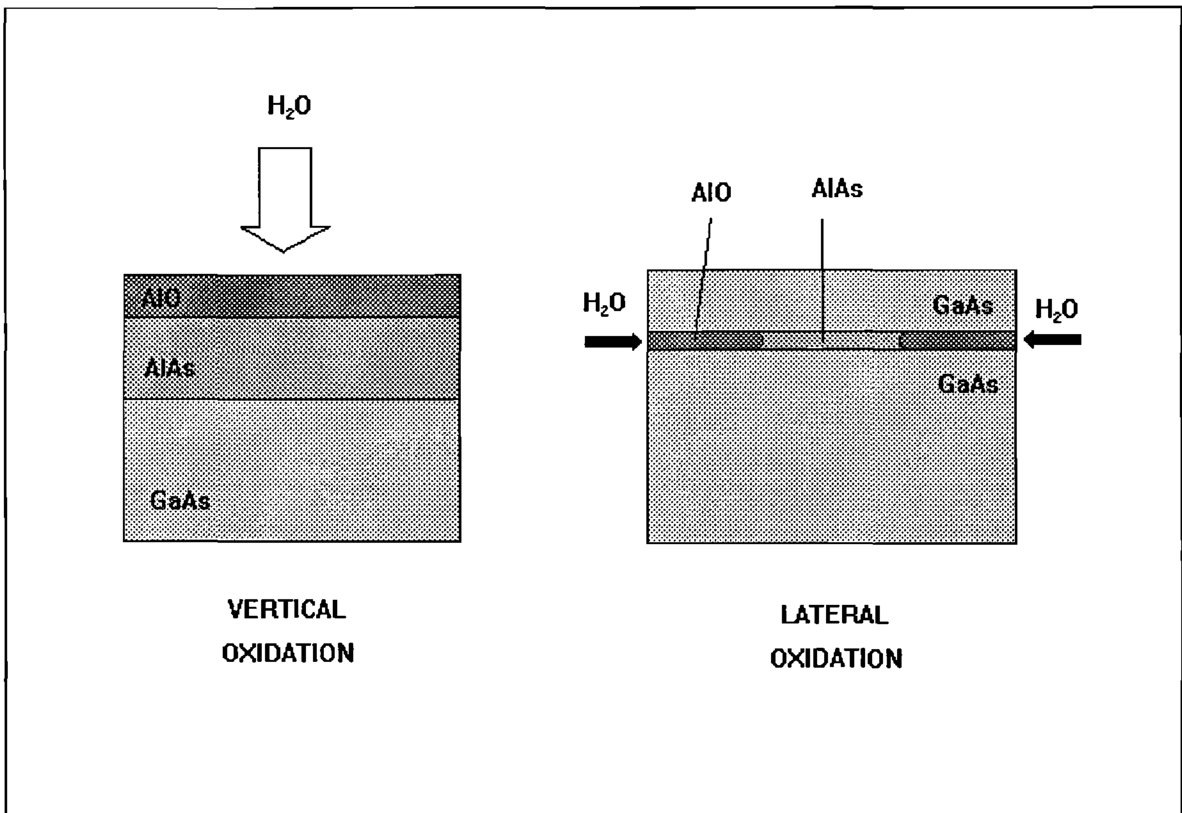

Figure 2.1: vertical and lateral oxidation

Vertical oxidation was the first historical way to wet oxidize AlAs; according to this process AlAs to be oxidized has obviously to lay on the top surface. The main application is merely the realization of passivated layers.

For lateral oxidation, an etching through the top layers is needed since the Al-rich compounds are buried under unaffected GaAs; the oxidation will then proceed from the exposed sidewalls to the inside of the structure. This process is the most interesting for device fabrication.
Homan et al. [18], after comparison of these two methods, stated that:

- vertical oxidation shows saturation for prolonged times
- lateral oxidation rate is about 2 times larger than vertical oxidation rate.

Only the second assertion is well established, since it was confirmed by many other researchers. Although the formed oxide is, in both cases, porous to a more or less extent, the higher oxidation rate for laterally oxidized layers can be explained by the contraction of the oxide layers due to less molar volume and the creation of transporting canals along the oxide/semiconductor interface. See the next paragraph for more information.

2.3 Structure of oxide

Transmission Electron Microscopy (TEM) is the most widely used characterization method for inspecting the structure of the oxide formed by wet selective oxidation. For the definition of the crystal lattice this is often complemented with electron diffraction patterns; other techniques available for the elemental analysis are Auger Electron Spectroscopy (AES) and Secondary Mass Ion Spectroscopy (SIMS). In the following a complete and chronological review of all the TEM-studies on wet oxidation in the last five years is given.

The first TEM-studies were carried out by Kish et al. [5] in 1992 in order to observe the interface $Al_xGa_{1-x}As$/oxide (x=0.5 and x=0.8) after vertical oxidation; they found no differences between the structure of the oxides from $Al_xGa_{1-x}As$ with different Al-composition, being both essentially amorphous with a rather smooth interface.
The presence of small crystalline granules, inherently present in the oxide, were wrongly attributed to electron beam irradiation damage. The smoothness of the boundary at the $Al_xGa_{1-x}As$ native oxide/semiconductor interface had been improved by employing $In_{0.5}(Al_xGa_{1-x})_{0.5}P$ "stop layers": since the phosphorous compounds oxidizes at a much slower rate, they effectively serve to stop the oxidation process. TEM inspection revealed a much more smooth interface.

In 1993 Sugg et al. [6] stated, after a TEM study of vertically oxidized $Al_{0.8}Ga_{0.2}As$, that the oxide had an amorphous structure with fine-grains embedded and that the oxide/ semiconductor interface was uniform and abrupt.
With help of electron diffraction they identified the oxide to be one of the four modification of Al_2O_3 (η, γ, χ or δ); see appendix D for more information about the hydrates phases of Al_2O_3 and their dehydration products. Monohydrate AlO(OH) was also a possibility but it was present to a lesser degree than the other phases since it probably reacted with AlAs to form Al_2O_3 according to the reaction (4).

First observations about the strain field at the oxide/semiconductor interface were carried out by Choquette et al. [7]; they noticed no evidence of strain or other extended defects, as dislocations or crystalline defects, for $Al_{0.98}Ga_{0.02}As$-converted oxide but clear evidence of a strain field was observed near the interface of AlAs-converted oxide. This strain would cause the mechanical and thermal instability of the device containing AlAs oxide layers. Choquette ascribed this different behavior to the vertical shrinkage of the oxidized AlAs-layer (-12%) compared to the shrinkage of the oxidized $Al_{0.98}Ga_{0.02}As$-layer (-6.7%)

By electron diffraction the oxide converted from pure AlAs was finally identified as γ-Al_2O_3, a cubic structure of hydrated alumina; the measured lattice constant of 7.87Å was in perfect agreement with the theoretical lattice constant of 7.9Å. During this study Guha et al. [8] were also able to estimate the grain size of the polycrystalline γ-Al_2O_3, which turned out to be about 8 nm.

According to previous results, Guha stated that during the wet oxidation process most of the AlO(OH) formed was converted into γ-Al_2O_3 by removal of hydroxil group upon heating (see appendix D); according to this theoretical reaction, a volume shrinkage of about 50% would lead to enormous hydrostatic stress. By TEM inspection voids and canals were in fact clearly seen at the oxide/semiconductor interface and formation of these defects were believed to considerably reduce the stress in the whole structure.

The phenomenon of "canals" at the oxide-semiconductor interface can also explain the higher oxidation rate of laterally oxidized compared to vertically oxidized layers. The transport of the oxidizing species and products to and from the oxidation front through such canals along the oxide-semiconductor interface is fast and would explain the diffusion-unlimited and the linear reaction process in the lateral case.

The stresses due to the shrinkage also contribute to the formation of defects close to the oxide terminus and in the $Al_xGa_{1-x}As$ layers near the oxide-semiconductor interface. These defects were observed to be confined within a 300 nm $Al_xGa_{1-x}As$-layer adjacent to the oxide.

The crystallografic phase of the oxide formed by wet selective oxidation of $Al_xGa_{1-x}As$ (with x=0.98 and x=0.92) was confirmed to be polycrystalline γ-Al_2O_3 by further TEM-studies carried out by Twesten et al. [9]. At the oxide/semiconductor interface a region containing neither γ-Al_2O_3 grains nor monocrystalline $Al_xGa_{1-x}As$ was found; they claimed that this zone was an amorphous phase, probably hydrated alumina such as amorphous $Al(OH)_3$ or AlO(OH), and suggested that the reaction proceeded from an initially amorphous phase to the polycrystalline γ-Al_2O_3 according to equation (3). Due to the random distribution of fine γ-Al_2O_3-grains the hypothesis of the precipitation of a random precursor is also more reasonable than a direct crystal to crystal transformation.

A detailed analysis of the structure revealed the presence of 4 nm large Al_2O_3 grains surrounded by an amorphous matrix. Void cavities were again found in proximity of the oxide/semiconductor interface; they were surrounded by γ-Al_2O_3 grains and were placed about 15 nm from the interface and within 1 µm from it.

Other TEM images indicates that those cavities are not really voids but contain an amorphous material (probably $Al(OH)_3$); since these defects were only found in the

$Al_{0.98}Ga_{0.02}As$ converted oxide and not in the $Al_{0.92}Ga_{0.08}As$-oxide their origin was believed to be the result of a rapid reaction kinetics of the oxidation process ($Al_xGa_{1-x}As$ with x=0.98 has an oxidation rate more than five times greater than $Al_xGa_{1-x}As$ with x=0.92).

The most recent TEM-study was carried out by Takamori et al. [10] and was not in complete agreement with the previous results: voids or cavities near the oxide/semiconductor interface were in fact not reported, even from AlAs-converted oxide. By their high-resolution cross-sectional TEM images they stated that the oxide/semiconductor interface was about four monolayers thick and the width at the oxide terminus interface between converted and non-converted AlAs was about 6.5 nm.

2.4 Mechanism of wet oxidation

Possible oxidation reactions responsible for the phase transformation of AlAs into AlO_x were already suggested by Dallesasse.

To investigate the differences between oxides grown in room ambient or by wet selective oxidation Sugg et al. [4] cleaved a sample in two pieces consisting of 0.1 µm AlAs on a 0.5 µm GaAs layer; only one part was vertically oxidized by wet oxidation. After 80-days exposure of both samples to room ambient, a SIMS inspection (presented in fig.2.2) was carried out.

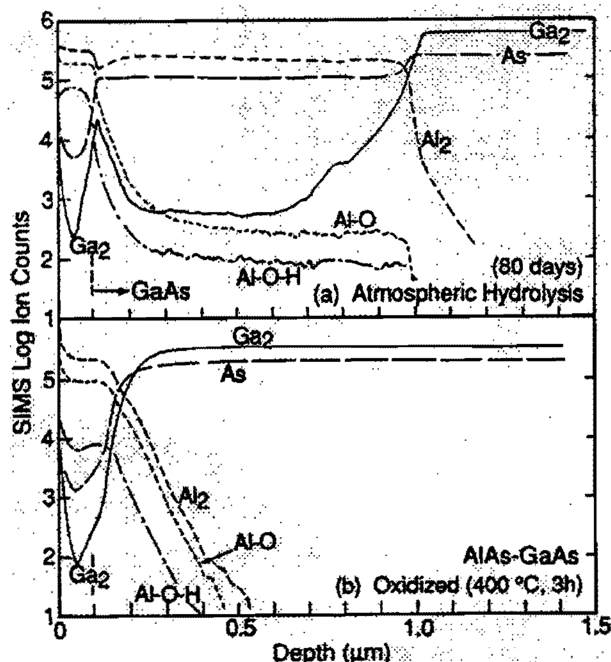

Figure 2.2: SIMS profiles after room-ambient exposure
(a) atmospherically hydrolized
(b) wet selectively oxidized

From these elemental profiles Sugg made the following observations:

- both samples have oxygen and hydrogen signals (Al-O-H-ion count) in the top 0.1 μm;
- the atmospherically hydrolyzed sample shows a significant Al-O-H-ion count as deep as 1.0 μm into the crystal.
- a Ga depletion is evident in the atmospherically hydrolyzed sample but not in the wet oxidized sample, indicating a chemical reaction and a degradation of the crystal in the former case.
- a selectivity in oxidation can be seen in the wet oxidized sample; AlAs easily oxidizes compared to GaAs. In further experiments was found that $Al_xGa_{1-x}As$ oxidizes more rapidly for higher Al-content, therefore the oxidation technique is called wet "selective" oxidation.

Sugg et al. ascribed reaction (3) to be the mechanism responsible for the atmospheric hydrolysis since the standard heat of formation of $Al(OH)_3$ is greater than that of either α-Al_2O_3, γ-Al_2O_3 or AlO(OH) at 300 K. Reaction (1) and (2) are more likely responsible for wet oxidation process.

The As depletion in the first 0.1 μm of the oxidize sample is one order of magnitude greater than for the hydrolyzed sample. This suggest that a second reaction takes place in the AlAs layer in the oxidized sample liberating still more As. The reaction may be:

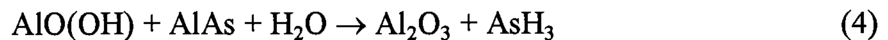

$$AlO(OH) + AlAs + H_2O \rightarrow Al_2O_3 + AsH_3 \qquad (4)$$

The greater As depletion in the AlAs layer of the oxidized sample indicates that As can play a significant role in the formation of a stable native oxide and may catalyze the reduction of hydroxyl (OH^-) groups in AlAs, since these hydroxyl groups are probably responsible for the instability of the atmospherically hydrolyzed sample.

2.5 Reaction or diffusion-limited process

One of the major mysteries of the wet oxidation mechanism has always been how the reactants and the products are transferred to and from the oxidation front through the Al_2O_3-layer. Although during the first historical experiments the oxidation was believed to be a diffusion-limited process, further studies established the oxidation to be a reaction-limited process. In a reaction-limited process the supply of oxidizing agents is sufficient and the reaction speed depends on how fast the species can react with each other. In a diffusion-limited process the supply of reactants is not sufficient and therefore the reaction speed is determined by how fast the species can reach the oxidation front.

The most important indicator for the type of process is the relation between oxide depth versus oxidation time. If this relation is linear, the process will be reaction-limited. If this relation is parabolic, the process will be diffusion-limited.

The temporal dependence of the oxidation thickness x_{ox} has been proposed by Ochiai [11] in analogy with the classical theory developed by Deal and Grove [12] about the thermal oxidation of silicon:

$$x_{ox}^2 + A \cdot x_{ox} = B \cdot t \tag{5}$$

where B is proportional to the diffusion constant of the water vapor through the oxide layer and B/A is a function of the reaction rate constant for AlAs oxidation and of the vapor transport coefficient [12].
In the limit of short oxidation times and thin oxide layers, equation (5) reduces to a linear growth law:

$$x_{ox} = \frac{B}{A} \cdot t \tag{6}$$

Alternatively, in the limit of long oxidation times and thicker oxides, or where oxidant diffusion across the oxide is the rate limiting mechanism, the oxidation follows a parabolic growth law:

$$x_{ox} = \sqrt{B \cdot t} \tag{7}$$

The reaction rate constant is smaller than the diffusion coefficient at lower temperatures (400-440 °C) resulting in a linear growth. For higher temperatures (500 °C) the reaction rate constant is larger than the diffusion coefficient resulting in a parabolic growth. For a given oxidation temperature the growth shifts from the linear to the parabolic region, as the oxidation progresses in time. Oxidation carried out at the lowest and highest temperatures lie in the linear and parabolic growth regions, respectively.
A diffusion-limited process indicates the formation of a protective, non-porous film, where, on the contrary, a reaction-limited process indicates the formation of a porous film.

In early studies (1992) parabolic growth laws were found by Kish et al. [13] and therefore the oxidation was believed to be controlled by the diffusion of the mobile ions (Al, Ga, O, OH); these ions diffuse via crystal defects in the oxide, thus the ion diffusion rate (oxidation rate) will depend on the diffusion rate of the crystal defects and on their concentration. However the data of Kish could also be fitted on a linear scale. This is depicted in figure 2.3 and 2.4.

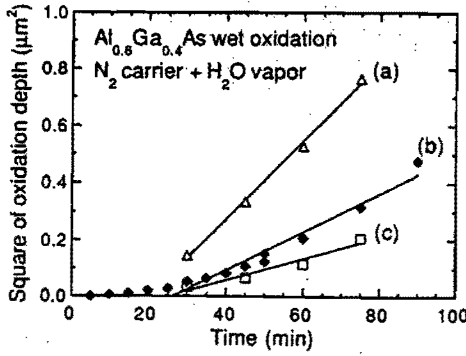

Fig. 2.3: square linear plot of oxidation depth vs. time
(a) $p = 9 \cdot 10^{18}$ T=500°C [13]
(b) $p = 10^{18}$ T=490°C [14]
(c) $p = 4 \cdot 10^{17}$ T=500°C [13]

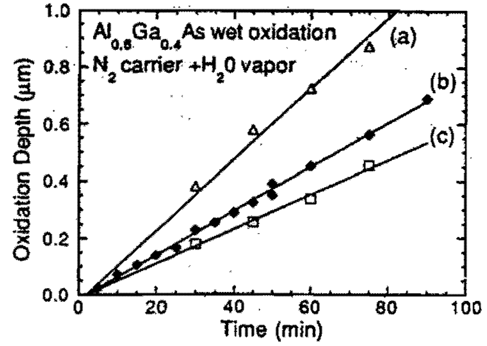

Fig.2.4:linear-linear plot of same data in fig.2.3 [14]

Several other scientists found linear growth laws [14,15,16,17,18]. From this it can be concluded that the oxidation mechanism is a reaction-rate limited rather than a diffusion-rate limited process and that the transport of the oxidizing species is explained by porosity of the oxide.

2.6 Parameters which influence the oxidation rate

2.6.1 Temperature dependence

As described in the previous paragraph the oxidation growth versus oxidation time for thin oxide layers fits a linear law $x_{ox} = k \cdot t$ where the rate constant $k = B/A$ has an Arrhenius-type dependence on temperature:

$$k = e^{-\left(\frac{E_a}{k_B T}\right)} \qquad (8)$$

where E_a is the activation energy of the oxidation process; the exponentially increasing of oxidation rate with increasing temperature has been verified in literature and many experimental data can fit equation (8).

Lee et al. [19] did an interesting study on the defect-free wet selective oxidation of AlAs: oxidation at 370°C revealed some defects on the oxide surface, at oxidation temperatures of 430°C also GaAs-layers started to oxidize and at 400°C the oxidation was stopped at the AlAs/GaAs interface and no defects were found on the surface.

2.6.2 Al-content

It is well established that wet oxidation is a selective process: oxidation rate is much higher for high Al-content AlGaAs compounds compared to low Al-content. It is therefore expected that the activation energy E_a of equation (8) will be lower for higher Al-content; by applying eq. (8) to data found in literature it will be clear that the activation energy E_a decreases for increasing Al-content ranging from 0.48eV (AlAs) to 3.15eV (n-$Al_{0.6}Ga_{0.4}As$).

A difference between the activation energy for p-doped $Al_{0.6}Ga_{0.4}As$ and n-doped $Al_{0.6}Ga_{0.4}As$ is also noticed, showing a higher oxidation rate for p-doped layers. The influence of doping on oxidation rate is discussed in paragraph 2.6.4.

Few studies have been carried out about the influence of Al-content on the oxidation rate. Results of these studies are depicted in the following diagrams.

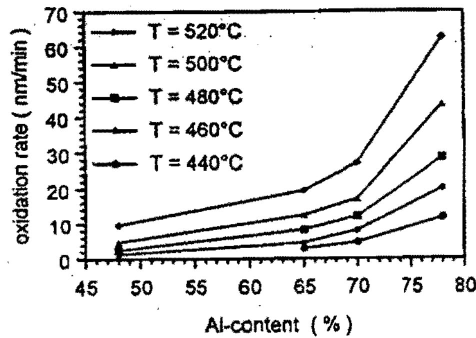

Figure 2.5: vertical oxidation rate vs. Al-content [15]

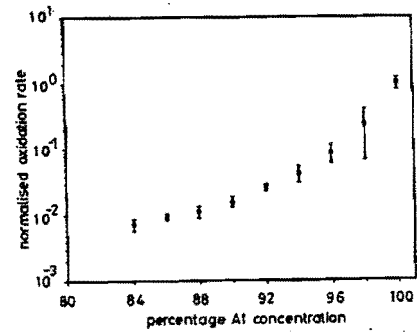

Figure 2.6: lateral oxidation rate vs. Al-content [42]

Ref.	Al molar fraction	T [°C]	oxidation rate [nm/min]
[7]	1	440	4000
	0.92	440	200
[9]	0.98	450	1125
	0.92	450	200
[16]	0.98	400	90
	0.98	425	260
	0.98	450	850
[17]	1	400	833
	0.937	400	196
	0.92	400	122
	0.86	400	24

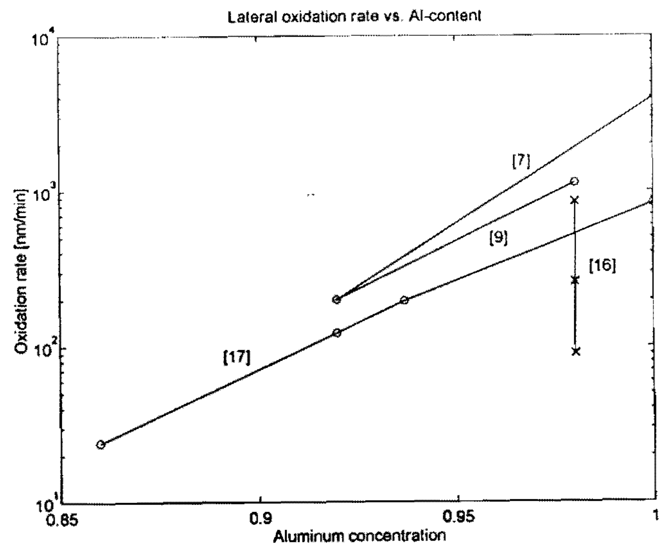

Figure 2.7: lateral oxidation rate vs Al-content

2.6.3 Crystallographic preference

During the first processing of VCSELs, containing AlAs-oxide current confinement layers, Huffaker et al. [20] observed a crystallographic preference for the oxidation process: during the lateral oxidation of circular mesas a square pattern appeared, showing that the oxidation rate was enhanced toward special directions. Huffaker ascribed this crystallographic preference to the graded superlattice layers grown during MBE between AlAs and GaAs and stated that this effect would disappear for the lateral oxidation of DBRs with abrupt interfaces.

Such statement has been verified by the oxidation of sample W872L99_B (n°15) shown in fig.4.7.3: the circular patterns around the oval defects indicate a complete oxidation of all the four AlAs-layers in the abrupt AlAs/GaAs multilayer and show a perfectly isotropic oxidation.

2.6.4 Doping type and level

An interesting but not fully established phenomenon is the effect of doping on the oxidation rate. Kish et al. [13] stated that the doping level only affects the oxidation rate and not the composition or the structure of the oxide; they conclude that this variation is due to a difference in the position of the Fermi level, and is not a specific property of the dopants themselves. Kish et al. believed that during the oxidation process the species diffused in the oxide through the crystal defects; hence the oxidation rate would be enhanced for larger concentration of defects, which is known to be a strong function of the position of the Fermi level in the crystal.

Although Kish rejected the influence of the doping species, Bun Lee et al. [21] attributed the enhanced oxidation rate to the type of doping species and noticed how this effect was most enhanced using carbon impurities as dopants. However the dependence of the oxidation rate on doping-type is not seen for higher Al-content compound [22]

2.6.5 Heterointerface structure

Kim et al. [17] investigated the effect of the AlAs/GaAs interface structure structure on the lateral oxidation rate. They observed that the oxidation rate of AlAs-layers in AlAs/GaAs multilayers is lower when 100Å-thin $Al_{0.72}Ga_{0.28}As$-layers are placed on both sides of AlAs compared to the case when abrupt interfaces between AlAs and GaAs are allowed. Kim ascribed this reduction in oxidation rate to a reduced stress due to the thin interface between the unaffected GaAs and the transforming and contracting Al-oxide. As a result the forming of canals would be disrupted leading to a reduction of water vapor supply and hence of oxidation rate.

Kim et al. also examined the influence of AlAs-layer thickness on the lateral oxidation rate: they found a very strong dependence for thicknesses less than 80 nm. For smaller thicknesses the rate decreases significantly, where for thicker layers the oxidation rate saturates; oxidation was completely prevented with AlAs-layers thinner than 11 nm.

CHAPTER 3

Manufacturing Process

3.1 Introduction

In order to carry out the selective wet oxidation of AlAs/GaAs multilayers, AlAs layers have to be exposed to a water vapour flow at 400°C. Stripe mesas were patterned through DBR structures in several samples by two different techniques: dry etching and wet etching.

For all of the dry etched samples (10 of 18) the TUE-VCSEL procedure, from step 1.1 to step 1.8, has been followed. See appendix C.2 for a detailed description of the processing. For the remaining samples a wet etching was performed following the procedure in appendix C.3.

Since a sharp difference was noticed between dry or wet etched mesas during wet oxidation of AlAs-layers a detailed description of these two processes is presented in the following paragraphs. The complete list of all the samples processed and their structure are shown in appendix A and appendix B respectively.

3.2 Wet chemical process

The native oxide layer on the surface of each sample is removed by rinsing in an ammonia solution NH_4OH:H_2O (1:10) for one minute followed by a further rinsing in acetone and isopropanol for two minutes each.

The used photoresist is the commercial AZ1505; the resist layer with a convenient thickness is obtained by spinning at 3000 rpm for 30 seconds. After the bake step (5 min @ 95°C) the sample with a hardened resist layer is ready for exposure. The light field mask containing stripe patterns is placed parallel to the longest cleaved edge, upon the sample with a Karl Züss mask aligner. Because the photoresist layer is thicker at the edges of the sample, there is no good conctact between the sample and the mask during exposure causing the geometry transferred to the sample to be larger than the mask geometry. To avoid this, resist on the sample's edges should be removed before aligning. Although our samples were usually small, the width of the stripe mesas (from 4 to 50 μm) was rarely critical and this procedure was not performed.

After exposure for 4 seconds (λ=0.4 μm) and developing in a (1:1) solution of positive photoresist developer (DE014) and water the sample is rinsed in deionized water for several minutes and then spinned dry. A hard bake of 10 minutes at 110°C prepares the sample for etching.

Wet chemical etching is done in a solution of phosphoric acid, hydrogen peroxide and methanol, H_3PO_4:H_2O_2:CH_3OH (1:1:3) at 0°C keeping the sample up side down in the non-stirred solution. By visual inspection it is possible to see when the top DBR in the sample has been etched: due to the different refractive index of GaAs and AlAs the surface of the sample will be of two different color as the etching proceeds through the stack of the DBR.

The etching rates measured by an alpha-step profiler for all the processed samples are shown in table III.1

Sample	**Wet etching rates [μm/min]**
W839L60	0.28
W516L34_a	0.24
W404L22_a	first mesa > 0.24 second mesa 0.27
W404L22_D	0.27
W404L22_E (*)	0.17
W404L22_F	0.23
W872L99_E	0.21

Tab. III.1: wet etching in H_3PO_4:H_2O_2:CH_3OH (1:1:3) @ 0°C
(*)The slow rate observed in sample W404L22_E was due to a more diluted solution.

After rinsing in deionized water, to remove the sticky etchant, the sample is then ready for the oxidation process.

Wet etching is not ideal for producing small devices because, although the sidewalls of the structure will be smooth, the underetch is always of the same order as the etching depth. A dry process will cause almost no underetching but the etched sidewalls will be rough. A wet etching and a dry etching profile are shown in fig. 3.1 and fig. 3.2 respectively. The SEM pictures show that the wet etching rates for AlAs and GaAs (dark and light layers, respectively) are not the same.

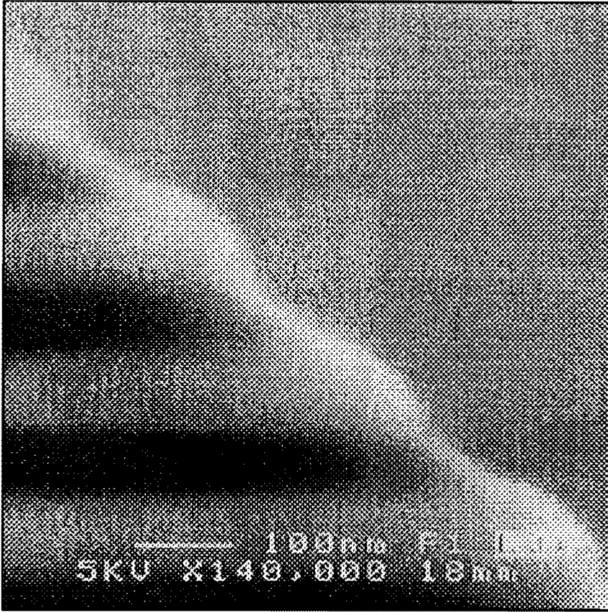

Figure 3.1: wet etching profile
etching rate for AlAs layers (black) is higher
than for GaAs layers (white)

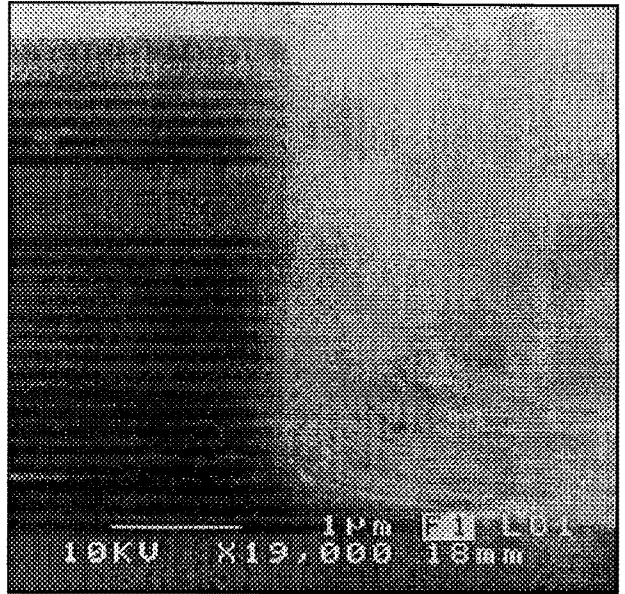

Figure 3.2: dry etching profile
vertical and rough sidewall
(on top of the mesa the SiN mask is present)

3.3 Dry process

Reactive ion etching is performed by the Electronic Device Group at T.U.E. with an Oxford Plasma Technology cluster tool. The detailed steps for the dry etching process used during the TUE-VCSEL fabrication are shown in appendix C.2.

For dry etching the cleaning procedure of the sample is the same as for wet etching; the definition of stripe geometry has to be performed with a dielectric mask since photoresist is not resistive enough to plasma damage. A Si_3N_4 layer, 300-nm thick, is deposited by PECVD and then patterned by using hard-baked photoresist as a mask and SF_6 and Ar as the etchants. Removing of the resist mask is accomplished by spraying acetone upon the sample but, in order to remove completely traces of organic material still present on the surface, a plasma etching with O_2 is necessary.

The sample is now ready for the etching; a non selective plasma reaction ion etching for AlAs and GaAs is used, based on $SiCl_4$ and Ar. Since uniform oxidation was not obtained after this process a general overview about plasma processing and about the RIE process in particular is presented in the next paragraph.

The etching rates estimated by an alpha step profiler during the monitoring of the process are shown in tab. III.2.

TAB III.2: Dry etching with Oxford 100 (non selective etching of GaAs and AlAs)

Name	**Size [cm x cm]**	**SiN mask thickness [nm]**	**Tencor after etching [μm]**	**Tencor after removing of SiN mask [μm]**	**Etching time**	**Dry etching rate [nm/min]**	**Etching rate of SiN [nm/min]**
W839L60_1	1.3 x 0.8	300 (assumption)	2.575 2.555 2.570 2.575	2.490 2.475 2.495 2.500	39' 41"	**62.7 ± 0.3**	5.5
W839L60_2	0.9 x 0.95	326 293 265 230	2.263 2.225 2.235 2.215		34'	**63.1 ± 0.8**	(1)
W404L22_b	0.73 x 0.98	330 -	I) 0.845 II) 2.090		19' 46' 36"	**44.5** **44.9**	3.3
W404L22_c	0.88 x 0.75	320 305	4.015 4.010		85'	**46.8** **46.9**	(2)
W4022_G	0.8 x 1	280	3.800 4.045		85'	**46.2 ±1.5**	(2)
W872L99_A					18' 20''	**40**	(2)
W495L33_A					27'	**138 (*)**	
W872L99_B	0.8 x 1.4				15'	**60**	2.97
W872L99_C	0.9 x 0.99					**55.5 ± 0.7**	3.17 ± 0.17
W872L99_D	1 x 1.4				15'	**224 (*)**	

(*) without sacrificial wafer
(1) assumption: SiN etching rate during the dry etching = 5.5 nm/min
(2) assumption: SiN etching rate during the dry etching = 3.3 nm/min
I) first mesa
II) second mesa

The wet oxidation of the AlAs layers has to be performed just after the etching: since the AlAs layers will be exposed to air, oxidation from the atmosphere can prevent the subsequent wet oxidation which results in an irregular profile of the oxidized layers.

The wet oxidation set-up is described in paragraph 4.1.

After oxidation the samples were examined by optical inspection and, after cleaving with a Loomis scriber, by SEM inspection.

3.4 Plasma etching theory

Plasma etching techniques are nowadays in wide use for the fabrication of optoelectronic devices due to excellent properties of anisotropy and selectivity.

Among the different types of dry etching developed at present we will focus on reactive ion etching (RIE) since this is one of the steps during the TUE-VCSEL fabrication. See appendix C.2 step 1.8 for an overview of the parameters.

Four main stages of this process can be recognized:

1. generation of Ar^+ ions and other reactive species (the ionization products of $SiCl_4$)
2. collimation/diffusion of ions to the surface of the sample
3. erosion of the material by ion bombardment and chemical reaction
4. discharge of the reaction products

It is well established that the RIE mechanism is partially chemical and partially physical (based on ion bombardment) but how the process in detail works and which mechanism is responsible for a high degree of anisotropy is still not clear.

According to recent developments in plasma processing for III-V compounds [24] two models have been proposed and are shown in fig.3.3 and fig.3.4

A **surface damaged induced anisotropy**

this model states that ion bombardment perpendicular to the sample breaks the bonds in the surface layer to make molecules ready to react with the chemical species in the plasma and to form volatile species. Since the wall of the etched structure is not bombarded, no chemical reaction take place there.

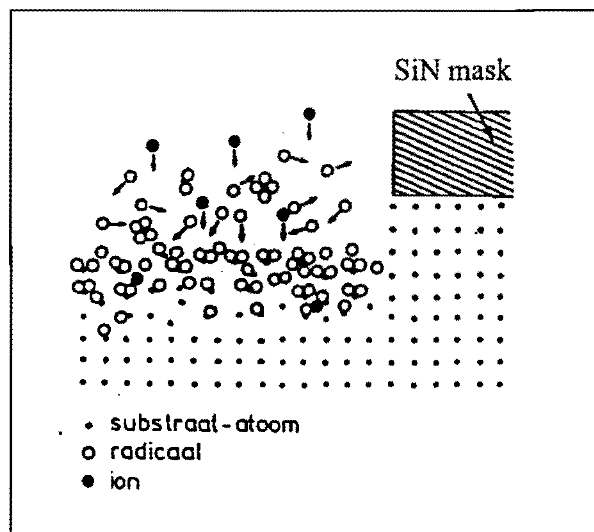

Fig.3.3: surface damaged induced anisotropy

B **surface inhibitors induced anisotropy**

this model states that chemical species react with the surface and form non-volatile products that will passivate the surface; on the areas bombarded, the passivating molecules are removed so the chemical reaction can continue.

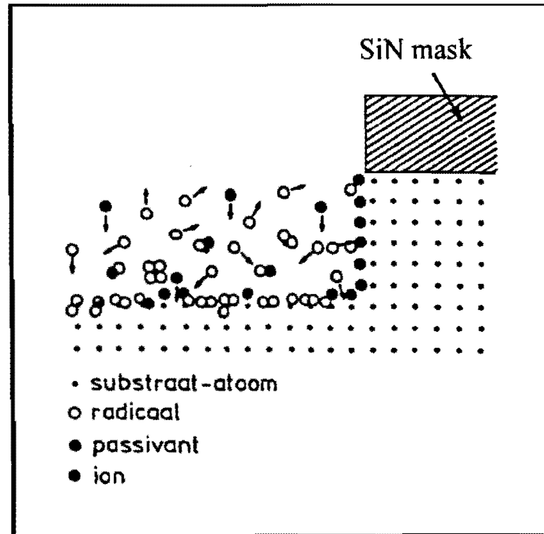

Fig.3.4: surface inhibitors induced anisotropy

The real mechanism will be in between both models depending on the etching parameters.

CHAPTER 4

Wet Selective Oxidation (experimental overview)

Introduction

Although wet selective oxidation, used in the fabrication of AlGaAs-based devices, is becoming an important technological step during the fabrication of new opto-electronic devices, its application is still nearly empirical.

The mechanism and the exact reactions that occur during the phase transformation of $Al_xGa_{1-x}As$ into γ-Al_2O_3 are in fact not well understood and many aspects of this process are still not under control.

In the framework of a general effort by several laboratories of research to improve the knowledge on wet oxidation we present in this section a review of all the observations carried out during this project.

Wet selective oxidation of several samples containing multilayers AlAs/$Al_xGa_{1-x}As$ (x varying from 0 to 0.8) was performed. Due to the scarcity of new grown material (the MBE facilities were in a tormented period of maintenance during this project) and to the questionable quality of some of the samples (we used old VCSEL material that was unsuitable for lasing operation) an exhaustive study on wet oxidation was not possible.

In spite of this, the contents of this work, comments and explanations about the oxidation process, will be usefull for future device developments, when new wafers, with low density of defects, will be available.

4.1 Experimental set up for wet oxidation

Wet oxidation is apparently a simple process; according to the theoretical reaction:

$$AlAs_{(s)} + H_2O_{(v)} \rightarrow Al_2O_{3\,(s)} + AsH_{3\,(v)}$$

water vapor has to be supplied to and arsine formed has to be removed from a sample at about 400°C.

To accomplish these requirements oxidation of AlAs layers was carried out in a 8-cm-diameter quartz tube placed inside a single-zone furnace with a variable temperature from 400°C to 450°C. A scheme of the set-up is shown in fig. 4.1.1.

The carrier gas is nitrogen and it feeds into a glass bubbler filled with deionized water at a flow rate of 0.5 l/min. The water in the bubbler is maintained at 95°C by manually adjustment of an electrical heater.

Samples are inserted and retracted from the hot furnace on a quartz slider with a ceramic push rod from one of the extremities of the quartz tube. This end of the tube is capped by a glass cover except for an exhaust line that takes away the poisonous arsine. To prevent condensation, the bubbler has been placed as closed as possible to the oven and the line between them has been isolated.

An aluminum hindrance has been inserted into the furnace in order to reduce the inner cross-section of the quartz tube in proximity of the sample from about 60 cm^2 to 6 cm^2. The water vapor was therefore forced to flow close to the sample with an increased velocity, about ten times greater (in literature flow rate greater than 0.5 l/min are used). Although this new configuration would prevent the flow to be laminar, uniform oxidations were still achieved and no differences in the oxidation rate were recorded.

An inclination of the sample to the incoming flow was also investigated; results of these different configurations are discussed in paragraph 4.2.

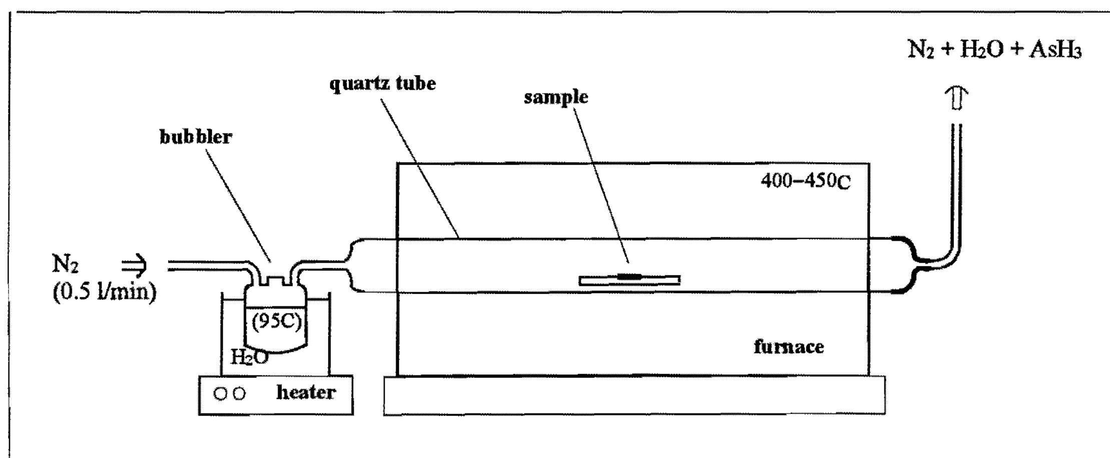

Fig.4.1.1: set-up for wet oxidation (old configuration)

Since the wet selective oxidation is still a non-uniform process it is desired to follow this process visually, therefore a special quartz-glass furnace is designed and is being fabricated.

A set-up of the new oxidation process is drawn in figure 4.1.2. During oxidation valve 1 is closed and valve 2 is opened. The N_2 bubbles at a flow rate of 0.6 l/min through the ionized water, which is indirectly heated to a temperature of about 95°C. The saturated water vapor is directed to the quartz glass furnace via heated supply lines to prevent condensation. The sample, heated to 400°C and exposed to this water vapor is oxidized which can be followed by the optical microscopy. The waste products are transported to a scrubber, which takes care of possible poisonous gases such as AsH_3.

The loading, heating and unloading of the sample can be done under pure N_2-flow, which is achieved by closing valve 2 and opening valve 1. This procedure would allow a better specification of the start of oxidation.

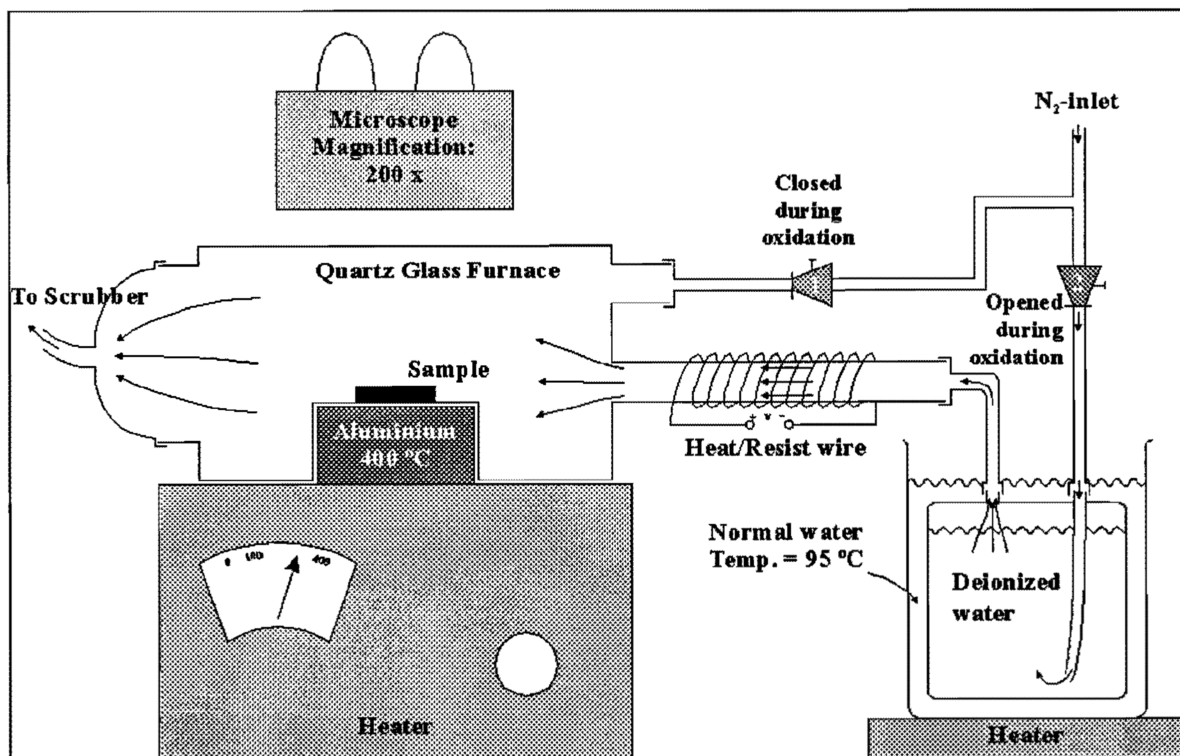

Figure 4.1.2: set-up for wet oxidation (new configuration)

4.2 Uniformity of wet oxidation

Results and general observations linked to the state-of-the-art in literature about wet selective oxidation of III-V compounds are shown in this section.
The first goal of this project was the achievement of uniform oxidation in order to obtain a reliable current constriction technique during the VCSEL processing (see appendix C.1, step g)
Stripe mesas containing DBRs with AlAs-layers to be laterally oxidized were etched and placed into a furnace at 400°C under a water vapor flow.
Two types of uniformity must be checked after oxidation:

1. **planar (or lateral) uniformity**: it means that the front of oxidation stays parallel to the sidewalls of the mesa during its growth;

2. **vertical uniformity**: it means that all the AlAs-layers in a DBR stack are oxidized to the same extension.

The former is checked by mere optical inspection just after oxidation: since AlO_x has a different refractive index (about 1.55) than AlAs, oxidized layers will be of a different color.
Verifying the vertical uniformity requires a sight into the structure; therefore after cleaving the stripes, only the SEM inspection can reveal if the lateral extension of the oxidation was uniform over all the AlAs-layers.
An example of planar uniformity and non-uniformity is shown in fig.4.2.1 and 4.2.2 respectively; they are the optical pictures of two 50μm-wide mesas oxidized with a different orientation to the incoming flow. Few oval defects can also be seen on the top of the samples (see paragraph 4.7.2). An example of vertical uniformity is depicted in fig. 4.2.4 and fig. 4.2.5.

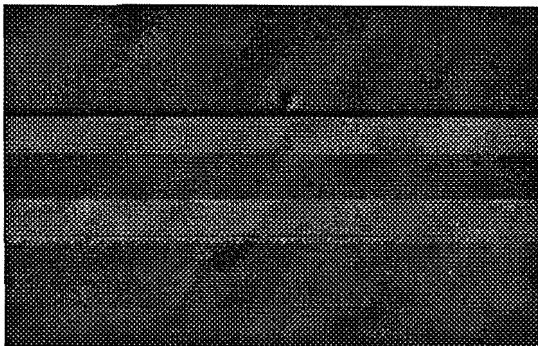

Figure 4.2.1: stripes parallel to N_2-flow

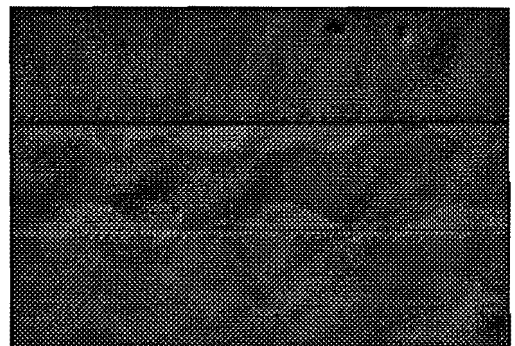

Figure 4.2.2: stripes perpendicular to flow

The final result of this research was that good uniformity (even higher than 3%) is achievable if the patterning of the mesas has been accomplished by wet etching while irregular profiles are obtained from dry etched samples.
The reasons for a large distribution in oxidation length has also been reported by other authors [10] and has not been identified yet.

Possible reasons for a non uniform oxidation are listed below; items D (with dry-etched mesas), E, F and H are related to the vertical uniformity; item G to planar uniformity; item B to both of them. Items A, C and D (with wet-etched mesas) will cause a general decreasing in oxidation rate over all the sample, but their influence on planar or vertical uniformity is still not clear.

A. **carrier gas not saturated with water vapor**;
the supply of water to the forming oxide can be interrupted if condensation occurs between the bubbler and the sample (see scheme in fig. 4.1.1). Heating of the supply line is therefore advisable.
The level of water vapor into the bubbler seems to influence [15] the amount of water vapor transferred to the furnace and therefore each oxidation should start with the same level of water. The temperature of the water in the bubbler is not critical and was constantly settled at 95°C.

B. **turbulent flow;**
turbulent condition in proximity of the sample is also a reasonable cause for a non uniform oxidation. We investigate such behavior by simultaneous oxidation of two samples with different orientation of the stripes to the incoming gas. Results are shown in appendix A (sample n°1).
Uniformity with stripes perpendicular to the flow was poor, probably due to a lack of water vapor carried by a turbulent flow of N_2 to random places on the sidewall. The gas flow in proximity of the sample when the stripes are parallel to the flow is laminar and the supply of water to the growing oxidation front results more regular. See figure 4.2.1 and 4.2.2.
Other test were carried out with the sample forming an angle of 20° to the quartz holder: no changes in oxidation uniformity were observed showing that the flow remains laminar. Later on all the oxidation tests were carried out without any inclination of the stripes.

C. **carrier gas speed**;
supply of water is also influenced by the flow of the carrier gas.
At temperatures of 400°-450°C the oxidation rate was found [15] independent from the gas flow for values in the range 1÷2 l/min; for higher temperature (480°C) the oxidation rate was not saturated. From this study it could be inferred that a limited supply of the oxidizing agent will occur if the flow is too high or too low.

Since the first experiments were carried out with a flow rate of 0.5 l/min and turned out in very irregular oxidation, we increased the gas velocity in proximity of the sample by inserting an aluminum hindrance into the furnace. Although this would prevent the flow to be laminar (higher values of mean velocities give a higher Reynold's number) uniform oxidation was still achieved.

D. **room ambient oxidation of AlAs**;
between the etching of the mesas and the wet oxidation, oxidation from the atmosphere will occur due to hydrolysis, see [1,2,4], and a very thin oxide layer will be formed covering the sidewalls.
If the mesa has been etched by a dry-process this oxidized layer will not be uniform due to the rough sidewalls and the contamination on it. See paragraph 3.4 (B). During the loading into the furnace the sample will stay for a few seconds at 400°C causing the oxide to densify [23] and prevent water vapor from penetrating and oxidizing the AlAs-layers; this will obviously prevent the oxidation profile to be vertically uniform.
If the mesa was etched by a wet-process the sidewalls will have a smoother surface and hence the room-ambient oxidized layer due to the unavoidable hydrolization will be more uniform. Oxidation from the atmosphere could hence explain the difference in oxidation uniformity noticed between dry or wet etched mesas, and will act together with the mechanism discussed in paragraph 4.2.2.

E. **stress relaxation**;
according to recent TEM inspection [8,9] canals and voids are believed to originate at the interface semiconductor/oxide due to the shrinkage of the forming oxide during lateral oxidation. Since these stress-relaxation phenomena could occur with different intensity through different AlAs-layers, oxidation rate will increase in those layers where wide canals had been formed.

F. **profile of mesas**;
the profile of the sidewall is also responsible for a non uniform profile of oxidation; larger surface exposed to oxidation will improve the amount of water vapor oxidizing the AlAs-layer and therefore the oxidation rate.
This effect is drafted in fig.4.2.3 and clearly shown in fig.4.2.6

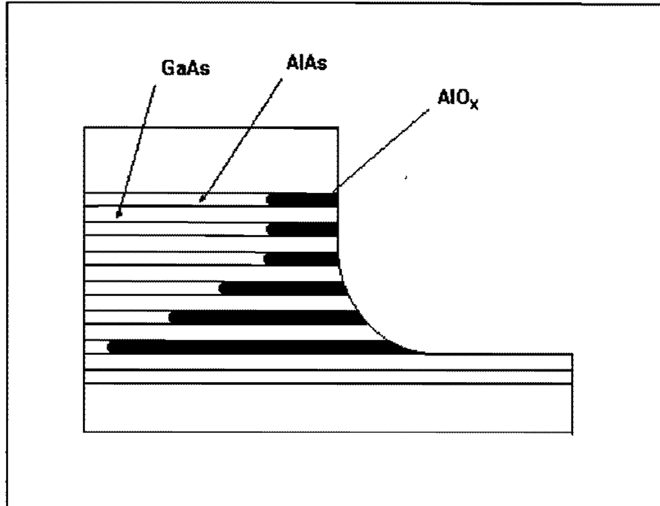

Figure 4.2.3: vertical non-uniformity due to the mesa's profile

G. **growth defects**;

Oval defects originating during crystal growth have been proved to increase the oxidation rate by a factor of about three depending on the size. With these problems we were concerned during the realisation of a visible light DBR

H **doping level and type**

AlAs-layers with different doping type and level will be oxidized at different rate causing the oxidation profile to be non vertically uniform (see paragraph 2.6.4).

In order to verify this effect sample n°10 (see Appendix A) was wet etched and wet oxidized; The top DBR AlAs-layers shown in fig.4.2.4 were p-doped ($2\ 10^{18}$ cm^{-3}) while the bottom DBR AlAs layers were n-doped ($5\ 10^{17}$ cm^{-3}).

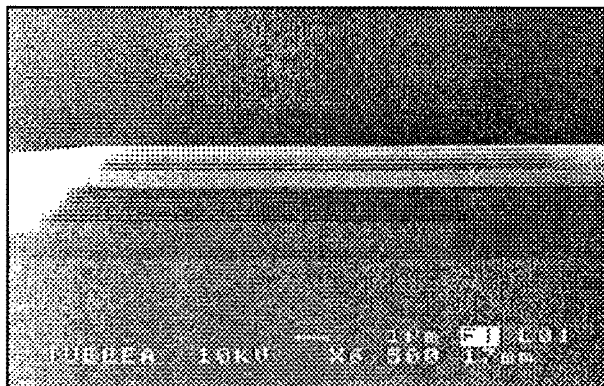

Fig.4.2.4: sample n°10
wet etched mesa, partially and laterally oxidized for 7 min.
(top DBR: p-doped; bottom DBR: n-doped)

Good vertical uniformity was achieved for both the p-doped and the n-doped layers. According to Kish et al. [13] oxidation rate for p-doped AlGaAs should be greater than for n-doped AlGaAs. Although in fig.4.2.4 a slight difference in oxidation rates can be inferred (2.7 μm/min for p-doping; 2.5 μm/min for n-doping), these effect was not observed for all the stripes of the sample. Therefore the dependence of oxidation rate on doping was not verified. Also in literature [22] this dependence was not seen for high Al-content AlGaAs compounds.

Due to the linking of these different mechanisms (most of them are believed to act at the same time during the oxidation) it is difficult to separate each contributions. This seems to be the main reason that has limited until now a full understanding of the oxidation process.

4.2.1 Oxidation of wet etched mesas

Uniform oxidation, both planar and vertical, was achieved with wet etched samples.
In fig.4.2.5 an example of a regular oxidation profile is shown.

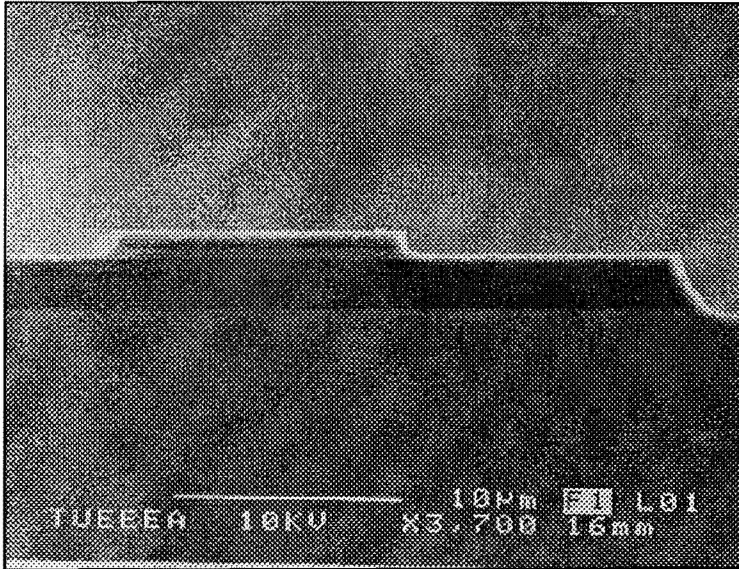

Fig.4.2.5: double mesa wet etched (sample n°6)
top DBR: completely oxidized
bottom DBR: partially oxidized

A top mesa (16-µm wide) containing a 5 pair AlAs/GaAs DBR has been defined over a bottom mesa containing a 15.5 AlAs/GaAs DBR by wet chemical etching in H_3PO_4:H_2O_2:H_2O (1:1:3) at 0°C. The sample was then oxidized for 7 min. @ 400°C .
The top DBR was over-oxidized while the bottom DBR was partially oxidized to an extension of 14 µm. The profile of oxidation nicely correlates with the mesa edge showing an oxidation rate of 2 µm/min.
This test was carried out in order to show the feasibility of a simultaneous oxidation of a top DBR and a current constriction layer (here replaced by the bottom DBR).
This experiment (the oxidation was uniform over all of the stripes of the sample) showed how the fabrication of an oxide/semiconductor DBR and the definition of a current constriction structure could be achieved by a single oxidation step when the VCSEL is fabricated with help of wet etched mesas.

4.2.2 Oxidation of dry etched mesas

With a dry process the good lateral uniformity obtained with a wet process (see figure 4.2.5) could not be reproduced.
The same double mesa structure described in the previous paragraph was patterned by two dry etching steps and oxidized at 400°C for 6 minutes (see appendix A, sample n°7).
The simultaneous and selective oxidation should have caused a complete oxidation of the AlAs-layers in the top DBR (16–μm wide stripes) and the partial oxidation of AlAs-layers in the top DBR (30–μm wide stripes) and in the bottom DBR (50–μm wide stripes).
The oxidation profile of this structure after cleavage is shown in fig.4.2.6

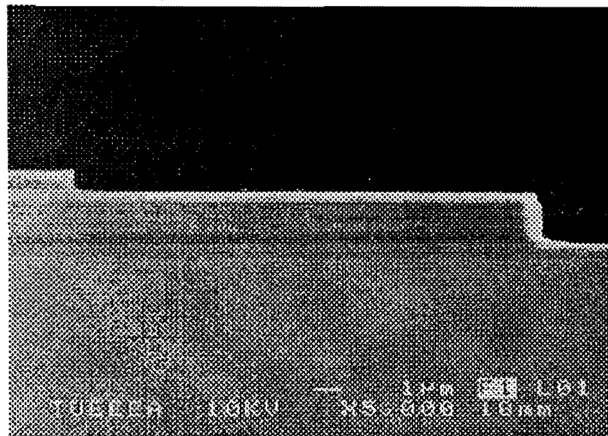

Fig.4.2.6: double mesa dry etched (sample n°7)
(the profile of the sidewall affects the oxidation rate)

The SEM inspection revealed a complete oxidation of the top DBR in all of the stripes and a non uniform vertical oxidation in the bottom DBR.
Planar uniformity was achieved because the profile shown in figure 4.2.6 was similar in all of the stripes. We make the following remarks about the shape of the oxidation profile:

- due to oblique slope of the etch profile at the bottom of the large mesa more water vapor can reach the oxidation front and therefore the oxidation rate will increase (about 3.3 μm/min)

- oxidation rate for the upper layers of bottom DBR is 0.6 μm/min with poor accuracy

- oxidation rate for top DBR was greater than 2.5 μm/min

In order to investigate the effects a plasma etching has on the oxidation profile the same structure was etched through both top and bottom DBR and partially wet oxidized.
The result is shown in fig.4.2.7

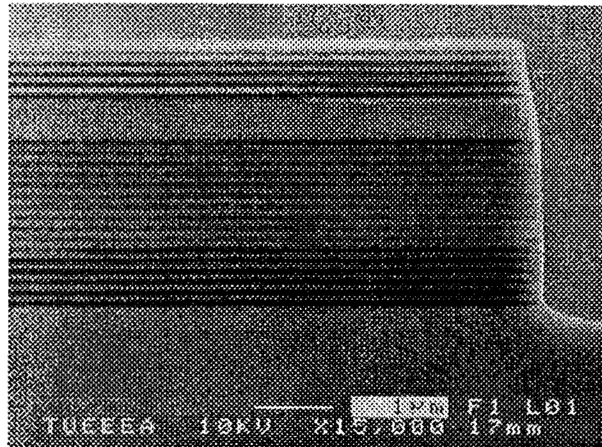

Fig.4.2.7: sample n°8
Dry etched mesa
inhibited oxidation due to contaminants on the sidewall
(the Si_3N_4 mask on top of the mesa is completely eroded)

AlAs-layers in the top DBR were oxidized at a rate of 3 µm/min while for the last six layers in the bottom DBR the rate was 2.8 µm/min. The first ten layers of bottom DBR were not oxidized at all.
This unexpected phenomenon was also observed by F. de Bruyn, a graduated student engaged with sealing problems during the VCSEL processing. The state-of-the-art literature does not give answer for this topic.
Nevertheless according to recent theories about plasma etching and the shape of the sidewalls of fig.4.2.7 some few considerations are possible.
Assuming the second model described in paragraph 3.4 (surface inhibitor induced anisotropy) to be the anisotropy mechanism of the etching during the TUE-VCSEL processing, the inhibition of oxidation would be explained by the formation of a thick passivating layer along the sidewall of the mesa.
This layer will have a thickness according to the time of permanence in the aggressive plasma ambient and there will be a threshold value of etching time (read thickness of passivation layer) after which a thick diffusion-limiting layer is formed. This threshold value is about 15-20 minutes for both the etching shown in fig.4.2.6 and 4.2.7.
The unaffected oxidation rate reported in the top DBR of fig.4.2.7 (the first exposed AlAs-layer stays in the plasma for nearly 85 min, the total length of the etching) is explained by the erosion of the Si_3N_4 mask.
During the plasma etching the mask is invariably eroded at a slow rate that we estimated 3.3 nm/min (see Tab III.2). Since the mask is usually thinner at the boundary of the stripes, the mask slowly erodes as etching proceeds; therefore in the middle of the stripe the SiN mask will be enough (300 nm) thick to prevent the etching of the underlying GaAs, but at the edges the GaAs will be exposed to ion bombardment and the etching will remove the passivation layer. In fig.4.2.8 a scheme of this mechanism is shown. The profile of fig.4.2.7 confirms this theory.

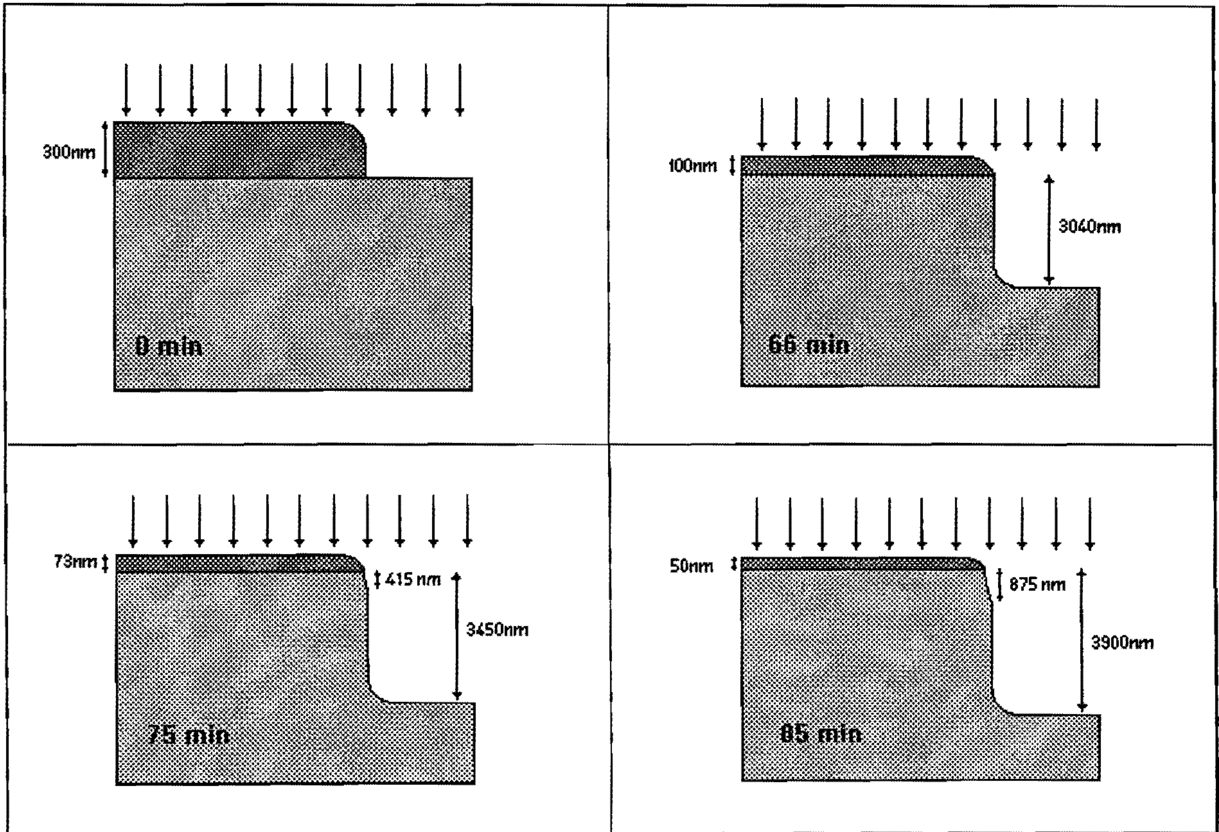

Figure 4.2.8: etching scheme

Assumptions: AlGaAs etching rate = 47 nm/min
Si_3N_4 etching rate = 3.3 nm/min
(data from Table III.2 sample W404L22_C)

Other tests were carried out with long etching times (more than 1 hour): the same etching profile and similar sharp transition between normally oxidized (2μm/min) and inhibited layers in the middle of the bottom DBR were found.
In fig.4.2.9 the threshold value over which oxidation is prevented is about 25 minutes but the transition is less sharp than in fig.4.2.7.

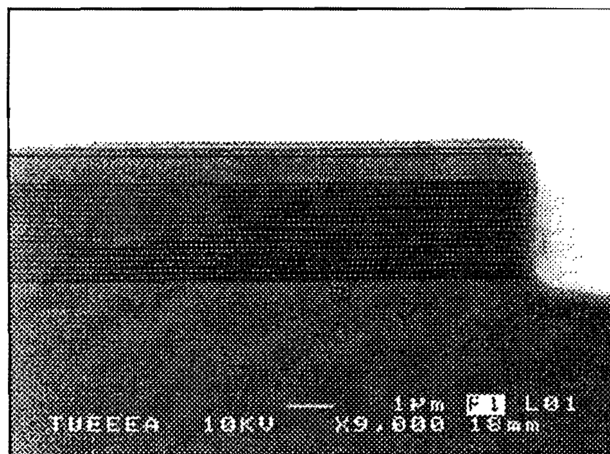
Fig.4.2.9: sample n°12

We suggest two ways to avoid the problems a dry etching causes on the subsequent wet oxidation process:

- **adjustment of dry etching parameters**

  In order to avoid the formation of a passivation layer some of the etching parameters should be changed. A decrease of pressure or frequency will increase the flow rate and the average energy of bombarding ions; this will promote the mechanism shown in fig.3.3 (surface damaged induced anisotropy) and therefore no passivation layer will be formed [25]. Increasing the mean power also modifies the ion energy but in the same time the density of the reactant species and therefore the formation of sticky compounds will be greater.

- **removal of passivation layer by means of a wet chemical etching**

  Since the wet etching has been proven to give an uniform profile of oxidation, a further step could be added after the dry etching in order to remove any compounds adsorbed on the sidewalls.

Both of these solutions will decrease the anisotropy of the etching and therefore a compromise between underetching and cleaning of the sidewalls has to be found.
We investigate the feasibility of a wet etching step to prepare the sidewalls for subsequent oxidation by a dip into a diluted solution NH_4OH:H_2O_2:H_2O (1:2:50) at room temperature for 10 seconds. Since the etching rate of this solution for AlGaAs is 40 Å/sec, this procedure works more as a cleaning step than as a real etching step, leaving the sidewalls of the mesa perpendicular and therefore the anisotropy of the plasma etching will not be losen.
The oxidation profile turned out to be more gradual, without the sharp transition between oxidized and non-oxidized layers, but top layers were still less oxidized than bottom ones.
We did not investigate further this procedure because higher times or higher concentrations would eliminate the benefits of a dry procedure.

4.3 Thermal stability of $Al_xGa_{1-x}As/Al_2O_3$ multilayers

4.3.1 Introduction

A rapid thermal annealing process (R.T.A) consists in the rapid exposure of a sample to high temperature in vacuum or gaseous ambient.
In the process layout for VCSELs fabricated at the Eindhoven University of Technology (TUE-VCSEL) two of these processes are used: the first one (10 min @ 450°C in Ar) is used to anneal the Si_3N_4 passivation layer which separates the p-contact pad from the n-doped GaAs contact layer; the second one (1 min @ 400°C in N_2) is used to anneal the n-metallisation to obtain ohmic contacts and reduce the series resistance (see appendix C.2, step 4.3 and 6.3).
In order to realize visible light emitting VCSELs the fabrication of a semiconductor-oxide Distributed Bragg Reflector (DBR) may be required. Therefore the thermal stability of such multilayers to the necessary annealing process has to be proved.
This section is intended to describe some experimental results about the subject and show how the mechanical stability of stripes containing completely oxidized DBRs has been proven to depend upon the time of the wet oxidation.
A list of all the samples which have been subjected to a RTA process is shown in Tab.IV.1.

4.3.2 First results

The first RTA-test was carried out with sample W839L60 at 450°C for 10 minutes and gave discouraging results: 30-μm stripes containing a top DBR $Al_{0.2}Ga_{0.8}As/AlO_x$ showed a complete de-adhesion between the oxide and semiconductor layers (see fig. 4.3.1).

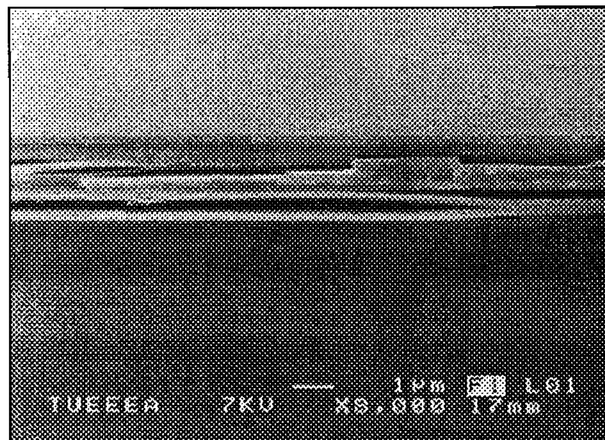

Fig: 4.3.1: sample n°1
abrupt $Al_{0.2}Ga_{0.8}As/AlO_x$ DBR after RTA (10'@450°C)

n°	Sample	Structure	Process	Wet oxidation	R.T.A.	Remarks
1	W839L60_2a2	$AlAs/Al_{0.2}Ga_{0.8}As$ (x 16)	30-µm stripes dry etched	14' @ 400°C	10' @ 450°C in Ar	complete delamination
2	W839L60_2b2	same as sample n°1	same as sample n°1	14' @ 400°C	10' @ 400°C in Ar	slight improvements
3	W516L34_a	AlAs/GaAs (x 9.5) (graded linear interfaces)	same as sample n°1	15' @ 400°C	1' @ 400°C in Ar	unaffected
4	W404L22_a	AlAs/GaAs x 9.5 (top) x 15.5(bottom) (graded linear interfaces)	16-µm stripes wet etched through the top DBR 50-µm stripes wet etched through the bottom DBR	7' @ 400°C	5' @ 400°C in Ar 10' @ 450°C in Ar	unaffected delamination
5	W404L22_b	same as sample n°4	16-µm stripes dry etched through the top DBR 50-µm stripes dry etched through the bottom DBR	6' @ 400°C	1' @ 420°C in Ar	unaffected
6	W495133_a1	same as sample n°4	30-µm stripes dry etc. through top and bottom DBR	15' @ 450°C	10' @ 470°C in Ar	complete delamination
7	W495133_a2	same as sample n°4	same as sample n°6	60' @ 450°C	10' @ 470°C in Ar	unaffected

Tab IV.1: rapid thermal annealing of semiconductor/oxide DBRs

An example of an oxidized DBR which could withstand such an annealing was not found in literature. M.H. MacDougal et al. [26] anneal their VCSELs containing top and bottom AlO_x/GaAs DBR at 400°C for 20 s, while delamination was observed in a VCSELs containing partially oxidized AlAs layers and annealed at 350°C for 30 s [7].

Since lack of adhesion is due to different thermal expansion of AlGaAs and AlO_x (about 5.9 10^{-6} K^{-1} and 8 10^{-6} K^{-1} respectively)during the raising of the temperature we first tried to reduce the shear stress by decreasing the stable temperature from 450°C to 400°C and the temperature growth rate from 35°C/s to about 2°C/s.

Slight improvements were achieved though almost all of the stripes showed openings and cracks at the oxide/semiconductor interfaces. In fig. 4.2.2 is shown one of the stripes still present after cleavage for the SEM inspection. Voids or extended porosity, not present in the as-oxidized sample, seem to appear in the AlGaAs layers after annealing.

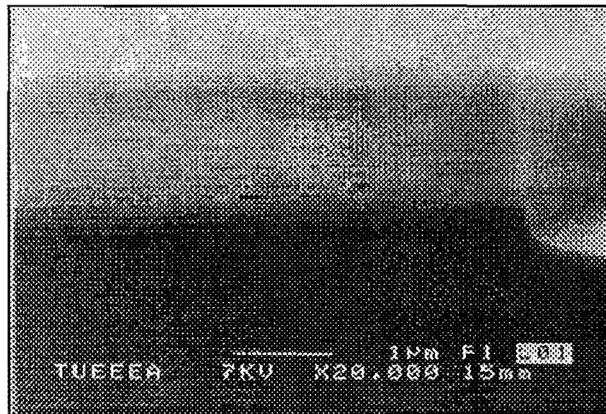

Fig. 4.3.2: sample n°2 RTA: 10' @ 400°C

4.3.3 Improvement in thermal stability

We suggest two methods to improve adhesion during a rapid thermal annealing process:

- use of graded interfaces between the DBR layers.
- over-oxidation

4.3.3.1 RTA of graded linear DBRs (AlO_x/GaAs)

The type of interface surrounding AlAs layers to be oxidized has been found [17] to influence the lateral oxidation rate: abrupt interfaces AlAs/GaAs show a relatively high oxidation rate due to transport canals formed at the oxide/semiconductor interface by the induced stress. On the other hand, the lateral oxidation rate was observed to decrease when

a 100Å thin $Al_{07}Ga_{0.3}As$ layer is added on both sides of the AlAs layer because the stress due to volumetric contraction of AlAs is less critical and the interfaces stronger.

During photoluminescence tests it was also found [27] that thin layers of $Al_{07}Ga_{0.3}As$ (300Å thick) between AlAs and GaAs allow the interface recombination to be lower, showing once again how the interface quality is improved when the AlAs to be oxidized is surrounded by very thin AlGaAs layers. J.A.Kash and at. also suggested that graded interfaces between the mirror layers of a DBR structure will play a similar role in preserving the low interface recombination at the GaAs/oxide interface.

We therefore decided to carry out RTA tests on completely oxidized DBRs with graded linear interfaces (158 Å thick). The samples (W516, W404 and W495) were old VCSEL material designed in order to reduce the electrical resistance of Bragg reflector and were grown by the MBE facilities in the Physics Department of the T.U.E.

The results are shown in Tab. IV.1 (samples 3,4 and 5); stripes containing the top DBRs completely wet oxidized were unaffected after RTA at a temperature higher than in the previous test, showing that the adhesion between AlO_x and GaAs is effectively enhanced by a non-abrupt interface.

4.3.3.2 Over-oxidation of AlAs layers in a DBR structure

Recently it has been found [28] that thermal stability of wet oxidized AlAs layers depends curiously on the length of time of oxidation.

Wet etched mesas (120μm x 300μm) containing a single AlAs layer (1000Å thick) surrounded by two linear graded regions (400 Å thick) were wet oxidized at 425°C in N_2/water mixture formed by bubbling N_2 in 90°C deionized water. The AlAs layer appears to be completely oxidized after 100 min. but the oxide is unstable and tends to crack during annealing.

The same wet oxidation process was carried out for 120 min. and the oxide was found to be very robust and more stable to temperature changes without cracking during the subsequent high temperature processes.

In order to check these statements we used an old VCSEL sample containing top (x 4.5) and bottom (x 15.5) DBRs AlAs/GaAs (677.6 Å /538 Å) with gradual compositional interfaces (158 Å thick).

See Tab. IV.1, samples n° 6 and n° 7, for a complete overview of the process; 30-μm wide stripes were dry etched through the top and bottom DBR; after cleaving in two pieces, we carried out a complete wet oxidation of all the stripes at 450°C for 15 min. (sample n°6) and 60 min. (sample n°7). The two samples were then put together into the rapid thermal annealer for 10 min at 470°C.

Differences between them by a simple optical inspection were evident: the over-oxidized sample appeared unaffected while the normal oxidized one showed lack of adhesion in all of the stripes, and particles due to completely delaminated DBR's were all over the surface.

In fig. 4.3.3 the two samples are shown.

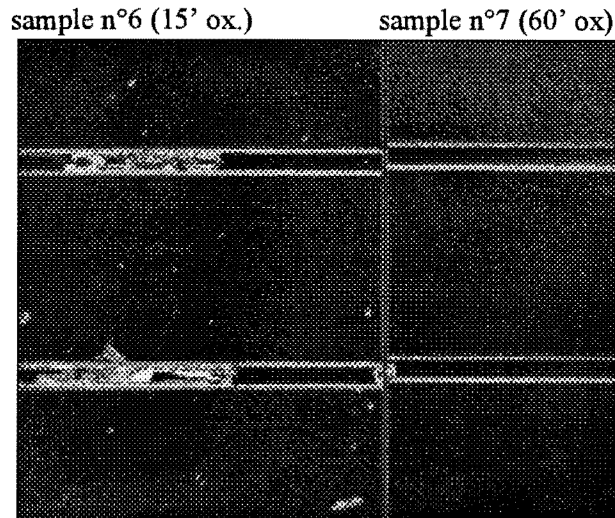

Figure 4.3.3: Top view of completely oxidized (left)
and over-oxidized (right) stripe mesas
containing sem/oxide DBR after RTA (10' @ 470°C)

Fig. 4.3.4 shows one of the over-oxidized stripes; although no lack of adhesion was found, a polycrystalline structure is evident in the GaAs layers (light layers on picture).

This anomalous behavior still remains unclear; nevertheless the same structure was found in other samples (wafer 872) oxidized for time as long as 60 min and T.Takamori [10] also observed oxidation of GaAs during wet oxidation of AlAs/GaAs multilayers at 450°C for 60 minutes.

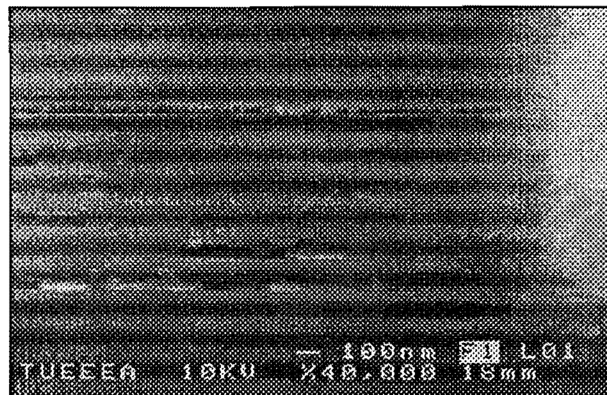

Figure 4.3.4: sample n°7

4.3.4 Conclusion

In order to verify the thermal stability of DBRs for visible light we made R.T.A. tests over a series of samples with different structures.

After proving how detrimental a thermal annealing could be for the adhesion of GaAs/AlO_x multilayers we verified two ways to improve their thermal stability.

- insertion of thin (about few nm) AlGaAs-layers between the AlAs and GaAs layers (see paragraph 4.3.3.1)
- extension of oxidation over the normal time required for a complete oxidation (see paragraph 4.3.3.2)

Nevertheless, due to lack of material (MBE system was particularly down in this period) other tests have to be done, in order to check:

1. the influence of interface on thermal stability (we think that even a few monolayers of AlGaAs could improve the adhesion between AlAs and GaAs after wet oxidation).
2. the oxidation time at which AlO_x/GaAs multilayers change abruptly their reaction after a RTA-process.

4.4 VERTICAL CONTRACTION OF WET OXIDIZED AlAs

4.4.1 Introduction

A completely wet oxidized AlAs layer should undergo a 50% volume contraction, according to the structural parameters of AlAs and γ-Al_2O_3 reported by Twesten et al. [9]. A shrinkage of this magnitude will induce considerable shear stress at the interfaces and will thereby affect the mechanical stability and optical properties in opto-electronic devices containing AlAs layers to be oxidized. Due to thermal annealing, or to mere aging of the structure, the induced stress can give rise to a complete delamination of polycrystalline oxide layers from the surrounding epitaxially grown material.

In spite of this, during phase transformation of AlAs into oxide, shrinkage along planar direction is prevented by the relatively strong adhesion to the surrounding layers; on the contrary, along the direction perpendicular to the layers (referred here also as vertical or growth direction) AlAs is relatively free to shrink.

In table IV.2 is shown, in chronological order, the exhaustive list of scientific publications about the shrinkage valuation of wet oxidized $Al_xGa_{1-x}As$ layers. Although the list is not complete or completely free from contradiction a mean value of 10% can be assumed for the vertical contraction. Such a small value, referred to the theoretical one, could be explained by a porous oxide present at the interfaces in the surroundings layers; porosity is also suggested by the linear kinetics, reaction limited, of the oxidation process [11].

Considering data from table IV.2 we can make the following remarks. Apparently inexplicable volume expansion observed by Tsang (1978) is certainly due to retention of As in form of As_2O_3; a mixture of 80% O_2 and 20% N_2 was in fact used and at 100°C arsenic oxide is not volatile. In subsequent experiments on wet oxidation, oxygen contamination was avoided and formation of As_2O_3 prevented; a depletion of As from the wet oxidized layers has been proved by several SIMS (secondary ion mass spectroscopy) studies [4,5,6], and all arsenic volatile reactants such as AsH_3 cause a moderate shrinkage of the structure.

Data recorded lately by optical methods and detailed TEM studies are more in agreement with a mean value of -10% but too parameters were varying, therefore is not possible to argue which one has induced this slight dispersion of data.

Year	Reference	Method	Material	Thickness	Structure	Wet ox. parameters	Shrinkage
1978	Tsang APL 33 (5) p.426	Talystep profiler	AlAs	300 Å ÷ 3000 Å	(v.o.)	80% O_2 + 20% N_2 + water vapor 15'÷ 60' @ 100°C	**volume expansion + 80 %**
1991	Sugg APL 58 (11)p.1199	TEM	AlAs	0.1 μm	(v. o.)	3h @ 400°C	**- (30÷40) %**
1994	MacDougal E.L. 30 (14) p.1147	matching with reflectivity spectrum	AlAs	1600 Å	(l.o.) DBR AlAS/GaAs (x3)	45' @ 425°C	**- 12.1 %**
1995	MacDougal PTL 7 (4) p.385	matching with ref. spectrum	AlAs	1330 Å	(l.o.) DBR AlAs/(GaAl)InP (x 4.5)	45' @ 425°C	**- (9 ÷ 12) %**
1996	Twesten APL 69 (1) p.15	TEM	$Al_{0.92}Ga_{0.08}As$ $Al_{0.98}Ga_{0.02}As$	840 Å	(l.o.) DBR AlAS/GaAs (x22) parabolic compositional grading single layer	40' @ 450°C	**- (6.7 ± 0.2) %** **≈ -5 %**
1996	Takamori APL 69 (5) p.659	H.R.TEM	AlAs	670 Å	(l.o.) AlAs/GaAs (x20)	1h @ 450°C	**- 15 %**

Tab. IV.2: shrinkage valuation in literature (l.o.:lateral oxidation; v.o.: vertical oxidation)

4.4.2 Shrinkage valuation

In order to fabricate a DBR mirror for visible light (λ=650nm)with alternate $Al_{0.5}Ga_{0.5}As/Al_2O_3$ layers the optical length in each layer must be designed to be exactly a quarter of wavelength of the light to be reflected. Its reflectivity is based on the costructive interference of the waves reflected by each AlGaAs/GaAs interfaces. Therefore thickness and refractive index in each layer have to be very well known.

Although the thickness of epitaxially grown layers can be known with good accuracy from the growth parameters (temperature of crucibles and shutter's opening times), nothing can be said about the thickness of the oxide since the shrinkage of the AlAs layers during the transformation into alumina is relatively unknown.

Assuming a vertical contraction of 10% evaluation of shrinkage of a single 700 Å thin AlAs layer would imply a resolution of less than 25 monolayers; such definition has only been achieved by TEM inspection (experimental tool not available at the T.U.E).

We therefore try to carry out the same valuation by measuring the total contraction of AlAs/GaAs DBR-structures during complete and selective wet oxidation. Three different methods has been used: SEM inspection, Talystep profiler and AFM inspection in air.

4.4.2.1 SEM inspection

Valuation of shrinkage by SEM-studies is not feasible due to lack of definition of the recorded images. In fig.4.4.1 the top DBR with ten AlAs layers completely oxidized (on the right) has been placed close to the bottom DBR not oxidized (on the left). We can recognize a difference of about one semi-period (77 nm) of the structure and therefore a shrinkage of about -11%. Although this value is in agreement with the α-step measurements on the same structure nothing can be said about the accuracy of this method.

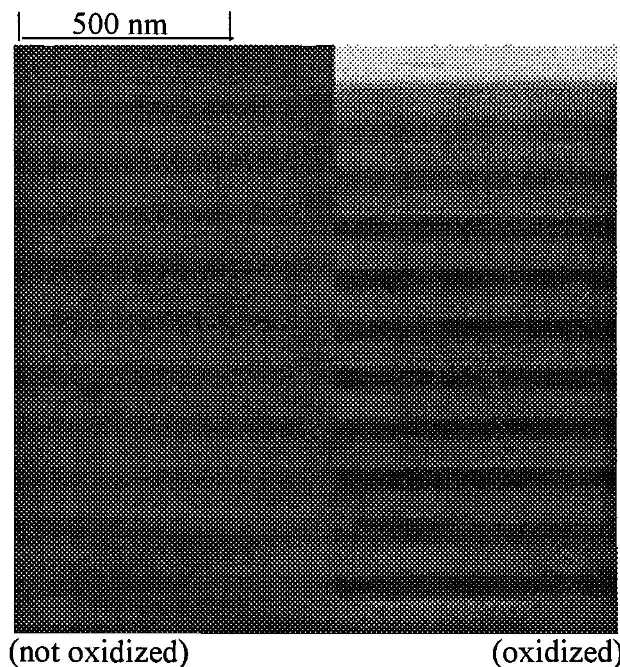

Fig.4.4.1: vertical contraction of sample W516L33_a by SEM inspection

By mere analysis of several pictures we also found that the thicknesses of unoxidized AlAs layers evaluated by the SEM are about 20% less than the growth menu value and that there is a correlation between SEM and growth menu values depending on the magnification of the SEM.
In conclusion, shrinkage valuation by SEM inspection can only be qualitative even when the measurements are carried out over a large number of AlAs layers.

4.4.2.2 Alpha-step inspection

Assuming a theoretical shrinkage of 10%, stripe mesas containing a 10 pair (AlAs/GaAs) DBR (700Å/700Å) should undergo, during selective wet oxidation, to a vertical contraction of 70 nm.
A shrinkage of this magnitude is easily measurable by the α-step profiler (resolution: 5nm) available at the Electronic Device Group.The results of the inspection over different samples are shown in table IV.2 and in fig.4.4.2.
Wafer W839 and W872 have an $Al_{0.2}Ga_{0.8}As/AlAs$ DBR structure and an $Al_{0.5}Ga_{0.5}As/AlAs$ DBR respectively, both with abrupt interfaces; wafer W404 has an AlAs/GaAs DBR with linear graded interfaces.
We define the shrinkage of a single AlAs layer as:

$$z_shr = \frac{S' - S}{n \cdot t_{AlAs}} \cdot 100\% \qquad \Delta z_shr = \frac{\Delta S' + \Delta S}{n \cdot t_{AlAs}} \cdot 100\%$$

where:

- S: height of the stripe before wet oxidation
- S’: height of the stripe after wet oxidation
- n_s: number of AlAs layers actually oxidized (from SEM inspection)
- t_{AlAs}: thickness of a single AlAs layer before wet oxidation (from growth menu)

The absolute resolutions are assumed to be ΔS = ΔS’ = 5 nm and $\Delta t_{AlAs} = 0$.
We operate in the μm-range (accuracy of ± 5 nm) in order to take into account the roughness of the surface, particularly after oxidation, and the unknown error on t_{AlAs}.

n°	SAMPLE	WET OX.	S [nm]	S' [nm]	n_s	t_{AlAs} [Å]	Z_SHR [%]
2	W839L60_1	9'+10'+30' @ 400°C	-	-	16	712	**-(0.4 ÷ 5.7)**
4	W839L60_2	14' @ 400°C	-	-	16	712	**-(1.8 ÷ 6.7)**
6	W404L22_a	7' @ 400°C c.o. (top DBR) p.o. (bottom DBR)	2745 2850	3720 2750	5 16	677.6 677.6	**-(7.4 ± 2.9)** **-(9.2 ± 0.9)**
8	W404L22_c	p.o. 7' @ 400°C	3975 4010	3930 3960	9	677.6	**-(7.4 ± 1.6)** **-(8.8 ± 1.6)**
10	W404L22_E	p.o. 5' @ 400°C	2305	2225	13	677.6	**-(9.1 ± 1.1)**
14	W872_A	c.o. 2h @ 450°C	990	933	4	1117 (*)	**-(12.8 ± 2.2)**
18	W872_E	c.o, 20' @ 400°C	905	855	4	1117 (*)	**-(11.2 ± 2.2)**

Tab. IV.2: alpha-step measures

(*) real thickness of AlAs from difractometry measurement
c.o. complete oxidation
p.o. partial oxidation

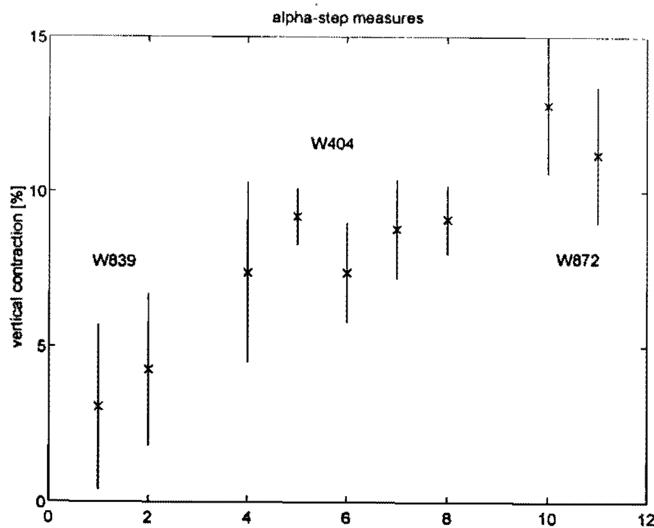

Figure.4.2.2: shrinkage valuation by alpha-step (data from table IV.2)

4.4.3 Conclusion

Values on samples n°2 and n°4 (those numbers are consistent with Appendix A) are not reliable because of the not complete and irregular oxidation; dispersion of data is also due to presence of several oval defects on the surface.

By alpha-step measurement we measure a mean shrinkage of about -8.4% for structure W404 (graded linear DBR) and -12% for wafer W872 (abrupt DBR). These results correlate with results known from literature (see table IV.2); vertical contraction is less in a graded interfaced DBR (Twesten) than in a DBR with abrupt interfaces. However this difference could also be ascribed to a slight different composition of the material to be oxidized ($Al_{0.92}Ga_{0.08}As$ for Twesten, AlAs for other authors).

A detailed study on the subject has still to be performed; some parameters that could influence the amount of shrinkage are:

1) thickness and composition of AlGaAs layer to be oxidized
2) thickness and composition of surrounding layers
3) temperature and time of wet oxidation

4.5 A.F.M. inspection

4.5.1 Introduction

An Atomic Force Microscope (AFM) has been used to estimate the shrinkage along growth direction which an AlAs layer in a DBR structure undergoes during wet oxidation in γ-Al_2O_3. The AFM, a commercial Rasterscope 3000 of DME Industries, was available at the Physics Department of Politecnico di Torino and works without vacuum conditions. The measurements were carried out in the Laboratory of Physics of prof. Renato Gonnelli

We used sample W872_C containing a superlattice AlAs/GaAs for the AFM calibration and sample W404_E and W516_A containing respectively partially and completely oxidized DBRs for shrinkage valuation (see growth menu on appendix B).

4.5.2 Preparation of the samples

The samples were cleaved in air at room temperature just before the AFM inspection and then mounted vertically by simple glueing on a magnetic holder. Inserting the holder inside the AFM chamber is quite a critical procedure: the maximum distance in totally released position between the AFM tip and the magnetic plate on which the sample has to be mounted is about one millimeter; as we need to investigate the fresh cleaved surface, we have to cleave a sample, usually 600-µm thick, in pieces of less than one millimeter width: this is a hard work because, according to an empirical rule, surfaces are well cleaved when the width is approximately 2.5 times the thickness. Anyway this has been accomplished for sample w404, but in order to have a cleaved surface nearly atomically planar, we decide to polish the sample up to a thickness of a hundred of microns; the polishing procedure consists in the removing of the substrate down to 150 µm (see the Polishing Manual, Philips Veldhoven, July 1987).

Samples has been glued with a wax upside down on a quartz disc heated at about 100°C together with 150-µm thick quartz samples, which act as stopping layers. All the pieces are equally distributed along the edge of the disc to insure a stable rotation. The removing of surplus wax has been done by placing the disc, covered with a filtration paper, into a vacuum press; finally, after cooling down and curing of the wax, the disc with the sample is placed in a polishing rotating machine and pressed by a variable weight.

The polishing is accomplished by 3-µm alumina powder and water as lubricant. After rinsing in water and drying, the samples are removed from the holder in hot trichloro ethylene, which dissolves the wax. Rinsing in the same liquid and in isopropanol will complete the cleaning procedure.

4.5.3 Measures

The edge of the cleaved surface was scanned with a silicon tip in contact mode at a constant force of 0.2 nN. Unfortunately our AFM was not provided with samples for an accurate calibration of the piezo-scanners along the direction perpendicular to the cleaved surface, therefore information about the movement of the tip along the z-direction are only qualitative.

As we operate in air oxidation of both GaAs and AlAs is unavoidable and we could not define an abrupt interface between GaAs and AlAs. All we were able to see was a periodic profile with alternating valleys (dark zone on AFM images) and peaks (bright zone) [29]. In the non oxidized DBR the peaks are AlAs layers (see for example fig. 4.5.2) and the valley are GaAs layers due to the higher rate of ambient oxidation of AlAs, while in the oxidized DBR the wet oxidized AlAs is the valleys and oxidized GaAs is the peak.

We measured the shrinkage which an AlAs layer undergoes during wet oxidation by comparing the steps of the AFM periodic image in the DBR wet oxidized and not oxidized for sample W516 and the contraction due to a partial lateral oxidation for sample W404. The way we analyze the images is discussed in appendix 4.5(B).

Sample W872

This sample includes a superlattice AlAs/GaAs (500Å/500Å) grown purposely to calibrate the MBE system after more than one year of inactivity.

From the growth menu the step of this periodic structure should be 100 nm.

On average we found that the real thickness is about (5.1 ± 0.2) % less than the growth menu value. This result is perfectly in agreement with the measure taken by reflectivity measurements in the Quantum Optic Group by Martin van Exter from the University of Leiden.

The AFM images of this structure are shown in fig.4.5.1, fig.4.5.2 and fig.4.5.3.

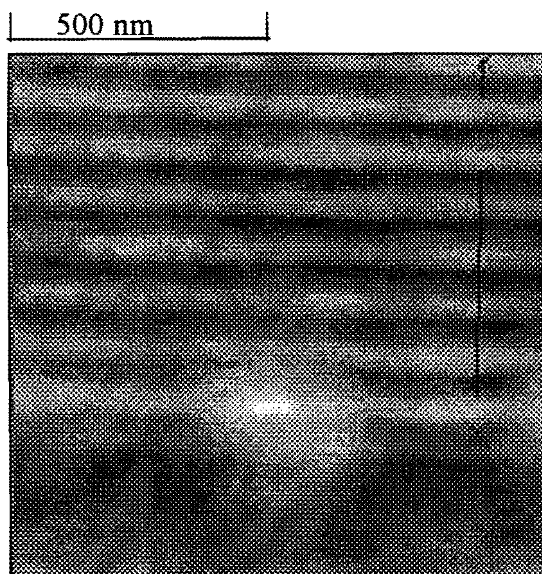

Fig.4.5.1: superlattice W872 (bottom layers)

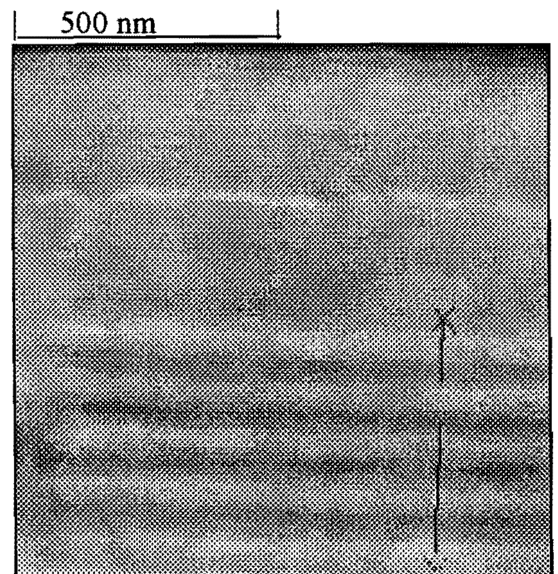

Fig.4.5.2: superlattice W872 (top layers)

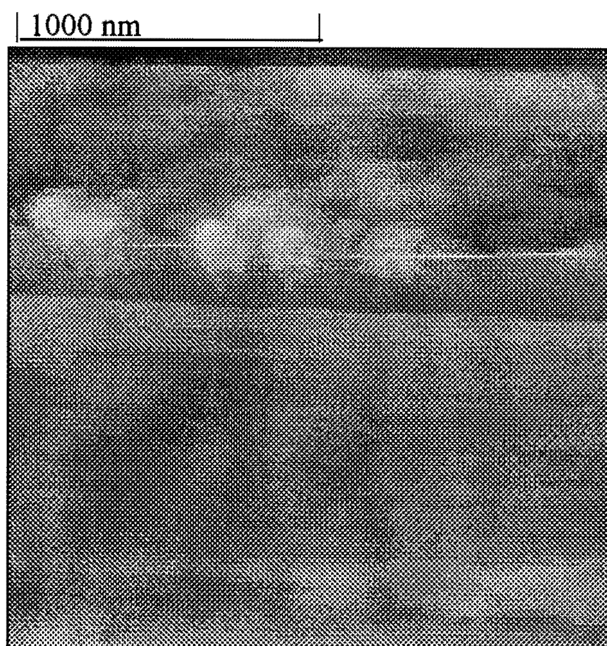

Fig.4.5.3: superlattice W872
the crystalline area above the SL is probably oxidized GaAs
(see SEM picture in fig. 4.7.4)

Sample W404

We used the sample W404L22_E which has the VCSEL structure shown in appendix B; 50-μm wide stripes were wet etched through the top DBR until the middle of the bottom DBR, then the sample was laterally wet oxidized for 7 min. @ 400°C to an extension of (13.6 ± 0.9) μm for the top DBR and (12.4 ± 0.9) μm for the first eight pairs of bottom DBR.

The SEM picture of a cleaved stripe is shown in fig.4.5.4; the lightest layers are GaAs while the darkest ones are AlAs and, even more dark, AlAs oxidized into γ-Al_2O_3.

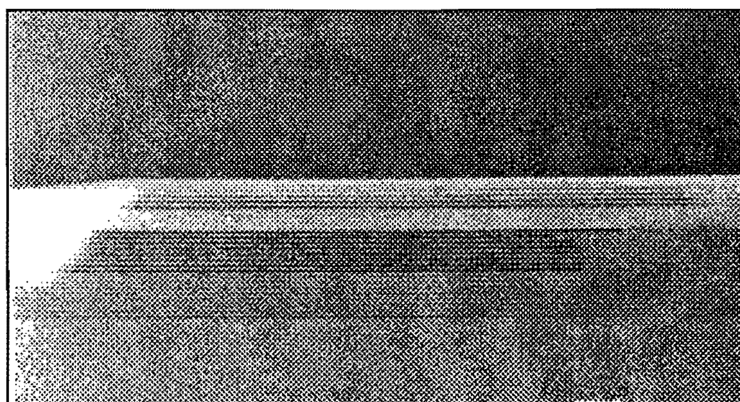

Fig.4.5.4: wet etched 50 μm stripe partially oxidized (W404)

The AFM images shown in the following were recorded in the middle of one of the stripes, in a region where the first eight AlAs layers of the bottom DBR are not oxidized.

From fig.4.5.5 we measure the total thickness of the bottom DBR to be (2.338 ± 0.016) μm; this value is about 2.5 % less than the growth menu value (2.397 μm).

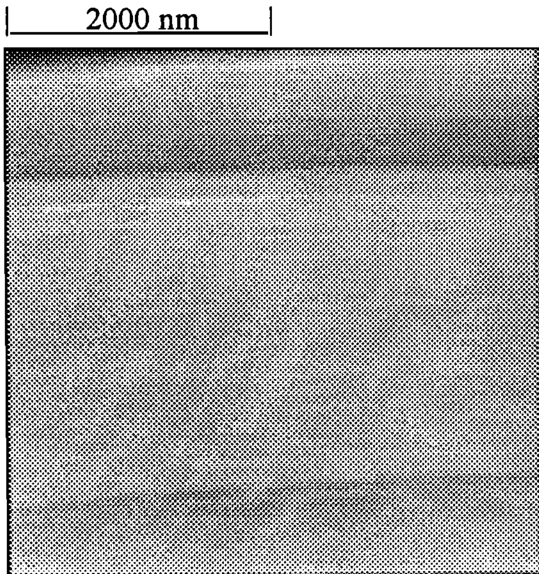

Fig. 4.5.5: W404 (bottom DBR)

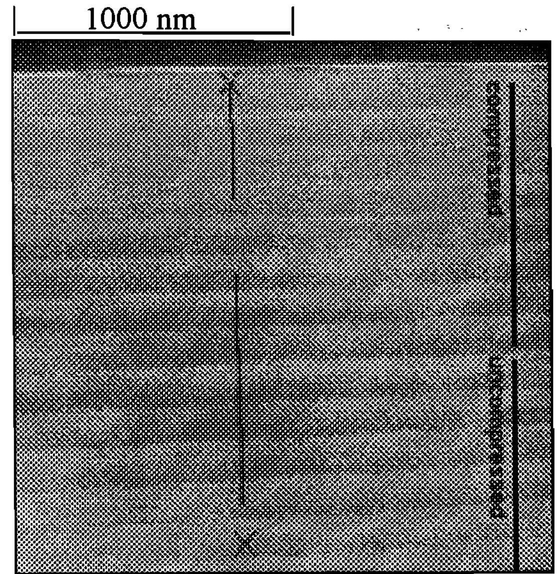

Fig.4.5.6: W404 (bottom DBR)

In fig.4.5.6 are shown the first thirteen pairs of the bottom DBR; the first eight are compressed due to the shrinkage of the lateral AlAs oxidized, while the others are uncompressed. From the periodic profile we estimate a step of

$$p' = (1343 \pm 11)\ \text{Å for compressed layers}$$

$$p = (1465 \pm 19)\ \text{Å for uncompressed}$$

The error associated to each measure has been calculated as follows: as the AFM images has 256 x 256 points the distance between two adjacent points is 7.8 nm. This is assumed to be the absolute error for each measured value.

As p' was the mean of seven periods and p of four periods the errors are $\Delta p' = 1.11$ nm and $\Delta p = 1.95$ nm respectively. Those errors are nearly the same if evaluated by the method shown in appendix 4.5(B).

According to (1) from appendix 4.5(B) the shrinkage is:

$$z_shr = (-18.8 \pm 4.6)\ \%$$

Note that from the growth menu one period of the DBR should be 1532 Å; this corresponds to a difference of -4.3% between the growth menu value and the AFM measure.

From fig. 4.5.7 and fig.4.5.8 which are the enlargement of fig. 4.5.6, we can get similar results; the periods of compressed and uncompressed layers are 1334 Å and 1446 Å respectively (5.6% less than the growth menu value).

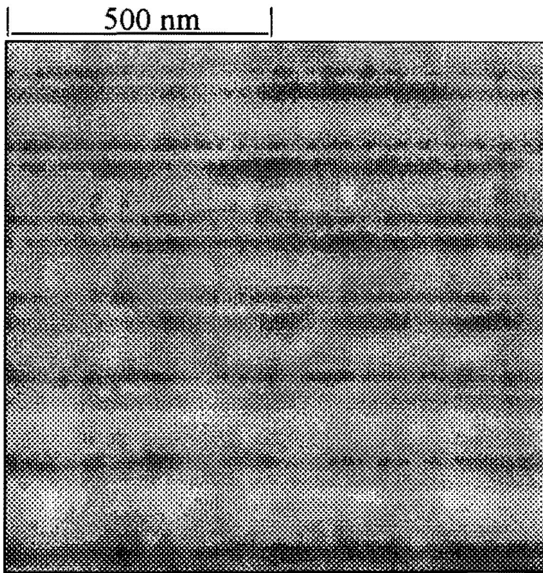

Fig.4.5.7: W404 (bottom DBR)

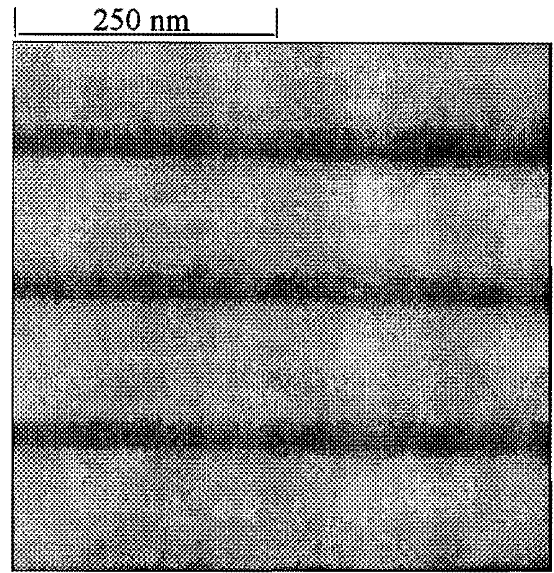

Fig.4.5.8: W404 (bottom DBR)

With the same assumptions of the previous case we estimate the z-shrinkage to be

$$z_shr \approx -17.5\ \%$$

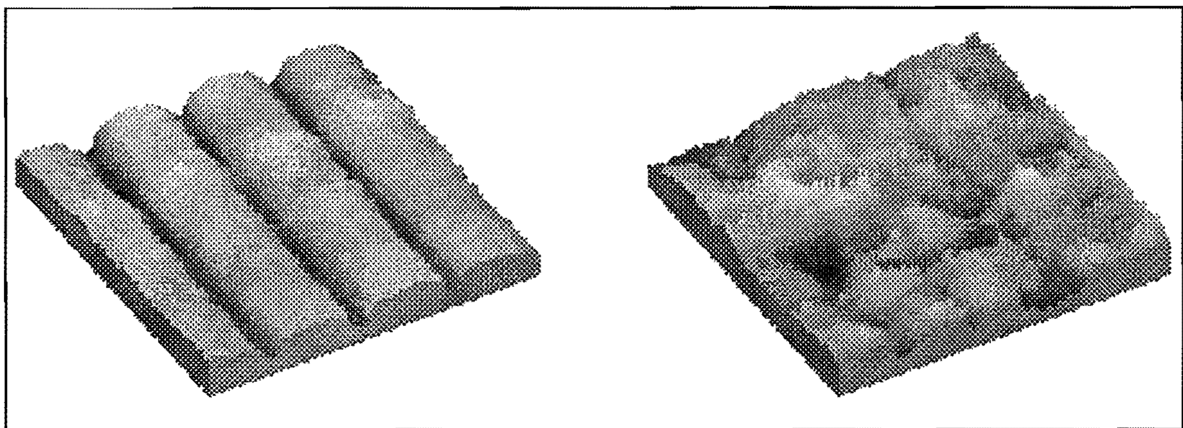

Fig.4.5.9: one day exposure to air one week exposure to air

Finally on fig.4.5.9 is shown what happened to the surface of our sample after one week: on the left we have the normal DBR structure, recorded one day after the cleavage, while on the right is shown nearly the same area of the sample after one week exposure to the atmosphere.

It's difficult to say if the roughness is due to the oxidation or to the instability of the image; in any case, looking at the profile of the structure, we still can recognize a periodic structure.

Sample W516

Complete oxidation of 30-µm wide stripes wet etched was achieved after 15' @ 400°C and, in order to check the thermal stability of the oxide, the sample was then annealed at 400°C for one minute in Ar.

|__500 nm_|

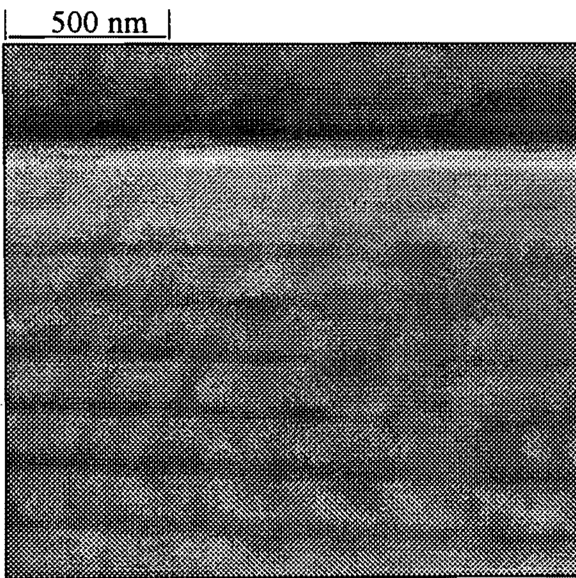

Fig.4.5.10: W516 (non oxidized)

|__250 nm ___|

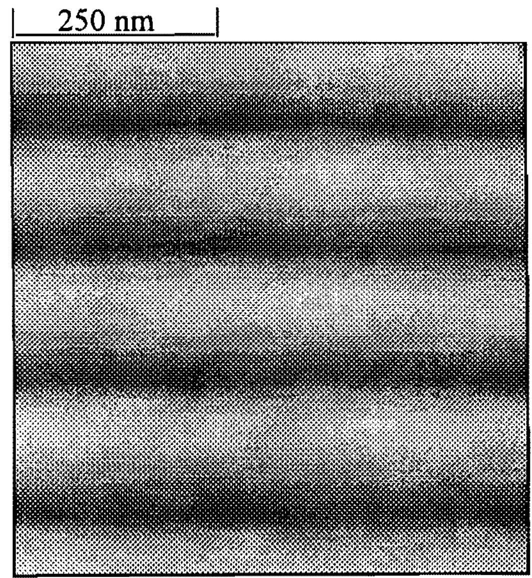

Fig.4.5.11: W516 (oxidized)

From fig.4.5.10 and fig.4.5.11 we measure:

$$p = (1836 \pm 19)\ \text{Å}$$

$$p' = (1643 \pm 10)\ \text{Å}$$

and, according to (1)

$$z_shr = (-23.8 \pm 3.6)\ \%$$

4.5.4 Conclusion

1. thickness evaluation of GaAs/AlAs multilayers with an AFM working in air is feasible;

2. wafer W872 had been grown with accuracy of about 5% and the measure is in good agreement with the optical evaluation carried out by Martin van Exter, showing the reliability of the AFM;

shrinkage of the AlAs layer in sample w404 is found to be -18.8 % while in sample w516 it is -23.8 %; as the two samples have the same DBR structure, the higher shrinkage for w516 is probably correlated to the thermal annealing process and the subsequent transformation of small quantity of residual Al-hydroxide still present after oxidation in Al_2O_3 [9]. The lower shrinkage of w404 is also due to the AlAs non-oxidized which will be in compression, and will retain the laterally oxidized parts.

APPENDIX 4.5(B)

Each image has been recorded with definition of 256 x 256 spots and has to be converted to a file ASCII; then each matrix can be inspected by a Matlab program written on purpose, which allows to cut a section in every place of the image, to deduct the parabolic component due to the hysteresis of the piezo scanner and finally to calculate the periodicity as:

$$\bar{p} = \frac{1}{N}\sum_{1}^{N} p_i \qquad \Delta p = \frac{1}{N}\sqrt{\sum_{1}^{N} (p_i - \bar{p})^2}$$

where N is the number of steps considered and p_i is one of the step defined as distance between two peaks or two valley depending on the quality of the image.
At least six evaluations have been done on each image.
In the next page is shown an example of a profile extracted from fig.4.5.1 and elaborated.

The shrinkage has been evaluated as follow:

from the growth menu we learn that one period (p_{gr}=1531.6 Å) of the DBR structure in sample w404 and w516 is formed by:

	158	Å	linear graded region
	538	Å	GaAs
	158	Å	linear graded region
t_{gr}=	677.6	Å	AlAs

If we name:

p: period before oxidation (by AFM measurement)
p': period after oxidation (by AFM measurement)
t: thickness of a single AlAs layer before oxidation defined as $(p/p_{gr}) \cdot t_{gr}$

(we make the assumption that the proportions between the growth menu values and the real structure are the same)

the shrinkage a single AlAs layer undergoes during wet oxidation turns out to be:

$$z_shr = \frac{p'-p}{t} \qquad \Delta z_shr = \frac{\Delta p'-\Delta p}{t} \qquad (1)$$

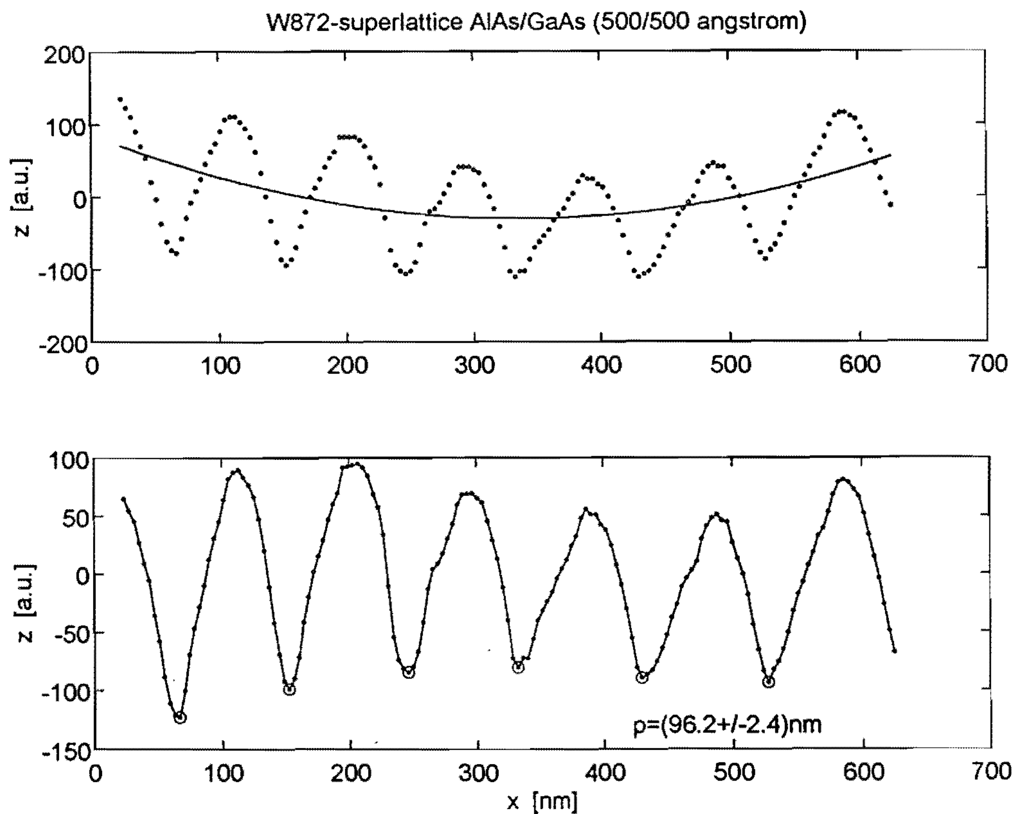

Figure 4.5.12: cross section of fig. 4.5.1

4.6 Weight loss during wet oxidation of AlAs

Although the final product of wet oxidation of AlAs has been proved [9,8] to be the cubic phase γ-Al_2O_3 the exact reactions that take place during this transformation are unknown untill now. The general mechanism for the transformation of AlAs into AlO_x by a water vapour flow at 400°C÷450°C is obviously hydrolysis but how AlAs degrades into a dense nanocrystalline phase through the formation of different Al-hydrates like bohemite AlO(OH) and gibbsite $Al(OH)_3$ is unclear (see appendix D for a review on aluminum based hydroxides)

Possible reactions could be :

		weight loss	**volume contraction (*)**
(1)	$2\ AlAs + 3\ H_2O \rightarrow Al_2O_3 + 2\ AsH_3$	49.97 %	49.1 %
(2)	$AlAs + 2\ H_2O \rightarrow AlO(OH) + AsH_3$	41.13 %	≈ 50 %
(3)	$AlAs + 3\ H_2O \rightarrow Al(OH)_3 + AsH_3$	23.45 %	6.6 %

(*) the volume per Al atom in AlAs is 45.5 $Å^3$ while in γ-Al_2O_3 and $Al(OH)_3$ is 23.1 $Å^3$ and 42.5 $Å^3$ respectively [9].

The high quality of the native oxides is due to the formation of stable AlO(OH) and Al_2O_3 while $Al(OH)_3$ and related compounds are believed to be formed during room-ambient destructive hydrolysis.

Supposing a complete transformation of AlAs into oxide according to equation (1) a sample (1x1 cm^2 large) containing a top DBR structure with 10 AlAs layers (700 Å thick) should undergo to a weight loss of 128 µg. Although this value is much lower than the total weight of the sample (about 250 mg) it is still measurable with a microbalance (resolution ± 1 µg).

A stripe mesa geometry has been defined on our samples in order to expose the AlAs layers. We then used the microbalance CAMN C-30 to measure the weight of the samples before and after oxidation and to estimate the weight loss percentage of AlAs transforming in γ-Al_2O_3.

We define the weight loss percentage as

$$w\% = \frac{W_1 - W_2}{W_t} \cdot 100\%$$

where:

W_1: weight of the sample just before oxidation
W_2: weight of the sample just after oxidation
W_t: theoretical weight of AlAs exposed to oxidation defined as

$$W_t = \rho \cdot n_s \cdot L_s \cdot s \cdot n_{Al} \cdot t_{Al}:$$

ρ: density of AlAs (= 3.732 g/cm^3)
n_s: number of stripes
L_s: lenght of the stripe
s: width of the stripe
n_{AlAs}: number of AlAs layers exposed to oxidation
t_{AlAs}: thickness of one AlAs layer (from growth menu)

The geometrical parameters have all been estimated by the growth menu or by the Polyvar optical microscope.
The accuracy of the balance CAMN C-30, in the range of 200mg, is ± 1 μg; we verified this accuracy by checking the weight of two samples three days after the first measurement: differences were less than 1 μg.
Results about weight losses during wet oxidation are shown in table IV.4.
In order to check the reliability of the balance we monitored the weight of the sample during some of the technological steps of the normal VCSEL process.
In table IV.3 the results about the gain and loss in weight during SiN deposition are reported.

n°	Sample	W1 [mg]	W2 [mg]	A [cm^2]	t_{SiN} [nm]	ρ_{SiN} [g/cm^3]
14	W872L99_A	181.913	181.950	0.82 x 0.81	317 ± 10	**1.76 ± 0.15**
13	W495L33_A	212.099	212.149	1.1 x 0.7	318.5 ± 10	**2.04 ± 0.16**
16	W872L99_C	252.337	252.378	0.90 x 0.99	243.5 ± 5.5	**1.89 ± 0.32**

Tab. IV.3

where

W_1 (W_2): weight before (after) deposition
A: area of the sample
t_{SiN}: thickness of Si_3N_4 mask (by average of Talystep measurements)

n°	SAMPLE	W_1 ± 0.001 mg [mg]	W_2 ± 0.001mg [mg]	WEIGHT LOSS ± 2 μg [μg]	W_t [μg]	w%	n_s	L_s [μm]	s [μm]	n_{AlAs}	t_{AlAs} [Å]
4	W839L60_2	203.555	203.544	11	21.2	**(51.9 ± 9.4) %**	24	7187 (1)	28.9	16	712
5	W516L34_a	152.900	152.885	15	≈ 14.2	- (2)	25	≈ 8000	28	10	677.6
6	W404L22_a	226.800	226.785	15	30.4 ± 3.8	**(49.3 ± 12.7) %**	21	11061 (1)	14 (top) 28.2 ± 2 (bottom)	5 16	677.6
7	W404L22_b	189.059	189.047	12	-	- (3)	-	-	-	-	-
8	W404L22_C	166.511	166.499	12	-	- (3)	-	-	-	-	-
9	W404L22_D	171.125	171.117	8	-	- (3)	-	-	-	-	-
10	W404L22_E	190.211	190.203	8	15.2 ± 1.3	**(52.6 ± 17.6) %**	23	7950	25.2 ± 2 (4)	13	677.6
11	W404L22_F	156.151	156.148	3	-	- (3)	-	-	-	-	-
13	W495L33_A1 _A2	94.534 116.069	94.517 116.017	17 52	17.8 22.7	**95 %** **229 %**	11 14	10348	29.5	21	677.6
14	W872L99_A	181.785	181.651	134	≈ 111.3	**120 %**	27	8100	293	4	1164
16	W872L99_C	252.485	252.378	111	≈ 130.4	**85 %**	180	9930	42	4	1164
18	W872L99_E	150.552	150.512	40	83.3	**(48 ± 2.4) %**	142	7553	44.7	4	1164

Tab.IV.4: weight loss during oxidation

(1) this is a mean value assuming an exact value for n_s; the sample had been cleaved in four pieces and the values L_s and n_s for each of them are not shown.
(2) this measure is not significant: traces of photoresist were present on the bottom surface of the sample during wet oxidation.
(3) oxidation front was too irregular therefore valuation of W_t was impossible.
(4) from SEM inspection.

The values measured are obviously different from the theoretical Si_3N_4 density (about 3.4 g/cm^3) because the Si_3N_4 layer deposited by PECVD is never stochiometric.
A bad quality of the Si_3N_4 layer deposited (low density) could also explain the failure of the sealing process against oxidation by a simple Si_3N_4 deposition.

We also measured the weight loss during dry etching: for sample W404L22_c (n°8) and W404L22_G (n°12) differences between the measured values and the theoretical weight of the etched material were less than 1.2 % and 1.6 % respectively.

Conclusion

Measures on sample n°4, n°6 and n°10 are not in disagreement with the theoretical reaction (1) but the accuracy is poor due to the small quantity of AlAs oxidized (about 20μg).
However, weight loss in sample W872L99_E is (48 ± 2.4)% and it is in good agreement with the theory (50%) because only 4-μm canals were etched and therefore almost all the AlAs present in the DBR has been oxidized. This sample shows that the wet oxidation process could be monitored by weight measure if the amount of oxide to be formed is over a certain level.
The measurements on sample n°13, n°14 and n°16 are not reliable since in these samples $Al_{0.5}Ga_{0.5}As$ and GaAs were oxidized.

4.7 Distributed Bragg Reflector for visible light

4.7.1 Introduction

A Distributed Bragg Reflector (DBR) is a stack of alternating layers with different refractive indices. Due to subsequent reflections on each interface, high reflectivity can be obtained. Design rules for a DBR at resonant wavelength λ_0 are very simple:

$$L_1 = \frac{\lambda_0}{4n_1} \qquad\qquad L_2 = \frac{\lambda_0}{4n_2}$$

where L_1, L_2 and n_1,n_2 are thicknesses and refractive indices of the two layers that form a single pair.

If the optical length, refractive index * geometrical thickness of each layer, is exactly a quarter of wavelength of the incident light, all the reflected waves will be in phase and the total reflectivity will even be in excess of 99%. The number of DBR pairs needed to reach the required reflectivity depends on the choice of material system; the reflectivity R at the resonant wavelength of a stack with N/2 non-absorbing dielectric pairs of indices n_i and n_{i+1} is given by:

$$R = \tanh^2\left[\sum_{i=1}^{N}\tanh^{-1}\left(\frac{|n_{i+1}-n_i|}{n_{i+1}+n_i}\right)\right] \tag{1}$$

Besides the required reflectivity, the thermal conductivity, the penetration depth of the light into the DBR and the width of the stopband are the most important parameters in the DBR design. In particular the bandwidth $\Delta\omega$, the band by which the reflectivity is more than 90%, is approximately

$$\frac{\Delta\omega}{\omega_0} = \frac{4}{\pi} asin\left(\frac{n_1 - n_2}{n_1 + n_2}\right) \tag{2}$$

In VCSEL's very high reflectivity mirrors are required on each side of the resonant cavity since the gain region is short, compared with that of edge emitting lasers. Epitaxial semiconductor DBR can be placed above and below the active region allowing the VCSEL to be grown in one step; however the refractive index ratio for typical epitaxial materials is low and many pairs should be grown in order to achieve a reflectivity of greater than 99% in order to reach the lasing condition.

A DBR composed by a stack of GaAs and AlAs layers should have for instance 20 pairs to reach a reflectivity of 99.6 % because of the small difference in refractive index between the two material (n_{GaAs} = 3.51; n_{AlAs} = 2.95); the stopband of such a structure at wavelength λ_0=1000 nm is only 110 nm.

The reflectivity and the spectral bandwidth is very sensitive to thickness and thickness uniformity of layers: to ensure alignment of the cavity resonance with the gain peak the requirements on the layer thickness precision are very stringent (about 1%).

A DBR composed by a multilayer of two materials that have a much larger refractive index difference will have several improvements:

- the number of pairs needed to achieve the same reflectivity will be decreased;
- the stopband will be strongly larger;
- the constrains about thickness control and thickness uniformity all over the sample will be less incisive.

To take advantage of this favorable properties we try to fabricate an epitaxially grown 4 pairs DBR for visible light (λ_0 = 650nm) with high reflectivity and wide stopband using alternate layers of $Al_{0.5}Ga_{0.5}As$ and AlO_x. Refractive index ratio for this couple of material is considerably high (about 2.25). We chose AlGaAs with x_{Al} = 0.5 in order to avoid absorption in the wavelength range of interest (note that λ_0=650 nm corresponds to 1.91 eV and the energy gap of $Al_{0.5}Ga_{0.5}As$ is approximately 2.49 eV).

The dielectric layers can be obtained by simple selective oxidation of epitaxially grown AlAs-layers but few data are available about the optical properties of the native oxide of AlAs. From literature [30] and from vertical contraction valuation by different techniques (see paragraph 4.4) we assume the refractive index of AlO_x to be 1.55 and shrinkage due to oxidation of AlAs to be about -10%.

According to equation (1) and (2) reflectivity and stopband should be 0.994 and 580 nm respectively. It should be noted that, in order to achieve the same reflectivity with a conventional semiconductor DBR ($Al_{0.5}Ga_{0.5}As$/AlAs), the number of pairs should be at least 34 and the time required for the growth will be in excess of 3 hours. Since this long time will not allow the MBE-growth to be uniform it is evident that thinner oxide based DBRs are necessary for future visible light emitting VCSELs.

Simulated reflectivity spectra for the new DBR structure AlGaAs/AlO_x and for the conventional AlAs/AlGaAs DBR have been calculated by a transfer matrix method and are shown in fig. 4.7.1

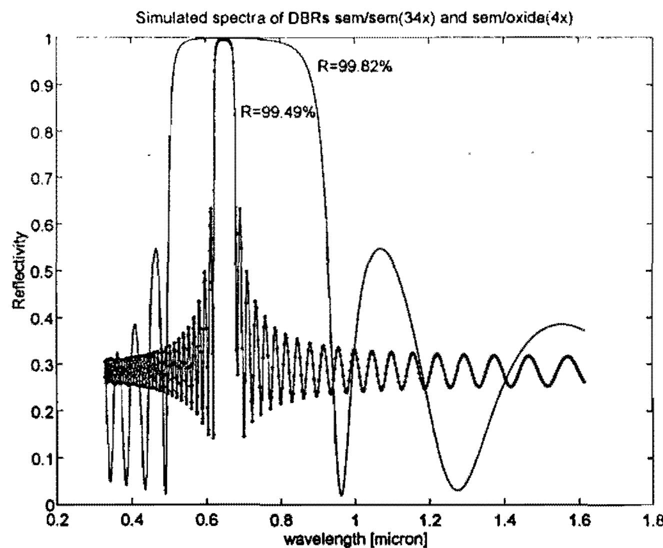

Figure 4.7.1 (reflectivity spectra simulated)

The wafer W872L99 containing the new DBR structure, was grown in November '96 by W.C.van der Vleuten with the MBE-system again available at the Physics Department of TUE after one year of inactivity. The detailed structure is shown in appendix B.

The DBR $Al_{0.5}Ga_{0.5}As/AlAs$ (466Å/1164Å) x 4 required a growth time of about 40 minutes. A 40Å GaAs capping layer on the surface is needed to prevent the under-laying $Al_{0.5}Ga_{0.5}As$ from room ambient oxidation which can lead to instable native oxide. The superlattice AlAs/GaAs was grown for calibration purpose of the MBE system and its total thickness was estimated to be 4-5% less than the growth menu value by AFM inspection (see fig. 4.5.1) carried out in the Physics Laboratories of Prof. R. Gonnelli of Politecnico di Torino and confirmed by reflectivity measurements done in the Quantum Optics group of University of Leiden by Dr. M. van Exter.

Surface quality of the wafer was questionable: lots of oval defects due to contamination of several impurities were present. In the next paragraph a complete classification of the so-called oval defects is discussed. All the deviations from the monocrystallinity of the structure W872 endangered the complete and uniform wet oxidation of the AlAs-layers and the reflectivity measurements; paragraph 4.7.3 will deal with those problems and the ways to avoid them.

4.7.2 Oval defect

The most common type of crystal growth defects observed in epilayers grown by MBE is the "oval defect", so called because of its appearance under optical microscope observation. It is typically 10-20μm in lengths and 5-10 μm in width [31] for a 1-2 μm-thick film (if the origin of these defects are from the substrate surface, the defect size would be larger, approximately in proportion to the thickness of the epilayer film). They can occur with densities ranging from 10^2 to 10^5 cm^{-2} and the orientation of the long-axis is parallel to the <1$\underline{1}$0> direction; this anisotropic growth may be related to the difference in the gallium surface diffusion constant that is larger along the <1$\underline{1}$0> direction than along the <110> direction [32]. A SEM picture of the cross-section of an oval defect is shown in fig. 4.7.2.

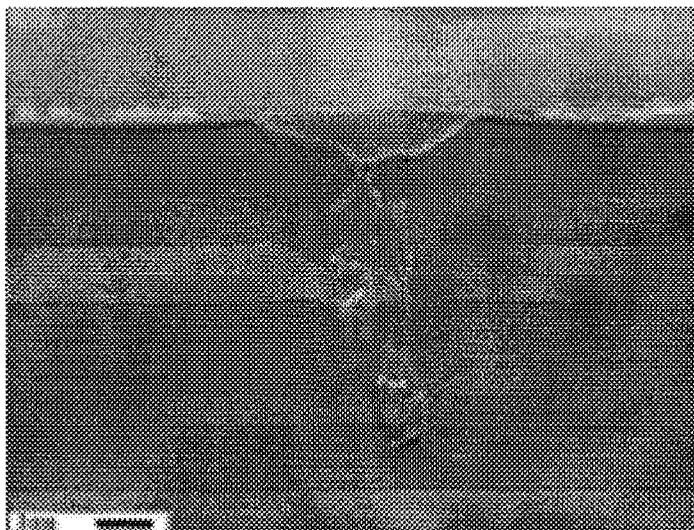

Figure 4.7.2: cross-section of oval defect

The factors causing the oval defects are not unique but several depend on the MBE-system employed and on the growth conditions used [33,34,35]. Experimentally the defect formation has been related to:

1) substrate preparation
2) excess of gallium ("gallium spitting")
3) As source cell
4) gallium oxides

1. inadequate substrate preparation can originate surface impurities on the substrate which interfere locally with the epitaxial growth [36]; the substrate is not a particular source of oval defects when the oval-defect density is proportional to the grown thickness.
   Two types of contamination can occur.

   Microscopic contamination: atoms can be adsorbed on the surface during the wet chemical cleaning step, from the atmosphere during the loading of the substrate or during the growth due to a leakage in the vacuum chamber.

   Macroscopic contamination: particles on the wafer surface prior to growth will produce oval defects characterized by a faceted pit because it provides a site for gallium agglomeration. Since the particle is not epitaxial to the substrate, no growth occurs on it and the oval defects grows up around the particle deriving its shape from the relative rates of growth parallel to the surface.

2. Oval defects can be originated by the formation of a liquid phase during growth; two different mechanism have been identified.
   I) Ga "spitting" from the Ga-crucible; it can occur by two different ways: (1) gallium which condenses at the front of the crucible falls back into the hot Ga melt, explodes and ejects globules of Ga from the crucible to the substrate; (2) uneven heating of the Ga melt due to localized increasing of temperature in critical places of the crucible walls induces violent turbulence and generation of Ga vapor from underneath the melt surface causing sudden release of bubbles and ejection of Ga droplets.
   II) agglomeration of Ga during growth: if the mean free path is long enough for gallium surface diffusion, Ga atoms will agglomerate into clusters [34].

3. Although the arsenic cell also contains some impurities generating oval defects, the defect density is easily decreased by a sufficient outgassing of the As cell and subsequent evaporation of all the impurities before growing [36].

4. Ga_2O (gallium suboxide) is an oxide species always observable in the gallium cell's effusate. Intentionally increasing the Ga_2O flux from the Ga effusion cell has been shown [37]to increase oval defect density; it is believed that this oxide transform into precipitates of Ga_2O_3 that nucleate gallium droplets, thus forming the precursor of the oval defects.

A detailed classification of all the oval defects grown by MBE can be found in reference [31]; by their surface appearance under optical microscope observation, they are divided into three group for convenience:

α-type: group of six different types of oval defects (designed α_1-α_6) all without a macroscopic core particulate. The origin of the α_1 , α_2 and α_5 is the microscopic contamination (probably carbon) both in solution and in vacuum environment; α_6 is due to contaminations of sulfur on the substrate [38] and α_3 and α_4 are originating from the locally enhanced anomalous GaAs growth due to the excess of Ga atoms [31].

β-type : group of oval defects with a macroscopic core particulate; the central part of this defect consists of polycrystalline GaAs and it is due to macroscopic contamination during inadequate substrate preparation.

γ-type : large macroscopic surface defect with an irregular shape; it can be eliminated by long outgassing procedure of the effusion cell and shutter assembly.

4.7.3 Realization of a semiconductor/oxide DBR

Wafer W872L99 has been grown on November 21th just after one of the openings of the MBE vacuum chamber for maintenance service (in that period several leakages were discovered).

Contaminants, probably carbon and oxygen, originating from the atmosphere before the loading of the substrate and from a leakage of the chamber during growth, were adsorbed on the surface and many oval defects were originated.

By optical inspection after growth the density of α_1 defects was in excess of $5 \cdot 10^6$ cm^{-2}; other defects, mainly α_4 and γ, were found with less density and larger dimensions.

Although the total density of growth defects was too much to obtain a high-reflectivity mirror (the optical properties of the sample are seriously degraded over a surface which is larger than the oval defect itself [39]) we have fabricated it in order to establish the technological steps for a selectively oxidized DBR; 4 and 8 μm wide canals have been defined by conventional photolithografic techniques with a dark-field mask and etched through the DBR; the sidewalls were than exposed to the usual oxidative flow at high temperatures. See samples n° 14 to 18 for an overview of the parameters.

High temperatures (450°C) and long times of oxidation (1 hour) were needed because of the large amount of AlAs to be oxidized: the canals were 300μm-spaced.

During selective oxidation several problems arose mainly due to the presence of the oval defects and the 300 μm spacing:

1) non-complete oxidation
2) non-uniform oxidation
3) unexpected oxidation of GaAs

Causes and cures to solve these problems are explained in the following:

1. in fig.4.7.3 the optical picture (100x) of sample W872L99_B (n°15) is shown; 60 minutes at 450°C were not enough to completely oxidize the structure. The arrows show the 8μm-canals while the five different shades of gray (from the darkest to the lighter) indicate the zones of the sample where none, one, two, three or four AlAs-layers of the DBR were oxidized.

Figure.4.7.3: enhanced oxidation around oval defects (sample n°15)

We observe that at the sides of the canals and around the oval defects all the four layers are oxidized (lightest) while in the middle of the 300μm-stripes none of the layers was oxidized (darkest). Such a difference in color is due to a difference in refractive index of AlAs and Al-oxide.

Causes:

(a) a dry etching could explain the prevention from oxidation as discussed in paragraph 4.2.2;

(b) after long times the oxidation law could become parabolic and even reach an asymptote;

Solutions:

(a) definition of canals by wet etching (see sample n°18, completely oxidized);

(b) number of canals can be increased using the same mask by a multi-exposure step (see sample n° 16, 17, 18 with canals about 50μm-spaced)

Increasing time and temperature of oxidation is not a solution because of GaAs oxidation problems (see later on).

2. in fig.4.7.3 an irregular front of oxidation is also clear;

   Causes:
   general causes were already proposed in paragraph 4.2. Presence of oval defects can also originate a non-uniform oxidation due to enhanced or prevented oxidation around them.
   In fig.4.7.3 all the oval defects increased the oxidation rate from about 2 to 3 times (depending on defect's dimension) and the front around them is also perfectly circular showing an isotropic oxidation.
   Explanations of the oxidation behavior around the oval defects to could be:

   - different composition of defect's core; enrichment or impoverishment of Al percentage could vary the oxidation rate due to the selectivity of the process.
   - infiltration of water vapor from the top surface to those defects uncovered by the Si_3N_4 mask;
   - polycrystallinity around defects can also increase the oxidation rate due to the formation of more canals among the GaAs grains for the water supply.

   Solutions:
   in order to prevent oxidation from the oval defects' core towards the inside of the structure, a sealing process has been performed. A rapid thermal annealing in H_2 and N_2 flow for 10 sec at 550°C just after the cleaning step of the sample has been proven to completely avoid oxidation, probably due to the formation of a thin and dense oxide layer all around the core's internal surface (see paragraph 4.2).

3. Oxidation of $Al_{0.5}Ga_{0.5}As$ and GaAs below the DBR structure (see the growth menu of W872 in appendix B) has been observed in all of the samples oxidized at temperatures higher than 425°C. See fig.4.7.4 and fig.4.5.3 (by AFM inspection). Although this behavior is in disagreement with all the literature about oxidation, Takamori also reported [10] oxidation of GaAs at 450°C for 60 minutes without providing explanation.

Figure 4.7.4: $Al_{0.5}Ga_{0.5}As$ and GaAs below the DBR are oxidized
due to high temperature and time of oxidation and bad quality of the wafer

This unexpected oxidation of GaAs could be related to the bad quality of the grown material and the lack of monocrystallinity around the defects.
Formation of GaAs oxide has been avoided when the oxidation was carried out at 400°C (see sample n°18).

4.7.4 Conclusion

The new process steps suitable to fabricate, from wafer W872, an oxide-based DBR were all developed and are listed below:

- sealing the oval defects
- definition of 50μm-spaced canals by multi-exposure
- etching canals by a wet process
- parameters of oxidation: 20min. @ 400°C

the surface of the sample is still unsuitable for reflectivity measurement due to the unavoidable presence of oval defects.
When the MBE system will be able to grow a new structure with less oval defects, the technological steps performed during this project will allow to fabricate the first DBR-mirrors for visible light emitting VCSELs

CHAPTER 5

Conclusion and acknowledgments

Conclusion

The Vertical Cavity Surface Emitting Laser (VCSEL) will receive more and more attention in the next future due to excellent properties like reduced size, low divergent circular output beam and two-dimensional laser array feasibility. The intra-cavity contacted VCSEL, developed at the Electronic Device Group of Technical University of Eindhoven is in particular a very promising device since the injection of the current through the DBRs is avoided resulting in low electrical series resistance and ultralow threshold current. This type of design will also be necessary for future light emitting VCSELs which use oxidized, and therefore non-conducting, Distributed Bragg Reflectors (DBRs).

During the processing stage of the new VCSEL the wet selective oxidation is one of the most critical steps. This relatively new process is becoming a powerful processing technique for many III-V semiconductor devices and a lot of research is aimed to better control the kinetics and the mechanism behind it in order to incorporate oxide-layers into all-epitaxially grown structures. However few information are at the moment available concerning the formation and the real structure of these oxides.

The main properties which make the wet selective oxidation of $Al_xGa_{1-x}As$ an interesting step for future optoelectronic device fabrication are:

- <u>selectivit</u>: the oxidation rates strongly depend on the Al-content in the III-V compound;
- <u>stability</u>: the formed oxides are mechanically as well as thermally very stable;
- <u>ease of processing</u>: a furnace at 400°C in a water vapor saturated environment is sufficient.

In contrast with these good features is the difficulty in obtaining a uniform and controllable profile of oxidation due to many parameters which act simultaneously and affect the process in an unknown manner.

During oxidation a complete depletion of As in form of the volatile AsH_3 is believed to occur resulting in a contraction of the oxide; the phase transformation of AlAs into oxide

is supposed to occur from an initially amorphous phase containing AlO(OH) and $Al(OH)_3$ compounds, due to the hydration process in heated water vapor, to the polycrystalline γ-Al_2O_3. Concerning the technological aspect of wet oxidation, a practical distinction has to be made between the oxides formed by vertical and lateral oxidation. While the vertical oxidation tends to show a diffusive character and saturation for longer time, the lateral oxidation stays reaction-limited and, due to the contraction of the oxide layers, "canals" and open porosity will originate along the oxide/semiconductor interface. The canals will allow a fast transport of the oxidizing species to and from the oxidation front and would explain the greater oxidation rates of lateral oxidation (about two times compared to vertical oxidation).

At the Electronic Device Group of T.U.E. the wet selective oxidation is used for realizing the current confinement, necessary in an intra-cavity contacted VCSEL; AlAs-layers adjacent to the active region are laterally oxidized in order to force the charge carriers to flow into the center of the active region. In the near future the same process will be used to realize semiconductor/oxides DBR necessary for visible light VCSELs. In the framework of these future developments, the experimental results obtained during this project will allow a better awareness of the process and a better controlled uniformity of the oxidized material. In particular several tests have been carried out in order to characterize the oxide with the tools available at the Electronic Device Group, and several attempts were made to avoid the effects that bad-quality MBE-grown wafers had over the uniformity of oxidation.

Several samples were etched by wet or dry process in order to expose the AlAs-layers for subsequent lateral oxidation with different conditions of time and temperature. A Taly-step profiler and an Atomic Force Microscope were employed in order to measure the vertical contraction these layers undergo during wet oxidation into γ-Al_2O_3. A microbalance has been used for the monitoring of the process and it was shown how the weight loss during oxidation could be estimated under particular conditions of measure. The thermal stability of GaAs/AlO_x DBRs was also investigated and interesting results about the effects of an over oxidation and a graded interface were verified. The different behavior of dry and wet etched mesas on oxidation was also analyzed and a theoretical explanation has been proposed.

These experiments on wet oxidation were carried out in order to prepare the fabrication of the next semiconductor/oxide DBRs necessary for a new generation of visible light VCSELs. The required steps were all defined but the final realization was not possible due to the bad crystal quality of the designed structure which affected the optical properties even before the oxidation process. It is expected that high reflectivity DBRs can be processed in the next future when new VCSEL material will be available.

Acknowledgements

I would like to thank all the people of the Electronic Devices Group who have assisted me during my working here: Barry Smallbrugge, who learned me the basic behavior inside a clean-room, Eric Jan Geluk, for his patience with the SEM and Martin Creusen for the writing out of this work.
I would also like to thank Prof, Kaufmann and Dr. Theo van de Roer for giving me the opportunity to work in this group. I am also grateful to Prof. Renato Gonnelli of Politecnico di Torino for allowing me the use of his A.F.M.
Especially thanks are also for my family who, even if far away from here, did a lot for me.
I'd finally like to thank the Politecnico di Torino and Socrates program for funding.

Overview of processed samples

In table A1 a list of all the samples processed during this selective oxidation project is presented. All the wafers were grown by the MBE facility in the Physical Department of T.U.E. by W.C. van der Vleuten; see appendix B for a detailed description of the structures.

Wafer W839L60 has a top (bottom) DBR consisting of alternate $Al_{0.2}Ga_{0.8}As/AlAs$ layers x 16 (x 25.5). Wafer W404L22 and W495L33 are structures with top (bottom) DBR AlAs/GaAs x 4.5 (x 15.5) and gradual compositional interfaces (158 Å thick) between AlAs and GaAs layers. W516L34 has the same structure of W404L22 but with a top (bottom) DBR x 9.5 (x 20.5). W872L99 has been grown for the visible light reflectors project and contains a DBR $Al_{0.5}Ga_{0.5}As/AlAs$ x 4.

n°	NAME	PURPOSE	PROCESS	RESULTS
1	W839L60	uniformity of oxidation profile depending on the orientation of the stripes	50-μm st. wet etched wet oxidation: 7 min @ 400°C	stripes parallel to N_2-flow: regular oxidation stripes perpendicular to N_2-flow:irregularoxidation
2	W839L60_1	complete oxidation of 30-μm stripes and partial oxidation of 50 μm stripes shrinkage valuation of completely and partially oxidized DBR	30 and 50-μm stripes dry etched removing of SiN before oxidation wet oxidation: 9 min @ 400°C put back into the furnace + 10 min @ 400°C put back into the furnace + 30 min @ 400°C RTA: 1 min. @ 400°C in Ar	ox. just around some defects irregular profile of oxidation complete oxidation of the stripes unaffected
3	W839L60_I	calibration of SEM	unprocessed	
4	W839L60_2	shrinkage valuation of AlAs during oxidation and behavior of a complete oxidized DBR to a rapid thermal annealing	30-μm st. dry etched through top DBR wet ox: 14 min @ 400°C RTA: sample _2a 10 min. @ 450°C in Ar (35°C/sec) sample _2b 10 min. @ 400°C in Ar (2°C/sec)	not complete around some defect complete deadhesion at sem/oxide interface almost complete deadhesion at sem/ox interface

5	W516L34_a	verify thermal stabilitiy of graded linear DBR after oxidation	30-μm st. wet etched through top DBR wet ox: 15 min @ 400°C (complete) RTA: sample _a2 1 min. @ 400°C in Ar	no delamination (DBR with gradual compositional interfaces)
6	W404L22_a	simultaneous complete ox. of top DBR and partial ox. of bottom DBR after a wet etching.	16-μm st. (top DBR) onto 50-μm st. (bottom DBR) wet etched wet ox: 7 min @ 400°C RTA: 5 min. @ 400°C in Ar	uniform profile of oxidation in bottom DBR (0.7 %) unaffected
7	W404L22_b	simultaneous complete ox. of top DBR and partial ox. of bottom DBR after a dry etching	16 and 30-μm stripes through top DBR onto 50 μm stripes through bottom DBR dry etched wet ox: 6 min @ 400°C RTA: 1 min. @ 420°C in Ar	top DBR: completely oxidized after removing of SiN bottom DBR: irregular profile of oxidation unaffected
8	W404L22_C	investigate the p and n type oxidation rates	50–μm stripes dry etched through top and bottom DBR wet ox: 7 min 10 sec @ 400°C	non uniform profile of oxidation (the first AlAs layers of bottom DBR were not oxidized)
9	W404L22_D		50–μm stripes wet etched through top and bottom DBR wet ox: 7 min @ 400°C	not oxidized (around some few defects only)
10	W404L22_E	investigate the p and n type oxidation rates	50–μm stripes wet etched wet ox: 5 min @ 400°C	uniformity of oxidation in top DBR: 2 % uniformity of oxidation in bottom DBR: 6.7 % enhanced ox. of p-type in few stripes

11	W404L22_F		50–μm stripes wet etched wet ox: 5 min @ 400°C	profile of oxidation very irregular
12	W404L22_G	investigate the influence of a wet clean in step before dry etching	50 μm stripes dry etched through top and bottom DBR G1: etched in NH_4OH:H_2O_2:H_2O (1:2:50) before ox. G2: not etched wet ox: 5 min @ 400°C	no differences in oxidation depth (only the shape of the profile was different)
13	W495L33_A	influences of an over-oxidation on the thermal stability of completed oxidized DBRs	30–μm stripes dry etched wet ox: A1:15 min @ 450°C A2:60 min @ 450°C RTA: 10 min @ 470°C	complete oxidation of all the stripes A1: complete delamination at sem/oxide interface A2: unaffected
14	W872L99_A	realization of AlGaAs/AlO_x DBR for reflectivity measurements	4–μm canals (300–μm spaced) dry etched wet ox: 2 hours @ 450°C	complete oxidation of AlAs in DBR oxidation of GaAs rough surface
15	W872L99_B	same as n° 14	8–μm canals (300–μm spaced) dry etched wet ox: 1 hour @ 450°C	not complete oxidation of AlAs in DBR isotropic enhanced oxidation around oval defects oxidation of GaAs
16	W872L99_C	same as n° 14	8–μm canals (44–μm spaced) dry etched sealing of defects (30 sec @ 550°C) wet ox: 1 hour @ 425°C	complete oxidation of AlAs in DBR oval defects sealed oxidation of $Al_{0.5}$ $Ga_{0.5}$ As

17	W872L99_D	same as n° 14	4–μm canals (50–μm spaced) dry etched sealing of defects (30 sec @ 550°C) wet ox: 1 hour @ 425°C	complete oxidation of AlAS in DBR oxidation of GaAs cracks at substrate/buffer interface
18	W872L99_E	same as n° 14	4–μm canals (50–μm spaced) wet etched sealing of defects (30 sec @ 550°C) wet ox: 2 0 min @ 400°C	complete oxidation of AlAs in DBR rough surface NO oxidation of GaAs

TAB A1: overview of processed samples

APPENDIX B

MBE-growth menus

B.1 Wafer W839L60

Layer no.	L_z [Å]	Material	Doping	type	Sub T [°C]	Loops
22	0	As	-	-	250	
21	200	GaAs	-	-	800	
20	400	$Al_{0.2}Ga_{0.8}As$	-	-	800	
19	712	AlAs	-	-	800	
18	609	$Al_{0.2}Ga_{0.8}As$	-	-	800	15
17	712	AlAs	-	-	800	15
16	357	$Al_{0.2}Ga_{0.8}As$	-	-	800	
15	507	$Al_{0.2}Ga_{0.8}As$	-	-	800	7
14	100	GaAs	-	-	800	7
13	200	$Al_{0.2}Ga_{0.8}As$	-	-	800	7
12	100	GaAs	-	-	800	7
11	200	$Al_{0.2}Ga_{0.8}As$	-	-	800	7
10	100	GaAs	-	-	800	7
9	864	$Al_{0.2}Ga_{0.8}As$	-	-	800	
8	712	AlAs	-	-	800	
7	609	$Al_{0.2}Ga_{0.8}As$	-	-	800	25
6	712	AlAs	-	-	800	25
5	1000	GaAs	-	-	800	
4	1000	GaAs	-	-	790	
3	1000	GaAs	-	-	775	
2	1000	GaAs	-	-	695	
1	1000	GaAs	-	-	610	

B.2 Wafer W404L22

Layer no.	L_z [Å]	Material	Doping	type	Sub T [°C]	Loops
38	0	As	-	-	400	
37	466	GaAs	$2\cdot10^{19}$	p	470	
36	538	GaAs	$2\cdot10^{18}$	p	470	
35	158.4	GaAs → AlAs (*)	$2\text{-}4\cdot10^{18}$	p	730	
34	677.6	AlAs	$2\cdot10^{18}$	p	730	
33	158.4	AlAs → GaAs	$4\text{-}2\cdot10^{18}$	p	730	4
32	200	GaAs	$2\cdot10^{18}$	p	730	4
31	338	GaAs	10^{18}	p	730	4
30	158.4	GaAs → AlAs	$2\text{-}4\cdot10^{18}$	p	730	4
29	677.6	AlAs	$2\cdot10^{18}$	p	730	4
28	158.4	AlAs → GaAs	0	-	730	
27	100	GaAs	0	-	730	
26	80	$In_{0.2}Ga_{0.8}As$	0	-	560	2
25	100	GaAs	0	-	560	2
24	240	GaAs	0	-	560	
23	466	GaAs	0	-	730	
22	80	$In_{0.2}Ga_{0.8}As$	0	-	560	3
21	100	GaAs	0	-	560	3
20	240	GaAs	0	-	560	
19	607	GaAs	0	-	730	
18	80	$In_{0.2}Ga_{0.8}As$	0	-	560	3
17	100	GaAs	0	-	560	3
16	240	GaAs	0	-	560	
15	607	GaAs	0	-	730	
14	80	$In_{0.2}Ga_{0.8}As$	0	-	560	3
13	100	GaAs	0	-	560	3
12	240	GaAs	0	-	560	
11	466	GaAs	0	-	730	
10	80	$In_{0.2}Ga_{0.8}As$	0	-	560	2
9	100	GaAs	0	-	560	2
8	0	As			560	
7	158.4	GaAs → AlAs	0	-	730	
6	677.6	AlAs	10^{18}	n	730	
5	158.4	AlAs → GaAs	$1\text{-}0.5\cdot10^{18}$	n	730	
4	538	GaAs	$5\cdot10^{17}$	n	730	15
3	158.4	GaAs → AlAs	$0.5\text{-}1\cdot10^{18}$	n	730	15
2	677.6	AlAs	10^{18}	n	730	15
1	158.4	AlAs → GaAs	$1\text{-}0.5\cdot10^{18}$	n	730	15

B.3 Wafer W495L33

Layer no.	L_z [Å]	Material	Doping	type	Sub T [°C]	Loops
38	0	As	-	-	400	
37	466	GaAs	$1.2 \cdot 10^{20}$	p	470	
36	538	GaAs	$2 \cdot 10^{18}$	p	470	
35	158.4	GaAs → AlAs	$2\text{-}4 \cdot 10^{18}$	p	730	
34	677.6	AlAs	$2 \cdot 10^{18}$	p	730	
33	158.4	AlAs → GaAs	$4\text{-}2 \cdot 10^{18}$	p	730	4
32	200	GaAs	$2 \cdot 10^{18}$	p	730	4
31	338	GaAs	10^{18}	p	730	4
30	158.4	GaAs → AlAs	$2\text{-}4 \cdot 10^{18}$	p	730	4
29	677.6	AlAs	$2 \cdot 10^{18}$	p	730	4
28	158.4	AlAs → GaAs	0	-	730	
27	100	GaAs	0	-	730	
26	80	$In_{0.2}Ga_{0.8}As$	0	-	560	2
25	100	GaAs	0	-	560	2
24	240	GaAs	0	-	560	
23	466	GaAs	0	-	730	
22	80	$In_{0.2}Ga_{0.8}As$	0	-	560	3
21	100	GaAs	0	-	560	3
20	240	GaAs	0	-	560	
19	607	GaAs	0	-	730	
18	80	$In_{0.2}Ga_{0.8}As$	0	-	560	3
17	100	GaAs	0	-	560	3
16	240	GaAs	0	-	560	
15	607	GaAs	0	-	730	
14	80	$In_{0.2}Ga_{0.8}As$	0	-	560	3
13	100	GaAs	0	-	560	3
12	240	GaAs	0	-	560	
11	466	GaAs	0	-	730	
10	80	$In_{0.2}Ga_{0.8}As$	0	-	560	2
9	100	GaAs	0	-	560	2
8	0	As			560	
7	158.4	GaAs → AlAs	0	-	730	
6	677.6	AlAs	10^{18}	n	730	
5	158.4	AlAs → GaAs	$1\text{-}0.5 \cdot 10^{18}$	n	730	
4	538	GaAs	$5 \cdot 10^{17}$	n	730	15
3	158.4	GaAs → AlAs	$0.5\text{-}1 \cdot 10^{18}$	n	730	15
2	677.6	AlAs	10^{18}	n	730	15
1	158.4	AlAs → GaAs	$1\text{-}0.5 \cdot 10^{18}$	n	730	15

B.4 Wafer W516L34

Layer no.	L_z [Å]	Material	Doping	type	Sub T [°C]	Loops
34	0	As	-	-	400	
33	466	GaAs	$1.08 \cdot 10^{20}$	p	470	
32	538	GaAs	$2 \cdot 10^{18}$	p	470	
31	158.4	GaAs → AlAs	$2\text{-}4 \cdot 10^{18}$	p	730	
30	677.6	AlAs	$2 \cdot 10^{18}$	p	730	
29	158.4	AlAs → GaAs	$4\text{-}2 \cdot 10^{18}$	p	730	9
28	200	GaAs	$2 \cdot 10^{18}$	p	730	9
27	338	GaAs	10^{18}	p	730	9
26	158.4	GaAs → AlAs	$2\text{-}4 \cdot 10^{18}$	p	730	9
25	677.6	AlAs	$2 \cdot 10^{18}$	p	730	9
24	158.4	AlAs → GaAs	0	-	730	
23	1200	GaAs	0	-	730	
22	100	GaAs	0	-	560	2
21	80	$In_{0.2}Ga_{0.8}As$	0	-	560	2
20	400	GaAs	0	-	560	
19	628	GaAs	0	-	730	
18	100	GaAs	0	-	560	2
17	80	$In_{0.2}Ga_{0.8}As$	0	-	560	2
16	400	GaAs	0	-	560	
15	628	GaAs	0	-	730	
14	100	GaAs	0	-	560	2
13	80	$In_{0.2}Ga_{0.8}As$	0	-	560	2
12	400	GaAs	0	-	560	
11	860	GaAs	0	-	730	
10	158.4	GaAs → AlAs	0	-	730	
9	677.6	AlAs	10^{18}	n	730	
8	158.4	AlAs → GaAs	$1\text{-}0.5 \cdot 10^{18}$	n	730	
7	538	GaAs	$5 \cdot 10^{17}$	n	730	20
6	158.4	GaAs → AlAs	$0.5\text{-}1 \cdot 10^{18}$	n	730	20
5	677.6	AlAs	10^{18}	n	730	20
4	158.4	AlAs → GaAs	$1\text{-}0.5 \cdot 10^{18}$	n	730	20
3	400	GaAs	$5 \cdot 10^{17}$	n	730	
2	400	GaAs	$5 \cdot 10^{17}$	n	730	
1	2000	GaAs	$5 \cdot 10^{17}$	n	730	

B.5 Wafer W872L99

Layer no.	L_z [Å]	Material	Doping	type	Sub T [°C]	Loops
15	40	GaAs	0	-	730	
14	466	$Al_{0.5}Ga_{0.5}As$	0	-	730	4
13	289	AlAs	0	-	730	4
12	2.8	GaAs	0	-	730	4
11	289	AlAs	0	-	730	4
10	2.8	GaAs	0	-	730	4
9	289	AlAs	0	-	730	4
8	2.8	GaAs	0	-	730	4
7	289	AlAs	0	-	730	4
6	1000	$Al_{0.5}Ga_{0.5}As$	0	-	730	
5	3000	GaAs	0	-	730	
4	500	GaAs	0	-	730	10
3	500	AlAs	0	-	730	10
2	1000	GaAs	0	-	730	
1	2000	GaAs	0	-	650	

(*) graded linear interface:

L_z [Å]	Material	Doping	type	Sub T [°C]
19.8	GaAs	$2 \cdot 10^{18}$	p	730
2.8	AlAs	$4 \cdot 10^{18}$	p	730
17	GaAs	$2 \cdot 10^{18}$	p	730
5.7	AlAs	$4 \cdot 10^{18}$	p	730
14.1	GaAs	$2 \cdot 10^{18}$	p	730
8.5	AlAs	$4 \cdot 10^{18}$	p	730
11.3	GaAs	$2 \cdot 10^{18}$	p	730
11.3	AlAs	$4 \cdot 10^{18}$	p	730
8.5	GaAs	$2 \cdot 10^{18}$	p	730
14.1	AlAs	$4 \cdot 10^{18}$	p	730
5.7	GaAs	$2 \cdot 10^{18}$	p	730
17.0	AlAs	$4 \cdot 10^{18}$	p	730
2.8	GaAs	$2 \cdot 10^{18}$	p	730
19.8	AlAs	$4 \cdot 10^{18}$	p	730

APPENDIX C

Recipes

Although fabrication and characterization of a complete VCSEL device was not one of the main goals for this project, in this section the total processing of the TUE-VCSEL is discussed
Realization of stripe mesas for mere oxidation purpose has in fact required the application of this procedure (in particular from step 1.1 to 1.8 and from step 1.10 to 3) and therefore a long and exacting work inside the clean-room.

C.1 Process overview

The processing consists of 5 mask-exposures. The total processing involves 13 major steps. A short description of every process step is given below accompanied with a clarifying figure.

(a)

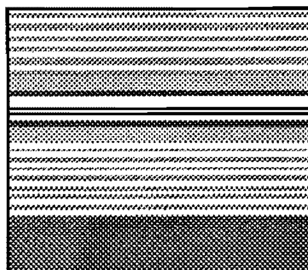

The wafer is grown by MBE at the Eindhoven University of Technology Physics Department. The exact structure of the wafers is given in appendix B. Information about exact thicknesses, doping levels, growth menus and motivations for the design can be found in [43].

(b)

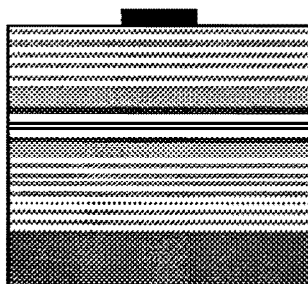

A 300 nm thick Si_3N_4-layer is deposited by Plasma Enhanced Chemical Vapor Deposition (PECVD), which is patterned by standard optical lithography.

(c)

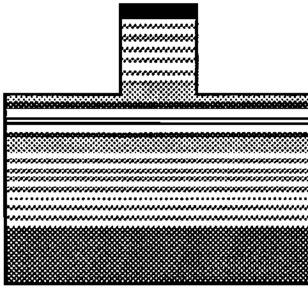

The first mesa is etched by Reactive Ion Etching (RIE). The etch has to stop in the heavily *p*-doped contact layer.

(d)

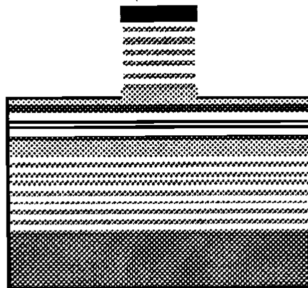

After the first mesa is etched the sealing process is done. This is done with a 10 seconds wet etch in a diluted solution, followed by a Rapid Thermal Anneal (RTA) step, which exposes the sample 30 seconds to an ambient of 90% N_2 and 10% H_2 or O_2 at 550 °C.

(e)

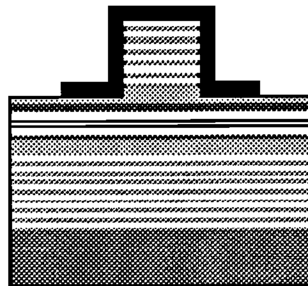

The fifth step involves the preparing of the mask for the second mesa. This is done by depositing a 900 nm thick Si_3N_4-layer by PECVD, patterned by standard optical lithography. The thick Si_3N_4-layer also serves as a protection coating against oxidation.

(f)

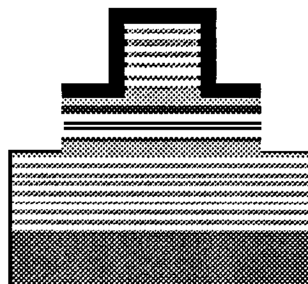

In this step, the second mesa is etched with RIE. Like in step (c), it is important to end in the heavily *n*-doped contact layer.

(g)

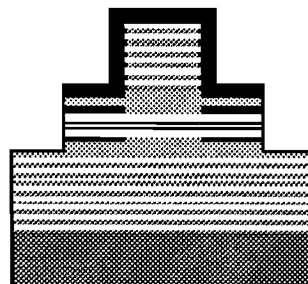

At this point, the current confinement can be realized. This is done by wet selective oxidation of the AlAs-layers surrounding the active region. The fabrication of the oxide will force the current to go through the active region under the top-DBR. The wet oxidation is carried out in a furnace heated to 400 °C, with a saturated H_2O (95 °C) ambient carried by a N_2-carrier gas (flowrate = 0.6 l/min).

(h)

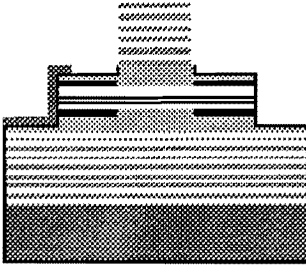

The following steps concern the metallization of the VCSEL. To be able to probe the VCSEL contact-pads have to be realized. Therefore, a passivation layer is created to separate the *p*- contact pad from the *n*-doped GaAs contact-layer. The passivation layer consists of a Si_3N_4-layer deposited by PECVD.

(i)

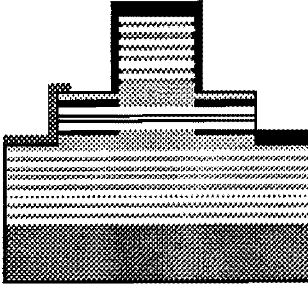

Step 8-10 concern the lift-off process for the *p*-metal contact. First a resist profile has to be generated with standard photolithography. At the places where resist is left no metal will remain after the lift-off process.

(l)

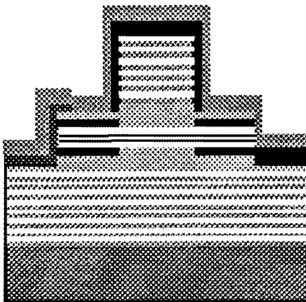

An angle-evaporation of the *p*-metal is done, because a large vertical step (about 1 μm) has to be covered with metal. The *p*-metal consists of TiAu

(m)

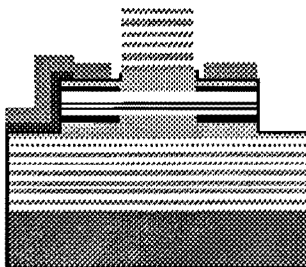

Lift-off. The resist is dissolved in acetone, removing the metal on top.

(n)

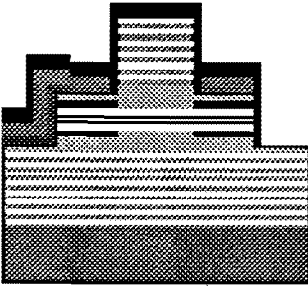

Process-steps 8-10 are repeated for the n-metal contact pads. Here again a standard photolithography is used to generate the resist profile.

(o)

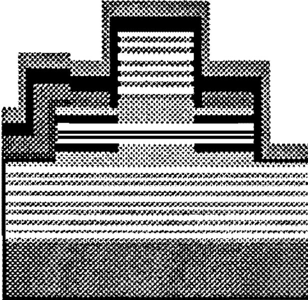

No angle metal-evaporation is done, since no large vertical step has to be covered with metal. The n-metal consists of GeNiAu

(p)

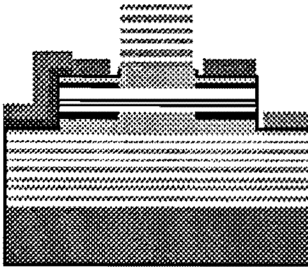

Lift-off. The resist is dissolved in an acetone solution. The on top situated metal is also removed

C.2 Probenprotokoll for the new TUE-VCSELs

1. Etch small mesa

1. 1 Cleaving

- cleave sample + N_2-blow (removal of particles)
- Remarks:

  - Sample size: 1.6 x 1 cm^2

  - Sample check (oval defects ?)

1.2 Cleaning

1.2.A

- 1 min NH_4OH: D.I. H_2O (1:10)
  water rinse (5 MΩ)
  N_2-blow dry

1.2.B

- Acetone 2 min, wet transfer,
  Isopropanol 2 min.
  N_2-blow dry

1.3 SiN_x deposition

- Cluster tool chamber 3
- Batch *AK-SiNx-dep*:

  NH_3= 30 sccm mixed with N_2= 100 sccm
  SiH_4= 4 sccm mixed with N_2= 50 sccm
  T=300 °C, P=250 W, p=200 mTorr
  deposition time: 5 min.
- Remarks:

  - deposition rate: 60 nm/min

  - layer thickness: 300 nm

  - Reflected power should be less than 10 W.

1.4 Lithography

- No Rapid Thermal Annealing
- No extra cleaning steps after deposition !

AZ1505	30 sec	3000 RPM
Softbake	95 °C	5 min
Mask exposure (mesa 1)	8 sec	UV 400
Intermediate bake !!	105 °C	5 min
Development (40:40 ml)	40 sec	

- water rinse (5 MΩ) and N_2-blow dry

1.5 Visual check

- Remarks:
  - 2μm mesas OK ?

1.6 Dry etch SiN_x

- Cluster tool chamber 1
- Batch *AK-SiNx-etch*:
  SF_6= 10 sccm mixed with Ar= 2 sccm
  T=20 °C, MW_{power}=400 W, RF_{power}=20 W
  etch time: 5 min.
- Remarks:
  - etch rate: 70 nm/min

1.7 Resist stripping

1.7.A

- with spray-bottle Acetone above waste container
- wet transfer to petri dishes:
- 1/2 min. Acetone
- 1/2 min. Isopropanol
- + N_2-blow dry

1.7.B

- Cluster tool chamber 1
- Batch *O2-etch*
  O_2= 30 sccm
  T= 20 °C, MW_{power}= 400 W, RF_{power}= 50 W
  etch time: 5 min.
- Remarks:
  - Visual check !

1.8 Dry etch small mesa

- Oxford 100
- Dummy run before real etch (same conditions)
- Process conditions *vcsel_ns.rec*:
  $SiCl_4$= 10 sccm mixed with Ar= 10 sccm
  T=20 °C, P= 50 W

p= 12 mTorr
etch time: 15 min, etch depth: ~3.0 μm

- Remarks:
  - Etch rates seem to depend on chamber-condition (influenced by oxygen plasma)
  - Etch rates depend on mask material and thickness
  - Etch rates depend on sample size
  - Argon is necessary for easier ignition and a more stable plasma.
  - Plasma damage up to 200 Å (Marijke Chang -> wet etch dip)
  - More anisotropic etch with lower pressure ? (10-15 mTorr)
  - $SiCl_4$ mixed with H_2O gives SiO_2 dust and poisonous HCl gas

1.9 Sealing top-DBR

1.9.A

- Room ambient hydrolysis
  Mesa height measurements by Tencor α-stepper
  Probably cleavage of samples
  In total about 10 minutes

1.9.B

- Dip in diluted wet-etch solution
  Etch solution: 1:2:50 = $NH_4OH:H_2O_2:H_2O$
  Etch temperature: room temperature
  Etch time: 10-12 seconds
- N_2-blow dry

1.9.C

- Rapid Thermal Anneal
  30 seconds at 550 °C in 10% O_2/H_2 and 90% N_2
  RTA-recipes: 550fo30s.1 or 550no30s.1
  by Deng and Deppe (Austin)
  [EL 32, 900]/[APL 68, 1948]

1.10 SiN_x deposition

- Cluster tool chamber 3
- Batch *AK-SiNx-dep*:
  NH_3= 30 sccm mixed with N_2= 100 sccm
  SiH_4= 4 sccm mixed with N_2= 50 sccm
  T=300 °C, P=250 W, p=200 mTorr
  deposition time: 5 min.
- Remarks:
  - deposition rate: 60 nm/min
  - layer thickness: 900 nm

2. *Etch large mesa*

Ammonia attacks AlAs/AlOx !!

2.1 Lithography

AZ4330	30 sec	5000 RPM
Softbake	95 °C	15 min
Mask exposure (mesa 2)	25 sec	UV 400
Development	170 sec	

- water rinse and N_2-blow dry
- Visual check !

Hard bake	105 °C	10 min

2.2 Dry Etch SiN_x

- Cluster tool chamber 1
- BatchName *AK-sin-etch:*
  SF_6= 10 sccm mixed with Ar= 2 sccm
  T=20 °C, MW_{power}=400 W, RF_{power}=20 W
  etch time: 5 min.
  etch rate: 70 nm/min

2.3 Resist stripping

2.3.A

- with spray-bottle acetone above waste container
  wet transfer to petri dishes:
  Acetone
  Isopropanol
  N_2-blow dry
- Remarks:
  - Visual check !

2.3.B

- Cluster tool chamber 1
- Batch *O2-etch*:
  O_2= 30 sccm
  T= 20 °C, MW_{power}= 400 W, RF_{power}= 50 W
  DC-bias: ~110
  etch time: 5 min.
- Remarks:
  - Visual check !

2.4 Dry etch large mesa

- Oxford 100
- Dummy run before real etch (same conditions)
- Process conditions *vcsel_ns.rec*:

  $SiCl_4$= 10 sccm mixed with Ar= 10 sccm
  T=20 °C, P= 50 W
  p= 12 mTorr
  etch time: 6 min, etch depth: ~1.0 μm

3. *Selective Oxidation AlAs*

3.1 AlAs constriction layer oxidation:

- Furnace temperature: 400 °C
- Water temperature: 92-95 °C
- N_2-flow: 500 ml/min
- Oxidation time: 7 min
- Oxidation depth: ~15 μm/side
- Remarks:

  - Oxidation rate of the p-type AlAs confinement layer is higher than the n-type AlAs confinement layer [Logboek Martin: p.130-p.132].

4. *Opening metalisation*

4.1 Dry Etch SiN_x

- Cluster tool chamber 1
- Batch *AK-SiNx-etch:*

  SF_6= 10 sccm mixed with Ar= 2 sccm
  T=20 °C, MW_{power}=400 W, RF_{power}=20 W
  etch time: 10 min.

4.2 SiN_x deposition

- Cluster tool chamber 3
- Batch *AK-SiNx-dep*:

  NH_3= 30 sccm mixed with N_2= 100 sccm
  SiH_4= 4 sccm mixed with N_2= 50 sccm
  T=300 °C, P=250 W, p=200 mTorr, deposition time: 5 min.
- Remarks:

  - deposition rate: 60 nm/min
  - layer thickness: 120 nm
  - Hivac time delay: 2 min

4.3 Annealing SiN_x-layer

- RTA
- Recipe 450a_m10.1

4.4 Lithography

AZ4330	30 sec	5000 RPM
Softbake	95 °C	15 min
Mask exposure (PN)	25 sec	UV 400
Development	170 sec	

- water rinse and N_2-blow dry
- Visual check !

Hard bake	105 °C	10 min

4.5 Dry Etch SiN_x

- Cluster tool chamber 1
- BatchName *AK-SiNx-etch:*

  SF_6= 10 sccm mixed with Ar= 2 sccm

  T=20 °C, MW_{power}=400 W, RF_{power}=20 W

  etch time: 2 min.

4.6 Resist stripping

4.6.A

- with spray-bottle Acetone above waste container
  wet transfer to petri dishes:
  Acetone
  Isopropanol
  + N_2-blow dry
- Remarks:
  - Visual check !

4.6.B

- Cluster tool chamber 1
- Batch *O2-etch*:
  O2= 30 sccm
  T= 20 °C, MW_{power}= 400 W, RF_{power}= 50 W
  DC-bias: ~110
  etch time: 5 min.
- Remarks:
  - Visual check !

5. P-metalization

5.1 Lithography

AZ4330	30 sec	5000 RPM
Softbake	95 °C	15 min
Mask exposure (P)	25 sec	UV 400
Development	170 sec	

- water rinse and N_2-blow dry
- No Hardbake !

5.2 P-metal evaporation

- Ti-Au (500 Å + 2500 Å)
- ~20 ° angle evaporation
- Lift-off

6. N-metalization

6.1 Lithography

AZ4330	30 sec	5000 RPM
Softbake	95 °C	15 min
Mask exposure (N)	25 sec	UV 400
Development	170 sec	

- water rinse and N_2-blow dry
- No Hardbake !

6.2 N-metal evaporation

- Ge-Ni-Au (200 Å + 150 Å + 2000 Å)
- Lift-off
- Remarks:
  Ge: doping (diffuses into the semiconductor)
  Au: lower serial resistance
  Ni: adhesion/ smoothens surface

6.3 Annealing contacts

- RTA
- Recipe *400n_m01.1*
  (1 min. In nitrogen ambient at 400 °C)

ARRAYS:

- first polish backside
- no lithography

C.3 Recipe for wet-etched mesa's

1.1 Cleaning

1.1.A

- 1 min NH_4OH: D.I. H_2O (1:10)
  water rinse (5 MΩ)
  N_2-blow dry

1.1.B

- Acetone 2 min, wet transfer,
  Isopropanol 2 min.
  N_2-blow dry

1.2 Lithography

AZ1505	30 sec	3000 RPM
Softbake	95 °C	5 min
Mask exposure (mesa 2)	4 sec	UV 400
Development (40:40 ml)	20-30 sec	

- + water rinse (5 MΩ) and N_2-blow dry
- Remarks:
  - 2μm mesas OK ?

Hard Bake	95 °C	10 min.

1.3 Wet etch mesa

- Etch solution 1:1:3 = H_3PO_4:H_2O_2:CH_4OH = 20:20:60 ml
- Etch temperature 0 °C
- Etch-time: determined by vision
- Remarks:
  - etch rate: 0.26-0.28 μm/min.

Aluminum oxides and hydroxides

The oxide, hydroxides and mixed oxyhydroxides of aluminum form a family of compounds that have immense technological importance [40].
Many substances of intermediate composition between the oxide Al_2O_3 and hydroxide $Al(OH)_3$ occur abundantly in nature and are even involved into the room ambient degradation and wet oxidation process of AlGaAs in opto-electronic devices.
In this appendix it is intended to give a general overview of the aluminum based hydroxides and their products of thermal decomposition.
In table B1 a list of all the Al-hydroxides is shown.

Composition		Mineralogical denomination	ALCOA(*) denomination
Al_2O_3		corundum	α-alumina
$Al(OH)_3$	$Al_2O_3 \cdot 3H_2O$	hydrargillite or gibbsite	α-trihydrate of alumina
$Al(OH)_3$	$Al_2O_3 \cdot 3H_2O$	bayerite	β-trihydrate of alumina
$Al(OH)_3$	$Al_2O_3 \cdot 3H_2O$	nordstrandite	-
$AlO(OH)$	$Al_2O_3 \cdot H_2O$	boehmite	α-monohydrate of alumina
$AlO(OH)$	$Al_2O_3 \cdot H_2O$	diaspore	β-monohydrate of alumina

Tab. B1: nomenclature of aluminum based hydroxides
(*) Aluminium Company of America

The term "alumina hydrate" used for $AlO(OH)$ and $Al(OH)_3$ are misleading; these compounds are in fact true hydroxides, with different cristalline structures than Al_2O_3 and not species in which water molecules have been absorbed. Anyway, aluminum oxide and hydroxide have a strong affinity for water (and for polar molecules in general) and therefore a surface layer of water will always be present.

α- Al_2O_3 : corundum or α-alumina crystallizes in the rhomboedral system. It is a white crystalline powder with a density of 4.0 g/cm^3 , a high hardness (Moh 9) and high melting point (2045°C); it is involatile, inert, a good electrical insulator and it resists hydration and attack by acids, in contrast to active aluminas which readily absorb water and dissolve in acids. As a result, it finds many applications in abrasives, refractories and structural ceramic. Pure α- Al_2O_3 may be prepared by calcination of various Al salts, γ-Al_2O_3 or any of the hydrous oxides above 1200°C.

γ- Al_2O_3: is the second modification of alumina and has less compact cubic close-packed structure; his structure is also referred as a defect spinel type (like a spinel but with a deficit of cations) and is composed of a face-centered cubic array of 32 oxygen atoms with the aluminum atoms randomly occupying $21\frac{1}{3}$ of the octahedral and 8 tetrahedral interstices. It can be prepared by low temperature (< 450°C) dehydration of gibbsite or bohemite. Unlike α- Al_2O_3, γ-Al_2O_3 is one of the so-called "activated alumina" and readily absorbs water and dissolves in acids. Progressive dehydration of γ-alumina leads to porous materials that have great value as catalyst, catalyst supports and ion-exchanges. On the aluminum metal surface another oxide is found; it has a defect NaCl structure in which aluminum cations occupy only two thirds of the octahedral holes.

α-Al(OH)$_3$ gibbsite (also known as **hydrargillite**): it is the principal constituent of bauxites of North and South America and is the more stable trihydroxide; it is prepared by slow precipitation from warm alkaline solution or by heating bayerite in sodium aluminate solution at 80°C. The crystal structure of gibbsite, like those of bayerite and nordstrandite, is based on a sequence of layers AB of closely-packed hydroxil ions, two-thirds of the octahedral holes being occupied with aluminum ions. The alternation of occupied and vacant octahedra causes the lattice to be slightly deformed, the empty octahedra being smaller than the filled octahedra.

β-Al(OH)$_3$ bayerite: it does not occur in nature and has a pseudotrigonal structure in which the approximately hexagonal close-packed arrangement of hydroxide ions is distorted by the metal ions, giving rise to O-Al-O sandwiches similar to those in gibbsite [42].

Nordstrandite: it rarely occurs in nature and its structure is based on an AB sequence of oxygen layers which are so aligned to place adjacent OH ions opposite to each other, making nostrandite structurally intermediate between gibbsite and bayerite.

Boehmite and **diaspore**: they are the two modifications of monohydrate of alumina AlO(OH); well-crystallized boehmite can be prepared by hydrothermal treatment of gibbsite in an autoclave at 300°C for 2 hours and is the principal constituent of European bauxites. Well-crystallized diaspore occurs in some types of clay and in bauxite; it can be prepared by hydrothermal treatment of boehmite (300°C and 500 atm) in 0.4 % aqueous NaOH. Between 275°C and 425°C and with a water vapour pressure in excess of 140 atm, all aluminium hydroxides and oxides are converted into diaspore when a seeding of this form is present [41].

Crystalline bohemite and diaspore are built up of double chains in which each Al atom has a neighbouring bridge oxygen of the other chain. The difference between the two modifications is due to the different arrangements of the extended double molecules.

Activated aluminas

When the hydroxides $Al(OH)_3$ and $AlO(OH)$ are heated strongly, they lose water and are converted ultimately into Al_2O_3 through a series of intermediate phases recognizable as structurally distinct by means of their X-ray powder diffraction spectra.
They have been classified as:

Phase	Lattice	Density [g/cm³]
γ	cubic	3.20
δ	rombic	3.20
η	cubic	
θ	monoclin	3.56
κ	rombic	
ρ	amorphe	
χ	cubic	

The intermediate phases encountered in a particular dehydration experiment depend critically on the starting material and its degree of crystallinity and on several process parameters like temperature, rate and time of heating, pressure, vapor or vacuum conditions. Possible reactions (data from [41] and [42]) are depicted in fig. D.1.

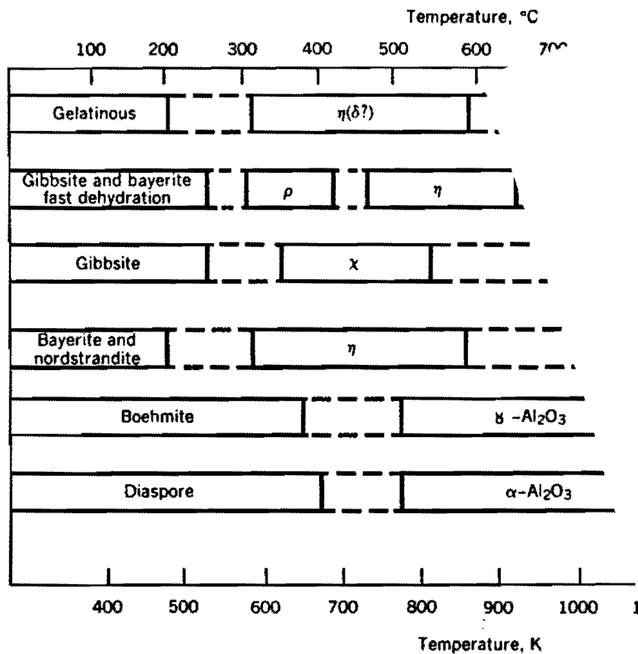

Figure D.1: decomposition sequence of hydrous aluminas

All of the intermediate dehydration products of the hydroxides contain a small proportion of hydroxil group, the proportion decreasing as the dehydration temperature increases.
Chemically it is convenient to classify them according to their reactivity, which can be related to their temperature of formation. Those species produced by dehydration of $Al(OH)_3$ or $AlO(OH)$ below 600°C (χ, ρ, η and γ alumina) are referred to as "low-temperature aluminas" or as γ-group of aluminas. They have formula $Al_2O_3 \cdot n\ H_2O$ $(0 < n < 0.6)$ and are

incompletely deactivated hydroxides. They are also called "activated aluminas" because of their adsorptive and catalytic activities. Those types of alumina obtained by dehydration at 900-1000°C, the "high temperature aluminas" or δ-group of aluminas, include κ, θ and δ alumina; these species are nearly anhydrous Al_2O_3.

According to fig. D.1, formation of γ-Al_2O_3 by hydrolysis of AlAs during the wet oxidation process seems to be originated directly from decomposition of bohemite AlO(OH). Dehydration of this hydroxide will obviously provoke generation of water vapor, breakdown of grains and therefore creation of pores (20÷40 Å); although the new oxide will have higher density than the hydroxide, such porosity will be conserved leading to huge specific surfaces. The specific surface of γ-Al_2O_3 (about $100m^2/g$) is less than the porosity of χ and κ aluminas, but enough to explain the high oxidation rates during the reaction limited wet oxidation process.

Phase diagrams of the Al_2O_3-H_2O and Al_2O_3-Ga_2O_3-H_2O system are presented in the following figures.

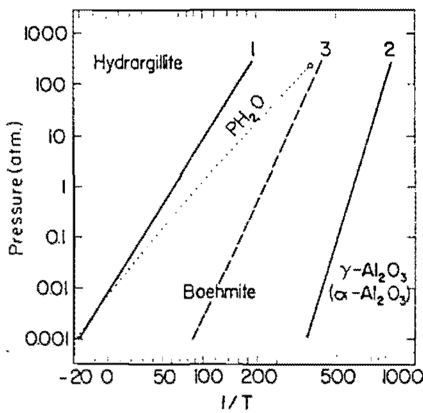

Figure D.2: system Al_2O_3-H_2O
K. Torkar and H. Worel, Monatsh. Chem., 743

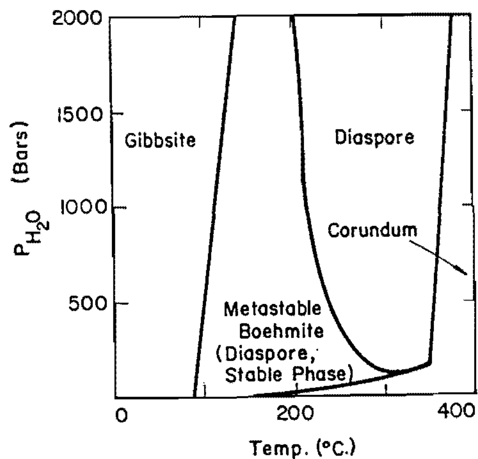

Figure D.3: system Al_2O_3-H_2O at low pressures
G.C. Kennedy, Am. J. Sci., 257, 568

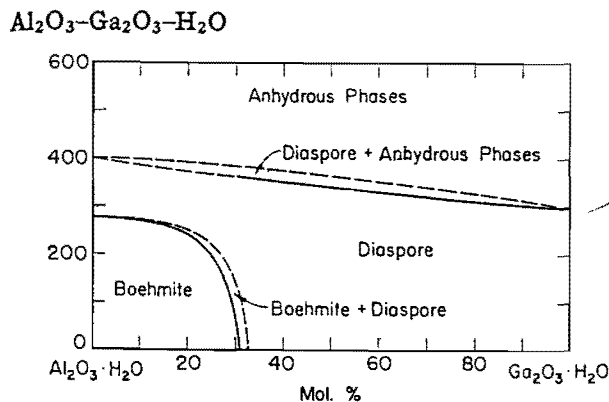

Figure D.4: system $Al_2O_3.H_2O$- Ga_2O_3-H_2O
V.G. Hill, R. Roy and E.F. Osborn, J. Am. Ceram. Soc., 35 [6] 139

REFERENCE

[1] Dallesasse, J.M. et al.
HYDROLYZATION OXIDATION OF $Al_xGa_{1-x}As$-AlAs-GaAs QUANTUM WELL HETEROSTRUCTURES AND SUPERLATTICES
Applied Physics Letters, Vol. 57(1990), No. 26, p. 2844-2846

[2] Dallesasse, J.M. et al.
ENVIRONMENTAL DEGRADATION OF $Al_xGa_{1-x}As$-GaAs QUANTUM-WELL HETEROSTRUCTURES
Journal of Applied Physics, Vol. 68(1990), No. 5, p. 2235-2238

[3] Dallesasse, J.M. et al.
NATIVE-OXIDE MASKED IMPURITY-INDUCED LAYER DISORDERING OF $Al_xGa_{1-x}As$ QUANTUM WELL HETEROSTRUCTURES
Applied Physics Letters, Vol. 58(1991), No. 9, p. 974-976

[4] Sugg, A.R. et al.
NATIVE OXIDE STABILIZATION OF AlAs-GaAs HETEROSTRUCTURES
Applied Physics Letters, Vol. 58(1991), No. 11, p. 1199-1201

[5] Kish, F.A. et al.
PROPERTIES AND USE OF $In_{0.5}(Al_XGa_{1-X})_{0.5}P$ AND $Al_XGa_{1-X}As$ NATIVE OXIDES IN HETEROSTRUCTURES LASERS
Journal of Electronic Materials, Vol. 12(1992), No. 21, p. 1133-1139

[6] Sugg, A.R. et al.
EFFECTS OF LOW-TEMPERATURE ANNEALING ON THE NATIVE OXIDE OF $Al_xGa_{1-x}As$
Journal of Applied Physics, Vol. 74(1993), No. 6, p. 3880-3885

[7] Choquette, K.D. et al.
SELECTIVE OXIDATION OF BURIED AlGaAs VERSUS AlAs LAYERS
Applied Physics Letters, Vol. 69(1996), No. 10, p. 1385-1387

[8] Guha, S. et al.
MICROSTRUCTURE OF AlGaAs-OXIDE HETEROLAYERS FORMED BY WET OXIDATION
Applied Physics Letters, Vol. 68(1996), No. 7, p. 906-908

[9] Twesten, R.D. et al.
MICROSTRUCTURE OF LATERALLY OXIDIZED $Al_xGa_{1-x}As$ LAYERS IN VERTICAL-CAVITY LASERS
Applied Physics Letters, Vol. 69(1996), No. 1, p. 19-21

[10] Takamori, T. et al.
INTERFACE STRUCTURE OF SELECTIVELY OXIDIZED AlAs/GaAs
Applied Physics Letters, Vol. 69(1996), No. 5, p. 19-21

[11] Ochiai, M. et al.
KINETICS OF THERMAL OXIDATION OF AlAs IN WATER VAPOR
Applied Physics Letters, Vol. 68(1996), No. 14, p. 1898-1900

[12] Deal B.E. and A.S. Grove
Journal of Applied Physics, Vol. 36(1965), p. 3770

[13] Kish, F.A. et al.
DEPENDENCE ON DOPING TYPE (p/n) OF THE WATER VAPOR OXIDATION OF HIGH-GAP $Al_xGa_{1-x}As$
Applied Physics Letters, Vol. 60(1992), No. 25, p. 3165-3167

[14] Burton, R.S. and T.E. Schlesinger
WET THERMAL OXIDATION OF $Al_xGa_{1-x}As$ COMPOUNDS
Journal of Applied Physics, Vol. 76(1994), No. 9, p. 5503-5507

[15] Nickel, H.
A DETAILED EXPERIMENTAL STUDY OF THE WET OXIDATION KINETICS OF $Al_xGa_{1-x}As$
Journal of Applied Physics, Vol. 78(1995), No. 8, p. 5201-5203

[16] Choquette, K.D.
FABRICATION AND PERFORMANCE OF SELECTIVELY OXIDIZED VERTICAL-CAVITY LASERS
IEEE Photonics Technology Letters, Vol. 7(1995), No. 11, p. 1237-1239

[17] Kim, J.-H. et al.
LATERAL WET OXIDATION OF $Al_xGa_{1-x}As$-GaAs DEPENDING ON ITS STRUCTURES
Applied Physics Letters, Vol. 69(1996), No. 22, p. 3357-3359

[18] Homan, O.J. et al.
FABRICATION AND CHARACTERISATION OF GaAs/AlGaAs QUANTUM-WELL LASERS USING THERMALLY OXIDISED AlGaAs
In: Nanofabrication technologies and device integration. Lindau (Germany), april 1994. Edited by: Wolfgang Karthe.
Bellingham, Washington: SPIE, 1994, p. 196-204
(Proceedings of the SPIE; vol. 2213)

[19] Lee, Y-S. et al.
WET OXIDATION OF AlAs GROWN BY MOLECULAR BEAM EPITAXY
Applied Physics Letters, Vol. 65(1994), No. 21, p. 2717-2719

[20] Huffaker, D.L. et al.
NATIVE-OXIDE DEFINED RING CONTACT FOR LOW THRESHOLD VERTICAL-CAVITY LASERS
Applied Physics Letters, Vol. 65(1994), No. 1, p. 97-99

[21] Bun Lee et al.
DEFECT-FREE GaAs CAP LAYER ON ALUMINIUM OXIDE GENERATED BY THERMAL OXIDATION OF AlAs
In: evolution of thin films and surface structure and morphology. Boston (USA), November 28 - December 2, 1994. Edited by: B.G. Demczyrk et al.
Pittsburgh: Materials Research Society, 1995.
(Materials Research Society symposium proceedings; vol. 355)

[22] Maranowski, S.A. et al.
PHOTON-INDUCED ANISOTROPIC OXIDATION ALONG P-N JUNCTIONS IN $Al_xGa_{1-x}As$-GaAs QUANTUM WELL HETEROSTRUCTURES
Applied Physics Letters, Vol. 62(1993), No. 17, p. 2087-2089

[23] Burton R.S.et al
SELF-ALIGNED NATIVE-OXIDE RIDGE-GEOMETRY AlGaAs-GaAs QUANTUM WELL HETEROSTRUCTURE LASER ARRAYS
Applied Physics Letters, Vol. 60(1992), No. 15, p. 1777

[24] P. van Dale, IMEC-University of Gent (INTEC)
PLASMA PROCESSING FOR III-V OPTOELECTRONIC MATERIAL AND DEVICES
Private communication

[25] Flammy D.L.
THE DESIGN OF PLASMA ETCHANTS
Chemistry and Plasma Processing, Vol.1, No 4 (1981)

[26] M.H. MacDougal
ELECTRICALLY PUMPED VERTICAL-CAVITY LASERS WITH Al_xO_y/GaAs REFLECTORS
IEEE P.T.L vol.8 n.3 (1996)

[27] Kash, J.A. et al.
RECOMBINATION IN GaAs AT THE AlAs OXIDE-GaAs INTERFACE
Applied Physics Letters, Vol. 67(1995), No. 21, p. 2022-2024

[28] A.E.Bond, C.K.Lin, M.H.Mac Dougal
BACKING REDUCTION IN MESFET'S USING AM AlAs NATIVE OXIDE BUFFER LAYER
University of Southern California, L.A. (unpublished)

[29] F. Reinhardt, B.Dwir
OXIDATION OF GaAs/AlGaAs HETEROSTRUCTURE STUDIED BY AFM IN AIR

Appl . Phys. Lett. 69 n.22 p.3168 (1996)

[30] Mac Dougal
WIDE-BANDWIDTH DISTRIBUTED BRAGG REFLECTORS USING OXIDE/GaAs MULTILAYERS
Electronic Letters Vol.30 No14 (1994) p. 1147-1149

[31] Fujiwara K.
CLASSIFICATION AND ORIGIN OF GaAs OVAL DEFECTS GROWN BY MOLECULAR BEAM EPITAXY
Journal of Crystal Growth Vol.80 (1987) p.104-112

[32] Sato F et al.
Annual Spring Meeting on Applied Physics of Japan
Tokyo 1986

[33] Fujiwara K. et al.
EFFECTS OF SUBSTRATE PREPARATION CONDITIONS ON GaAs OVAL DEFECTS GROWN BY MBE
Appl . Phys. Lett. Vol.48 p.701 (1986)

[34] Matteson S. and Shih H.D.
MORFOLOGICAL STUDIES OF OVAL DEFECTS IN GaAs EPITAXIAL LAYERS GROWN BY MBE
Appl . Phys. Lett. Vol.48 p.47 (1986)

[35] Nanbu k. et al.
J. Electrochem. Soc. Vol.133 (1986) p.601

[36] Akimoto K. et al.
ORIGIN OF OVAL DEFECTS IN GaAs LAYERS GROWN BY MBE
J. Crystal Growth Vol.73 (1985) p.117

[37] Metze G.M. et al.
AN INVESTIGATION OF GaAs FILMS GROWN BY MBE AT LOW SUBSTRATE TEMPERATURES AND GROWTH RATES
J. Vac. Sci. and Technol. B1 (1983) p.166

[38] Chai Y.G. et al.
ELIMINATION OF “PAIRS” DEFECTS FROM GaAs LAYERS GROWN BY MBE
Appl . Phys. Lett. Vol.47 p.1327 (1985)

[39] Baffleur M. et al.
SPATIALLY RESOLVED PHOTOLUMINESCENCE AT OVAL DEFECTS IN MBE GaAs LAYERS
J. Crystal Growth Vol.66 (1984) p.472

[40] C.Misra
Industrial Alumina Chemicals
The American Chemical Society, Washington, D.C. 1986

[41] B.G. Linsen
Physical and Chemical Aspects of Adsorbents and Catalysts
Academic Press, London (1970)

[42] A. Standen
Kirk-Othmer Encyclopedia of Chemical Technology
2nd ed., Vol 2, p. 41, Wilson Ed. N.Y. (1963)

[43] Creusen M.
DESIGN AND FABRICATION OF AN INTRA-CAVITY CONTACTED VERTICAL CAVITY SURFACE EMITTING LASER
Ontwerpers opleiding Fysische Instrumentatie, Technische Universiteit Eindhoven